FLUORESCENCE MODULATION AND APPLICATIONS OF SELF-ASSEMBLED *p*-PHENYLENEETHYNYLENE DERIVATIVES

THESIS SUBMITTED TO
COCHIN UNIVERSITY OF SCIENCE AND TECHNOLOGY
IN PARTIAL FULFILMENT OF THE REQUIREMENTS FOR THE DEGREE OF

DOCTOR OF PHILOSOPHY

in Chemistry Under the Faculty of Science

By

R. Thirumalai Kumaran

Under the Supervision of

Dr. A. Ajayaghosh

Photosciences and Photonics Section
Chemical Sciences and Technology Division
CSIR–National Institute for Interdisciplinary Science and Technology (CSIR–NIIST)
Thiruvananthapuram-695 019, Kerala

September 2017

Dedicated to

My Parents

DECLARATION

I hereby declare that the Ph. D. thesis entitled **"FLUORESCENCE MODULATION AND APPLICATIONS OF SELF-ASSEMBLED *p*-PHENYLENEETHYNYLENE DERIVATIVES"** is an independent work carried out by me at the Photosciences and Photonics Section, Chemical Sciences and Technology Division of the CSIR-National Institute for Interdisciplinary Science and Technology (CSIR-NIIST), Thiruvananthapuram, under the supervision of Dr. A. Ajayaghosh and the same has not been submitted elsewhere for a degree, diploma or title.

In keeping with the general practice of reporting scientific observations, due acknowledgement has been made wherever the work described is based on the findings of other investigators.

(R. Thirumalai Kumaran)

राष्ट्रीय अंतर्विषयी विज्ञान तथा प्रौद्योगिकी संस्थान
वैज्ञानिक तथा औद्योगिक अनुसंधान परिषद्
इंडस्ट्रियल इस्टेट पी.ओ., पाप्पनंकोड, तिरुवनंतपुरम, भारत-695 019

75 Years of CSIR Touching Lives

CSIR-NATIONAL INSTITUTE FOR INTERDISCIPLINARY SCIENCE & TECHNOLOGY (CSIR-NIIST)
Council of Scientific & Industrial Research
Industrial Estate P.O., Pappanamcode, Thiruvananthapuram, India-695 019

डॉ. ए. अजयघोष एफएनए, एफटीडब्ल्यूएएस
निदेशक

Dr. A. Ajayaghosh FNA, FTWAS
Director

September 13, 2017

CERTIFICATE

This is to certify that the work embodied in the Ph. D. thesis entitled **"FLUORESCENCE MODULATION AND APPLICATIONS OF SELF-ASSEMBLED *p*-PHENYLENE ETHYNYLENE DERIVATIVES"** has been carried out by **Mr. R. Thirumalai Kumaran** under my supervision and guidance at Photosciences and Photonics Section, Chemical Sciences and Technology Division of the CSIR-National Institute for Interdisciplinary Science and Technology (CSIR-NIIST), Thiruvananthapuram and the same has not been submitted elsewhere for a degree. To the best of my knowledge the thesis is a bonafide record of research carried out by **Mr. R. Thirumalai Kumaran** under my supervision. All the relevant corrections, modifications and recommendations suggested by the audience and the doctoral committee members during the pre-synopsis seminar of **Mr. R. Thirumalai Kumaran** have also been incorporated in the thesis.

A. Ajayaghosh

(Thesis Supervisor)

ACKNOWLEDGEMENTS

I have great pleasure in placing on record my deep sense of gratitude to Dr. A. Ajayaghosh, my thesis supervisor, for suggesting me the research problem and for his guidance, support and encouragement, leading to the successful completion of this work.

I would like to express my sincere thanks to Professor M. V. George for his constant support during the tenure of this work.

I wish to thank Dr. Suresh Das, and Dr. B. C. Pai, former Directors of CSIR-NIIST, Thiruvananthapuram for providing me the necessary facilities for carrying out the work.

I am extremely thankful to Dr. J. D. Sudha and Dr. Vakayil K. Praveen, for their valuable help, support, encouragement and care.

I sincerely thank Dr. K. R. Gopidas, Dr. D. Ramaiah, Dr. Joshy Joseph, Dr. K. N. Narayanan Unni, Dr. Biswapriya Deb, Dr. V. Karunakaran, Dr. K. Yoosaf, and Dr. C. Vijayakumar, present and former Scientists of the Photosciences and Photonics, for all the help and support extended to me.

I would like to thank Dr. S. Prathapan, Associate Professor, Department of Applied Chemistry, CUSAT, Cochin for his support and help.

I would like to thank Dr. Rakesh K. Mishra and Mr. Gourab Das for their support and help in carrying out my research work.

I thank all the members of the Photosciences and Photonics and in particular, Dr. S. Mahesh, Dr. S. Prasanthkumar, Dr. Anesh G., Dr. Krishnan Kartha, Dr. Anees P., Dr. Vishnu S., Dr. Sandeep C., Dr. Vedanarayan B., Dr. Rahul Dev Mukhopadhyay, Dr. Divya Susan Philips, Mr. Samrat Ghosh, Mr. Arindam Mal, Mr. Hifsudheen M., Mr. Satyajit Das, Dr. Manas Panda, Juliya A. P., Anisha P., Betzy B. and the members of other divisions of NIIST for their help and support.

I would like to thank Mr. Robert Philip, Mr. Chandrakanth C. K, Ms. S. Viji, Ms. Soumini Mathew, Mr. Adarsh, Mr. P. Preethanuj, Mr. T. Arun, Mr. Saran P., and Mr. R. Gokul for technical assistance and general help.

Words are inadequate to express my gratitude to my parents for their encouragement. I take this opportunity to pay respect to all my teachers who have guided me.

I sincerely thank Council of Scientific and Industrial Research (CSIR) and DST, Government of India for financial assistance.

R. Thirumalai Kumaran

CONTENTS

PREFACE

Design of linear π-conjugated systems is of significant interest due to their self-assembling and inherent optoelectronic properties. Various non-covalent interactions such as hydrogen bonding, π-π interactions, van der Waals forces and hydrophobic-hydrophilic interactions are responsible for the self-assembly and optical properties of these systems. Tuning the emission of these molecules with high efficiency and reproducibility without changing the chemical structure is of great importance to different practical applications such as optical recording, sensing and security labeling. The first chapter of the thesis gives an overview of the recent developments and applications of fluorescence modulation in self-assembled π-conjugated molecules by different external stimuli.

Synthesis, photophysical and self-assembling behavior of π-conjugated molecules **PE1** and **PE2** were discussed in Chapter 2. In these molecules, the triple bonded linear aromatic π-backbone (phenyleneethynylene, **PE**) is the fluorescent core, which is connected to a bulky end group through an amide or ester bond. The terminal bulky group is composed of flexible oxyethylene chains. In this work, a novel strategy of self-erasable writing using water as ink was introduced. The inherent blue fluorescence of **PE1** in the film state can be tuned to cyan by applying water. We also have exploited the hydrophobic-hydrophilic balance and the flexibility of hydrogen bonds to manipulate the packing mode of molecular self-assemblies leading to variation in exciton interaction and fluorescence color change.

Such materials may have tremendous potential as security labels for checking authenticity of the documents as well as for currency counterfeit prevention. The other molecule **PE2** was used for comparative studies, as the molecule does not show any distinct fluorescence color change with water.

Synthesis and properties of cyano substituted dodecyl chain functionalized linear *p*-phenyleneethynylene derivative **(PE-CN)** which can form two different types of aggregates depending upon the rate of cooling and concentration in *n*-decane are discussed in Chapter 3. This molecule was designed in such a way that it can take part in the formation of the aggregates predominately through hydrogen bonding or dipolar interaction depending upon conditions. Blue emitting aggregates were obtained upon slow cooling of a hot *n*-decane solution and are under the complete control of thermodynamics. However, fast cooling of a preheated solution resulted in the formation of the kinetically controlled green emitting aggregates that in turn returns to the most stable blue form while stirring and even with time. It is further necessary to mention that these two aggregates are having completely different molecular packing and distinct photophysical properties, which are proves by small angle X-ray scattering and also by the measurement of the charge carrier lifetime. Concentration also plays a major role in this case. This molecule also forms green transparent and blue opaque gels with different morphological features at relatively higher (30 mM) and lower (6 mM) concentrations, respectively. The cyano group has an important role in the interaction and in the molecular packing to generate different aggregates because the molecule, PE without cyano group does not show any such changes under the same conditions.

Synthesis, photophysical and self-assembling behavior of cyano substituted chiral alkyl chain functionalized *p*-phenyleneethynylene **PE-CN-Chiral** are described in Chapter 4. In this work, we have introduced the concept of modulating both the emission and CD signal of a π-assembly by the application of a single stimulus. **PE-CN-Chiral** forms blue emitting aggregates in *n*-decane at 1×10^{-3} M concentration showing a bisignate CD signal with a negative response at 400 nm followed by a positive signal at 315 nm. When trifluoroacetic acid (TFA) was added to the blue aggregates, the emission of the aggregates changed from blue to green along with the reversal of signs of the bisignate CD with time. Addition of TFA results in breaking of the hydrogen bonds within the molecular self-assembly which eventually allows the molecules to re-organize in a manner different from the initial assembly. Here, TFA acts as an external stimulus to trigger the packing of the molecules from blue to green-phase. Addition of TFA did not reflect in any significant fluorescence switching of an assembly formed by a molecule that lacks cyano moiety (**PE-Chiral**), rather, in this case, addition of TFA led the formation of monomers.

In summary, this thesis describes the design, synthesis and properties of few *p*-phenyleneethynylene systems. The self-assembly, photophysical and stimuli responsive behavior of these *p*-phenyleneethynylene systems and their applications in security labeling and sensing have been discussed.

Chapter 1

Emission Tunable Molecular Assemblies Based on π-Conjugated Systems

Abstract

Linear π-conjugated systems are of significant interest due to their inherent optoelectronic properties which can be manipulated through intermolecular interactions. In these, systems weak noncovalent interactions such as hydrogen bonding, π-π interactions, van der Waals force and hydrophobic-hydrophilic interactions can be used to control the self-assembly of molecules leading to tunable optical properties. Systematic studies on the factors/parameters that control the tunable luminescent behavior not only facilitates fundamental understanding of the system but also provides suitable direction for their practical utility in optical recording, sensing and security labeling. In this chapter, an overview of the recent developments of stimuli responsive fluorochromic molecules and their possible applications are described. The mechanism of variable optical response and the correlation with structural change has also been discussed. Lastly, the objectives and outline of the thesis are also presented.

1.1. Introduction

Supramolecular chemistry is the study of noncovalent interactions between molecules and is an extremely interdisciplinary field of science covering the chemical, physical and biological concepts.[1] This rapidly expanding area is attracting more attention due to its ability to utilize noncovalent interactions such as electrostatic, hydrophobic, van der Waals, hydrogen-bonding, halogen bonding and charge transfer interactions for constructing supramolecular materials with useful properties. These intermolecular interactions are weak in molecular level but become collectively strong at supramolecular level and are able to control material properties. Thus, it is of particular interest to utilize these interactions to organize molecules in a regular fashion to tune their optical and electronic properties. In this context, enormous attention has been paid to different linear π-systems such as *p*-phenyleneethynylenes (PE) [2], *p*-phenylenevinylenes (PV) and *p*-phenylenes. Owing to the linearly conjugated structures, these molecules are efficient in electronic communication with each other and are of prime interest for studying properties such as charge transport, energy transfer and luminescence behavior, which are essential for a wide variety of optoelectronic applications.[3]

1.2. Self-assembly and Optical Properties of PEs

Phenyleneethynylenes (PEs) are π-conjugated molecules with unique optical and electronic properties. The important structural characteristic of PE is the free rotation of the alkyne-aryl bonds that leads to the coexistence and rapid equilibration of coplanar and twisted structures (Figure 1.1). Recently, Garcia-Garibay and co-workers have demonstrated that, by controlling the extent of phenyl group rotation and the aggregation, one can obtain variable optoelectronic properties of PEs.[4] They also proposed that the equilibration process of PEs in solution do not have any consequences in the ground state, but upon electronic excitation, the rotation of alkyne-aryl single bonds lead to the changes in the bond order of the coplanar and twisted forms that results in emission spectral shifts.

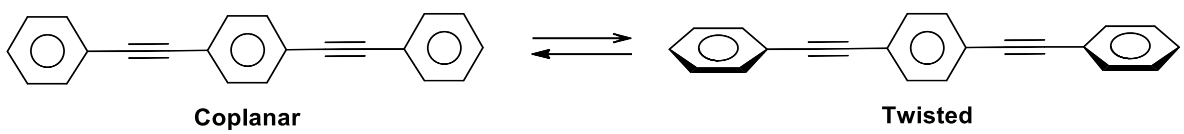

Figure 1.1. Coplanar and twisted conformations of *p*-phenyleneethynylene.

In general, spectral shift occurs due to the change in concentration or phase transitions of the chromophores, and they are interpreted in terms of excimer formation or excitonic coupling arising from co-facial aggregation. However, in the case of PEs, planarization of molecules gives rise to relatively modest emission shifts of ca. 20-30 nm (Figure 1.2), which preserve the vibronic structure of the monomer and retain a high emission quantum yield. This behavior is in contrast to that of aggregation induced large spectral shifts and loss of vibronic structures. The different spectral properties of twisted, coplanar and co-facial planar aggregate of PEs have been reported in solution, polymer film and in crystalline solid-state. For example, the excitation and emission spectra of the crystalline aggregates of PE derivative **1** was red-shifted by ca. 70-80 nm (Figure 1.2b, iii) with respect to the spectra obtained in dilute solutions. According to the results of optical studies, it was interpreted that relatively disordered aggregates may lead to planarization of the PE moieties before co-facial interaction (Figure 1.2c). This co-facial aggregate causes the red shift and broadening of the spectrum.

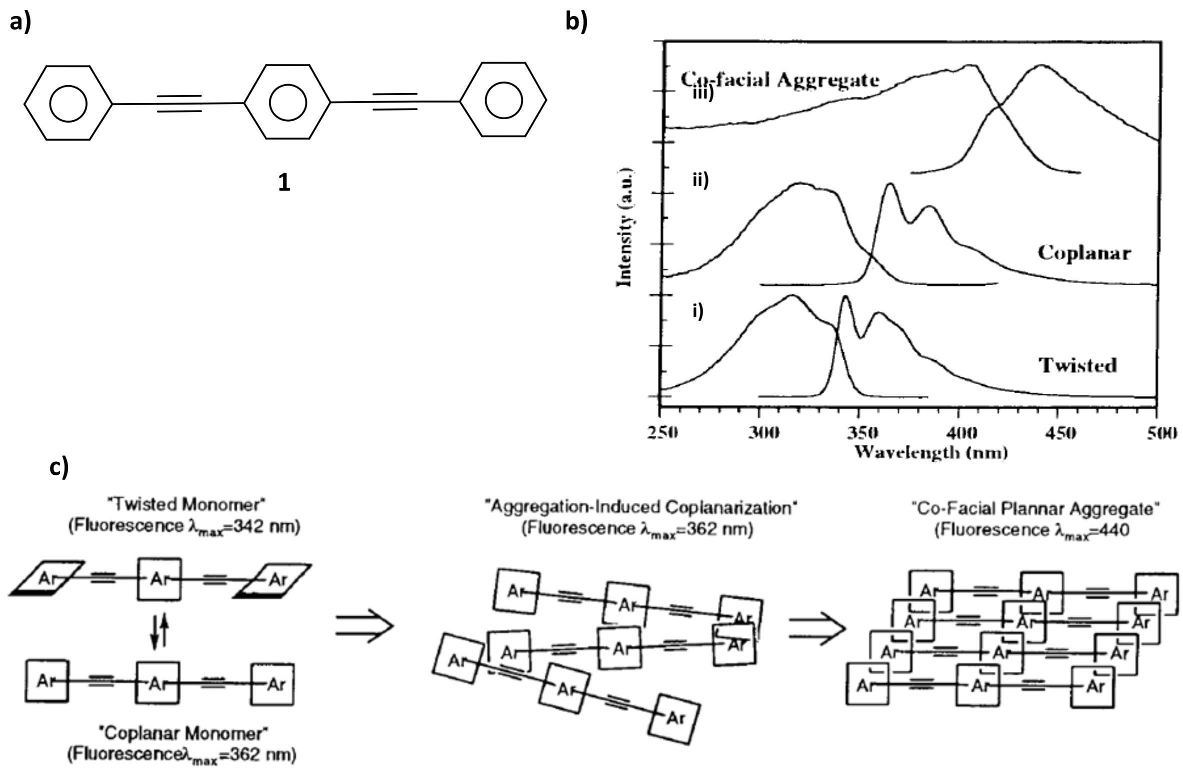

Figure 1.2. a) Molecular structure of **1**. b) Excitation (left) and emission (right) spectra of **1** in i) solution, ii) polymer film and iii) crystalline solid. c) Schematic representation of structural arrangements of **1** in twisted, coplanar and co-facial planar aggregate. (Adapted with permission from ref. 4a. Copyright 2001 American Chemical Society.)

In another interesting finding, Kulkarni and co-workers have investigated the correlation between molecule to molecule inter-planar distance with the solid state fluorescence property.[5] For this purpose, a series of alkoxy-substituted oligo(*p*-phenyleneethynelenes) (OPEs) (**2**-**7**) with varying alkyl chain lengths have been prepared (Figure 1.3a). Analysis of the crystal structure revealed that the interacting molecules are arranged in a nearly head to tail fashion, similar to *J*-aggregates (Figure 1.3b).

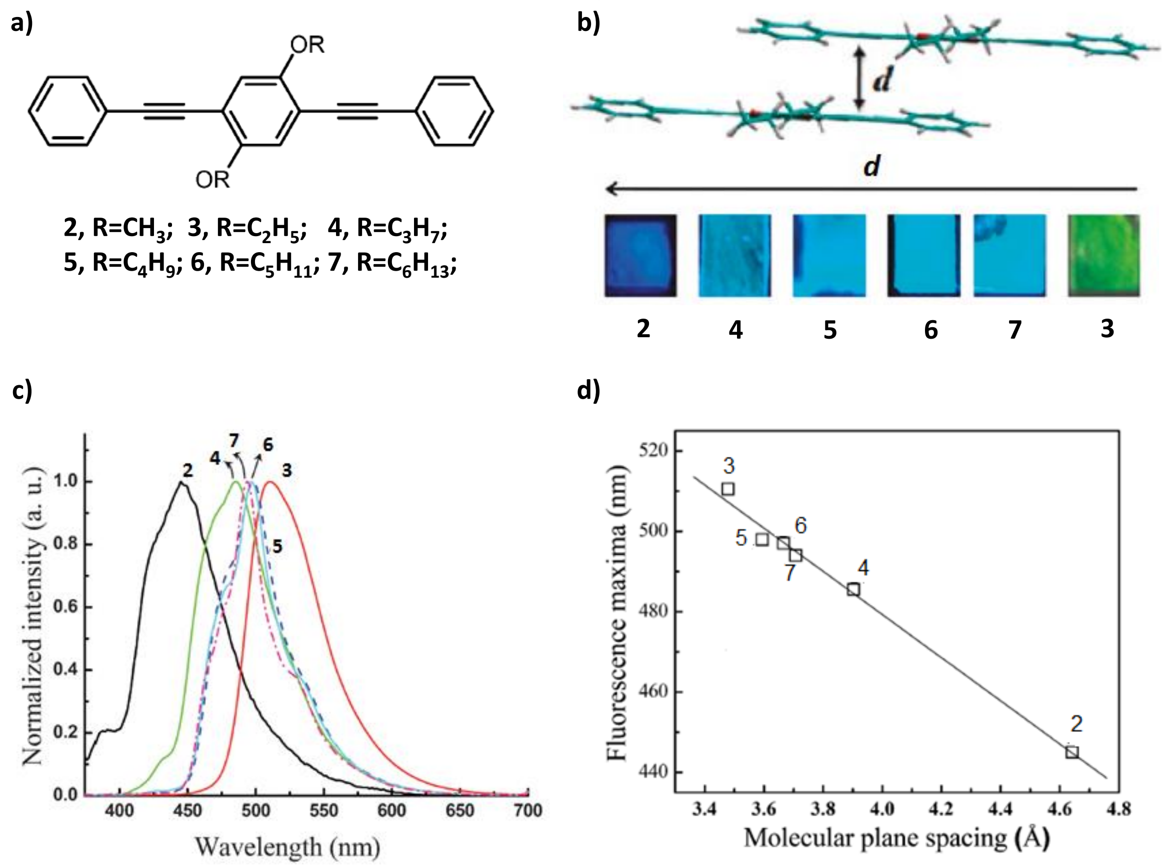

Figure 1.3. a) Molecular structures of PE derivatives **2**-**7**. b) Slip-stacked packing of molecules and the photographs of thin films of the molecules under 365 nm UV light, c) emission spectra and d) plot of intermolecular distance versus emission maximum of the molecules (**2**-**7**). (Adapted with permission from ref. 5a. Copyright 2009 The Royal Society of Chemistry.)

The inter-planar distance (*d*) between the molecular pairs forming the *J*-aggregates is varied between 3.48 to 4.65 Å. Furthermore, linear correlation was observed between the solid-state emission maxima and the spacing between the interacting OPE molecules (Figure 1.3d). As depicted in the figure when the *d* spacing increases, the emission maxima gradually shifted to lower wavelength. This behavior indicates that the solid-state emissions of **2-7** (Figure 1.3c) are governed by the extent of dipolar coupling between the chromophoric units which increases linearly with decrease in interplanar distance.

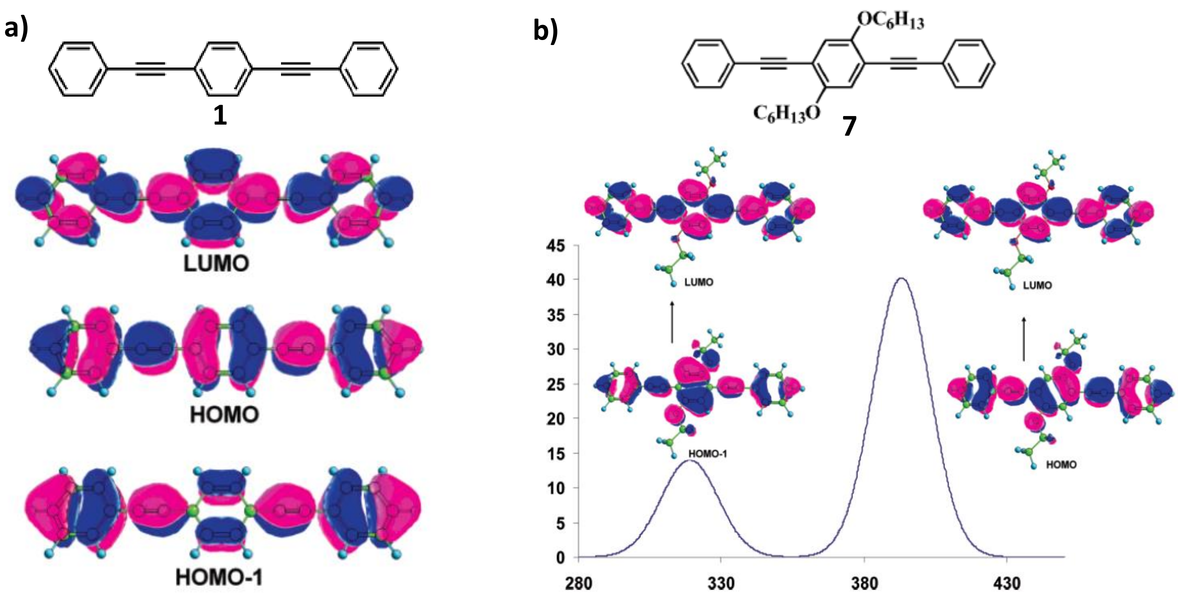

Figure 1.4. a) Molecular orbitals (MO) of compound **1**. b) Calculated absorption spectra of compound **7** and the peaks at 320 and 394 nm corresponding to MO transitions. (Adapted with permission from ref. 6. Copyright 2006 American Chemical Society.)

The variation in absorption property of alkyl chain substituted OPE **7** in comparison to unsubstituted OPE **1** was investigated using quantum chemical calculations (Figure 1.4).[6] The result showed a broad absorption feature for compound **1** due to the HOMO-LUMO transition, whereas substituted compound **7** possess two well-separated bands as shown in the Figure 1.4b. The reason for this behavior is the alkoxy substituent containing oxygen lone pairs that make resonance interaction with phenyl ring. This interaction alters the central arene π-orbitals of phenyleneethynylene, resulting in similar orbital features for HOMO and HOMO-1/HOMO-2. The electronic transition from the HOMO-1/HOMO-2 orbital to LUMO results in high-energy band at 320 nm. The red-shifted band at 394 nm is due to HOMO-LUMO transition.

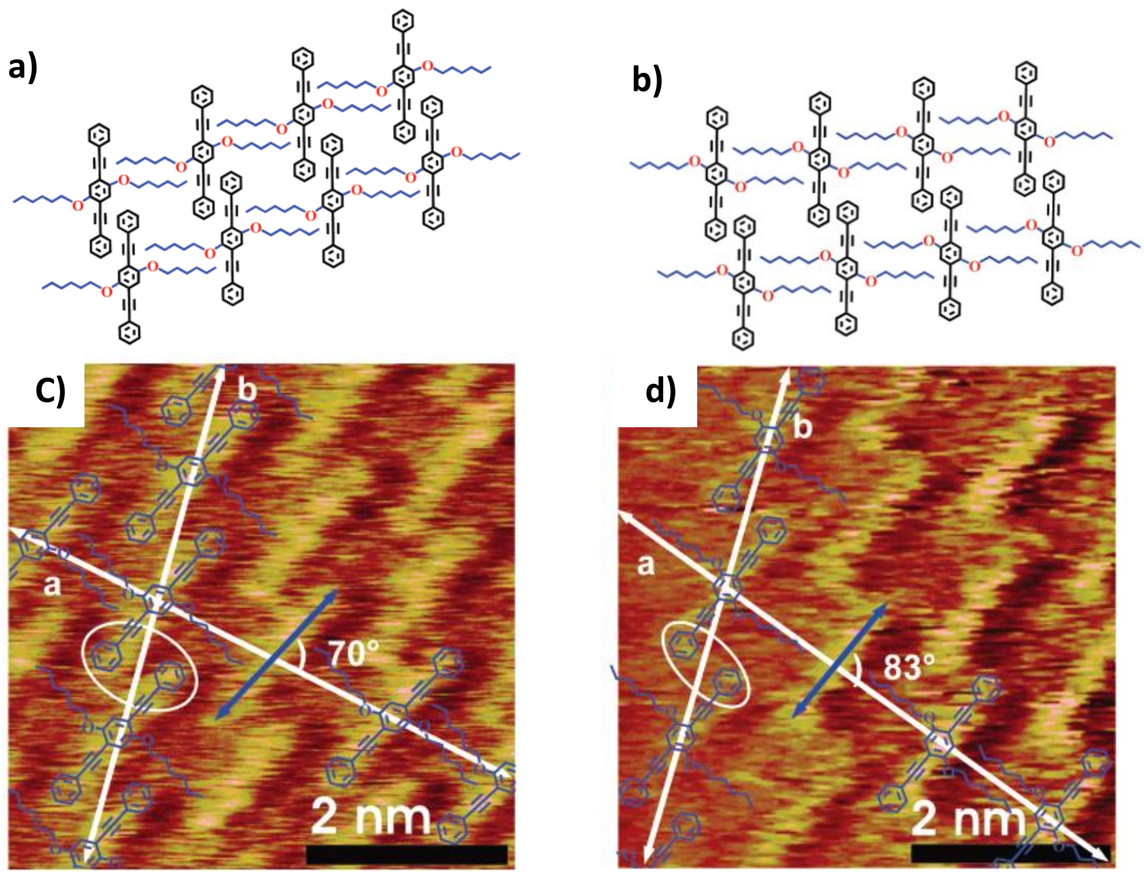

Figure 1.5. Schematic representation of interlocked 1D strips of molecular assemblies: a) type-I assembly, b) type-II assembly. STM images of **7** on HOPG showing: c) type-I assembly, d) type-II assembly. (Adapted with permission from ref. 7. Copyright 2007 American Chemical Society.)

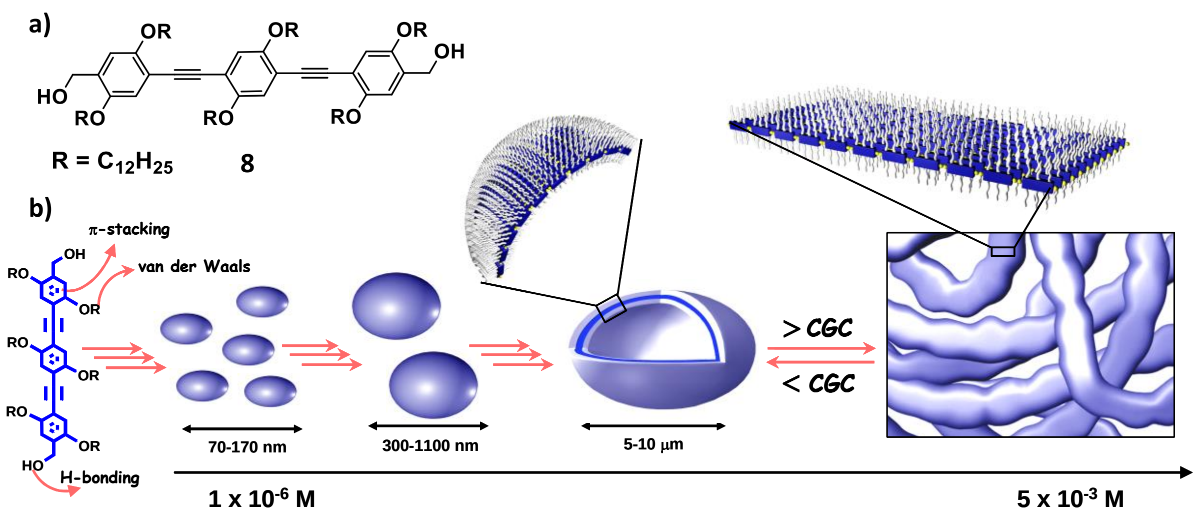

Figure 1.6. a) Molecular structure of compound **8**. b) Schematic representation of different stage self-assembly with varying concentrations. (Adapted with permission from ref. 8a. Copyright 2006 Wiley-VCH.)

Figure 1.5 depicts the self-organization of molecule **7** on a highly oriented pyrolytic graphite (HOPG) surface at ambient conditions, leading to various modes of intermolecular interactions.[7] In molecule **7**, the two terminal phenyl groups are connected to a central phenyl ring via acetylene linker which can self-organize in a skewed one-dimensional (1D) fashion. Detailed scanning tunneling microscopy (STM) studies revealed the existence of two types of molecular packing namely type-I and type-II, arising from different modes of CH···π interaction which was also supported by theoretical calculations (Figure 1.5c and 1.5d). The significant difference between the two assemblies is the extent to which molecule overlap with the other strips. In type-I assembly (Figure 1.5a), the aromatic moiety of one strip is inserted up to the acetylenic region of the other strip. However, in the case of type-II assembly (Figure 1.5b), the aromatic moiety of one strip is slightly inserted into the other strip.

The self-assembly and morphological features of OPEs were well studied by our group.[8,9] For example, compound **8** self-assembles in *n*-decane, resulting in the formation of nanovesicles, microspheres, superstructures and eventually to blue-emitting organogels (Figure 1.6).[8a] The morphology of these structures was confirmed by atomic force microscopy (AFM), scanning electron microscopy (SEM), transmission electron microscopy (TEM), dynamic light scattering (DLS) and optical microscopy analyses. At a concentration of 1×10^{-6} M, vesicles with an average size of 94 nm were formed, whereas at a concentration of 1×10^{-4} M, microspheres of 5-10 μm with strong blue fluorescence were obtained. However, at higher concentrations elongated giant structures of micrometer size were formed as evident from the SEM analysis. The absorption spectrum of **8** in *n*-decane showed a red-shifted shoulder at 419 nm corresponding to the initially formed kinetically controlled aggregates, which undergo a time-dependent transformation to more stable thermodynamically favored spherical aggregates. This work provides a very simple method for fabricating different morphological structures from the same solvent.

The effect of π-repeat units on the gelation and morphological behavior of three different OPEs was reported recently.[8b] All OPEs form fluorescent gels in non-polar solvents at low critical gel concentrations. The molecules **8**, **9** and **10** show blue, green and greenish yellow fluorescence color, respectively in gel state. The molecule-molecule and molecule-substrate interactions in these OPEs are strongly influenced by the conjugation length of the molecules. As the conjugation length increases, the stability of the aggregates and the gels also increase.

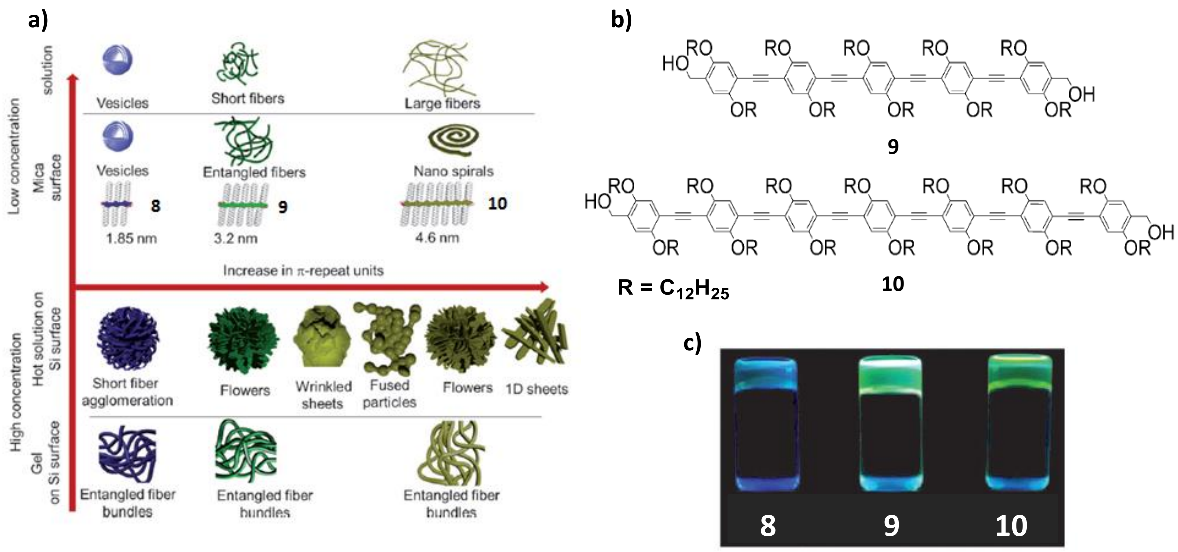

Figure 1.7. a) Schematic representation of the polymorphic structures of OPEs created by controlling the molecular interactions. b) Molecular structures of compound **9** and **10**. c) Photographs of *n*-decane gels under UV light. (Adapted with permission from ref. 8b Copyright 2012 Wiley-VCH.)

In general, silicon wafer suppresses substrate-molecule interactions, whereas mica surface facilitate such interactions. At lower concentrations in *n*-decane, **8** forms vesicular assemblies, molecule **9** forms entangled fibers whereas molecule **10** resulted in spiral assemblies on a mica surface (Figure 1.7). In a stark contrast, at higher concentrations, (in *n*-decane) **8** and **9** resulted super-bundles of fibers and flower like short-fiber agglomerates. The number of polymorphic structures increases on increasing the conjugation length, as seen in the case of molecule **10**. It shows a variety of exotic structures, the formation of which could be controlled by varying the substrate, concentration and humidity.

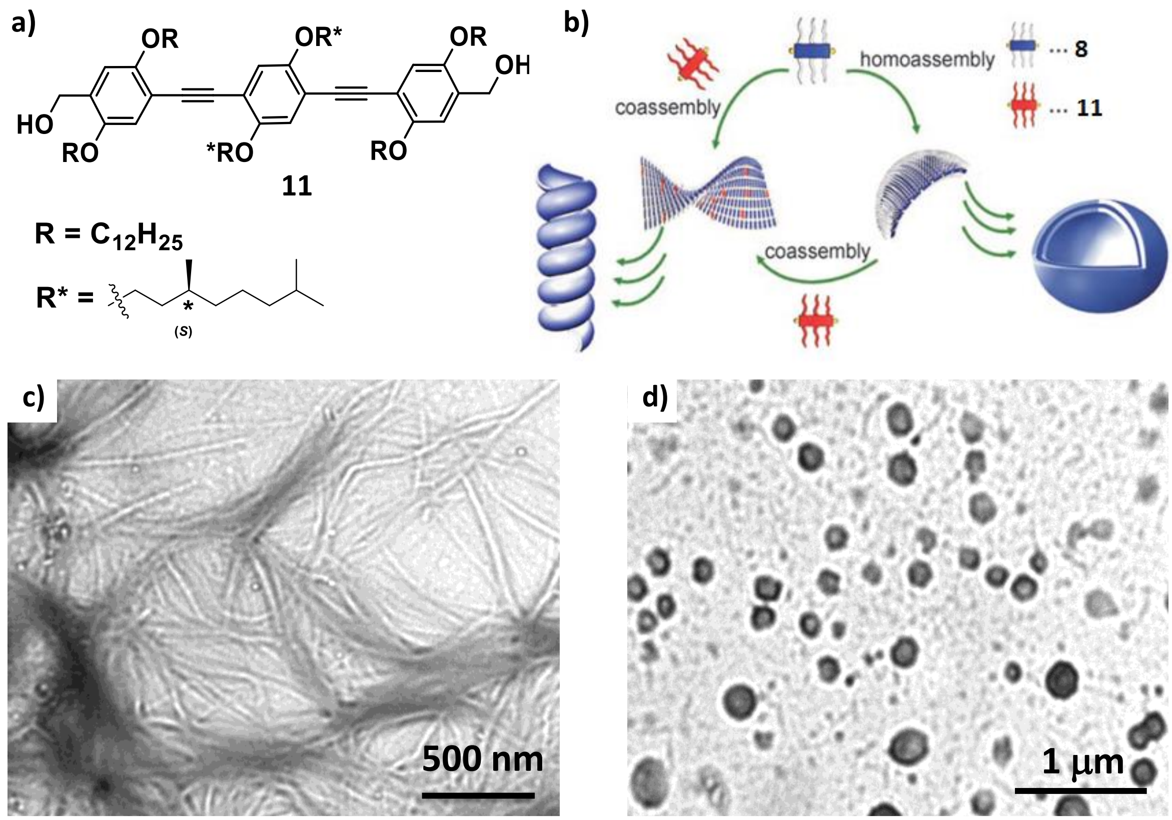

Figure 1.8. a) Molecular structure of compound **11**. b) Schematic representation of self-assembly processes to vesicles and subsequent transformation into helical tubes. c) TEM images of **8** with 25 mol% of **11** from *n*-decane (c = 1 × 10^{-5} M) at ambient conditions. d) TEM images of **8** from *n*-decane (c = 1 × 10^{-6} M) at ambient conditions. (Adapted with permission from ref. 9. Copyright 2006 Wiley-VCH.)

In another report from our group, the chirality-amplification and the morphological transition from vesicles to helical tubules during the co-assembly of chiral OPE **11** with its achiral analogue **8** have been demonstrated.[9] The molecules **8** and **11** in *n*-decane are silent to the circular dichroism (CD) effect, whereas the mixing of **8** with **11** (up to 30 mol %) resulted an induced CD effect in the co-assembled product that exhibited helical tubules-like morphology. AFM and TEM analyses of the drop cast samples of **8**, **11** and the co-assembled product showed vesicular morphology for **8**, nonspecific morphology for **11** and helical tubular morphology for the co-assembly respectively. Compound **8** when co-assembled with the chiral analogue **11**, the vesicular formation of **8** is hindered with the evolution of helical tubular structures. Simple mixing and sonication of **8** with **11** showed only weak CD signal and an irregular morphology, but the same mixture upon heating and cooling resulted in the complete transformation of the vesicles to helical tubular assemblies with strong exciton coupled CD signal (Figure 1.8).

1.3. Stimuli Responsive *p*-Phenyleneethynylenes

Kulkarni and co-workers have investigated the tunable fluorescence behavior of the OPE **2** by controlling the cooling rate from melt.[10] The films obtained after cooling exhibited a decrease in the emission intensity at 397 nm (peak 'C') when the cooling rate from the melt was increased from 2-13 °C min^{-1} (Figure 1.9b). This emission behavior was dependent on the thermal diffusivity of the surrounding medium; for instance, if the thermal diffusivity is higher, the emission of **2** showed a red shift of wavelengths.

Thomas and co-workers have demonstrated the mechano responsive fluorescence behavior of the OPE derivative **12**, which showed noncovalent interactions between aromatic rings on the side chains and main chains (Figure 1.10a).[11,12] In this compound, the perfluorobenzyl ester side chains interact co-facially with aromatic rings of the phenyleneethynylene unit resulting in a twisted central aryl ring. A film of **12** from dichloromethane solution exhibited piezochromic behavior. The absorbance and emission spectra of **12** in the film state are red shifted when compared to the solution state spectra. The film showed green emission with a maximum at 483 nm initially and when the film was heated to 110 °C for 15 min the emission maximum displayed 45-50 nm blue shifts (Figure 1.10). After grinding the film with a metal spatula the green emission was recovered and the subsequent reheating of the same film reverts back the blue emission.

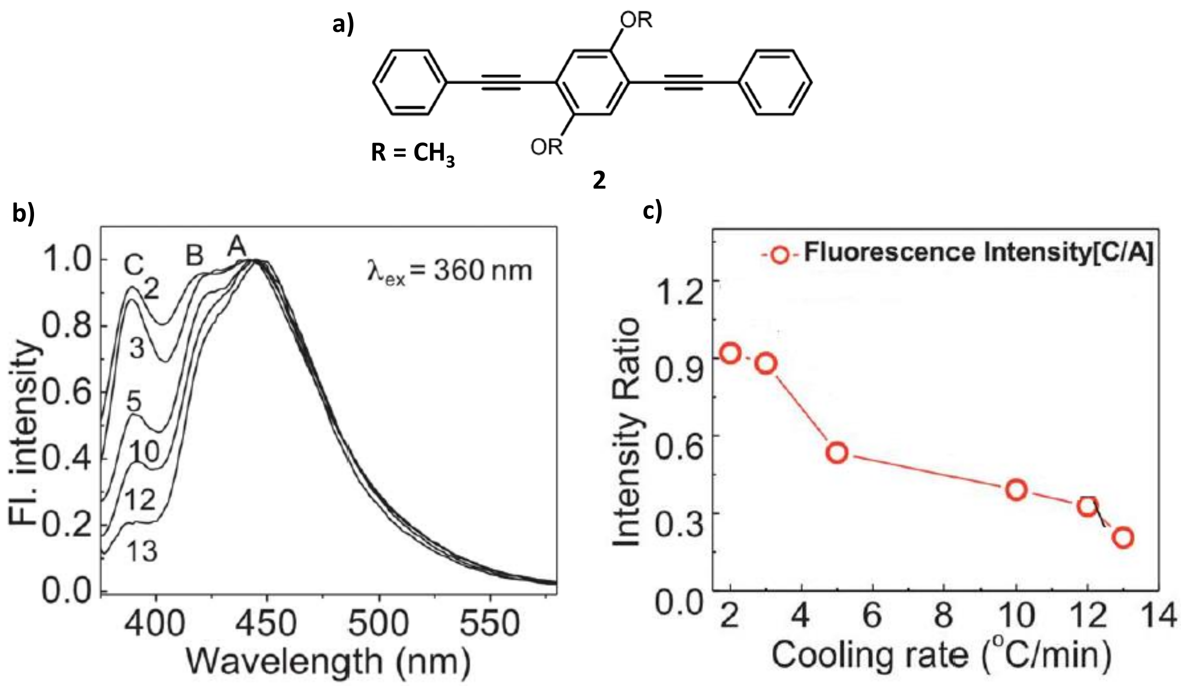

Figure 1.9. a) Molecular structure of compound **2**. b) Emission spectra of films formed from the melt at different cooling rates, 2-13 °C min^{-1}. Three different peaks in the emission spectra are labeled as A (444 nm), B (425 nm) and C (397 nm). The emission spectra are normalized with respect to peak A. c) Plot of intensity variation of peak C in the emission spectra with the cooling rate. (Adapted with permission from ref. 10. Copyright 2012 The Royal Society of Chemistry.)

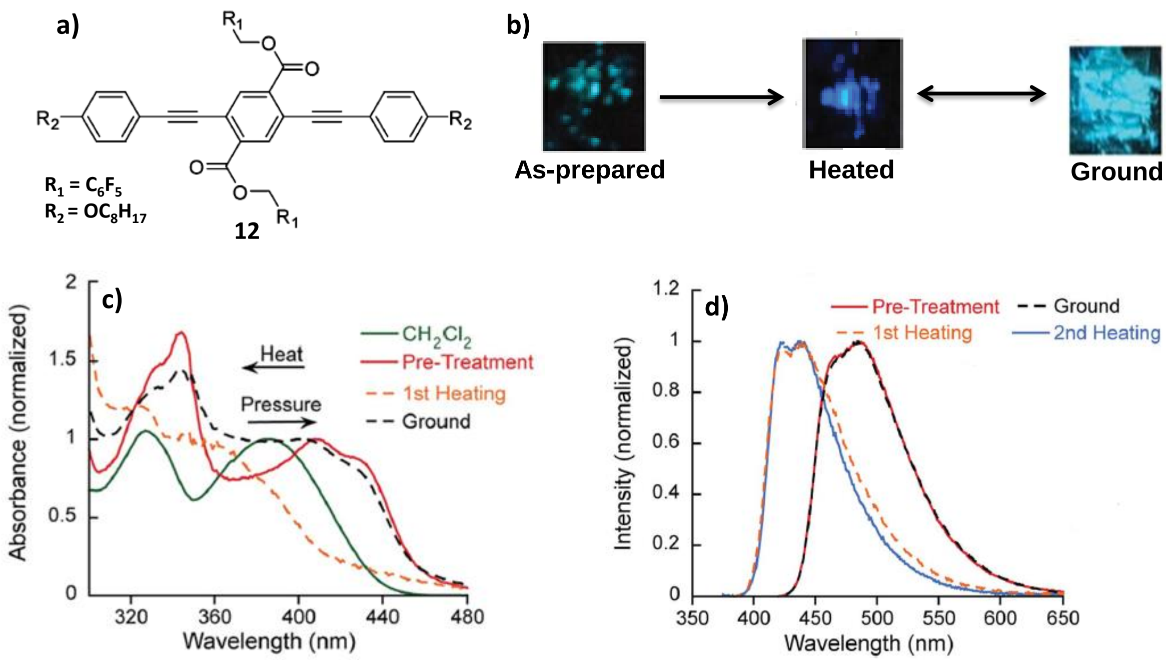

Figure 1.10. a) Molecular structure of compound **12**. b) Photographs of drop cast samples from dichloromethane with heating and grinding cycles under UV light. c) and d) Absorption and emission spectra of **12**, respectively. (Adapted with permission from ref. 11. Copyright 2014 The Royal Society of Chemistry.)

1.4. Water Responsive Fluorescent Molecular Assemblies

Recently, Kim and co-workers have reported water induced reversible switching of phosphorescence to fluorescence for a composite material of **13** and poly(vinyl alcohol) (PVA, Figure 1.11 a,b) .[13] The intermolecular halogen bonding interactions between the molecules **13** and hydrogen bonding interactions between **13** and the PVA matrix efficiently suppress the vibrational dissipation of excited state energy and produces bright room-temperature phosphorescence with quantum yields up to 24% (Figure 1.11). Unlike other room temperature phosphors,[14] the observed phosphorescence is originated from molecular assemblies and not from an isolated species. The designed organic phosphor **13** contains bromine and aldehyde groups for providing halogen bonding interactions in the assembly as well as for the generation of triplet-exciton. In addition, the carboxylic acid side chains present in the molecule enable strong hydrogen-bonds between the phosphor and the PVA matrix. The spin-orbit coupling is enhanced by intermolecular halogen bonding in molecular assemblies. Water is used as an external stimulus to break the molecular assembly, which leads to the decrease in spin-orbit coupling, resulting in fluorescence rather than phosphorescence emission. The long lifetime of 4.7 ms of **13** in PVA matrix (Figure 1.11d) clearly confirmed that the emission at 530 nm is phosphorescence.

The intensity of phosphorescence emission of the **13-**PVA system was strongly dependent on the air humidity (Figure 1.11c). When the humidity of the surrounding is increased, the phosphorescence emission at 530 nm showed a decrease in intensity, whereas the fluorescence emission peak at 437 nm remained unchanged. When humidity is high, more water was absorbed by the **13-**PVA system which leads to the breaking of the hydrogen bonding interactions between the PVA molecules, and between **13** and PVA matrix. Consequently, the motion of PVA molecules and the vibrational motion of **13** are enhanced, resulting in the decrease of phosphorescence quantum efficiency.

Tohnai and co-workers have reported the fluorescence modulation of an organic salt **14** by water inclusion in its crystalline state. [15] The organic salt **14** is composed of 9,10-*bis*(4-aminophenyl)anthracene and hypophosphorous acid (Figure 1.12a) which emits yellow-green fluorescence in the crystalline state and after water inclusion the crystal produced blue-green fluorescence. The external application of moisture for 2 h induced a fluorescence color change (Figure 1.12b). The water molecules induced fluorescence change arises from re-organization of anthracene moiety and is proven by single crystal X-ray studies.

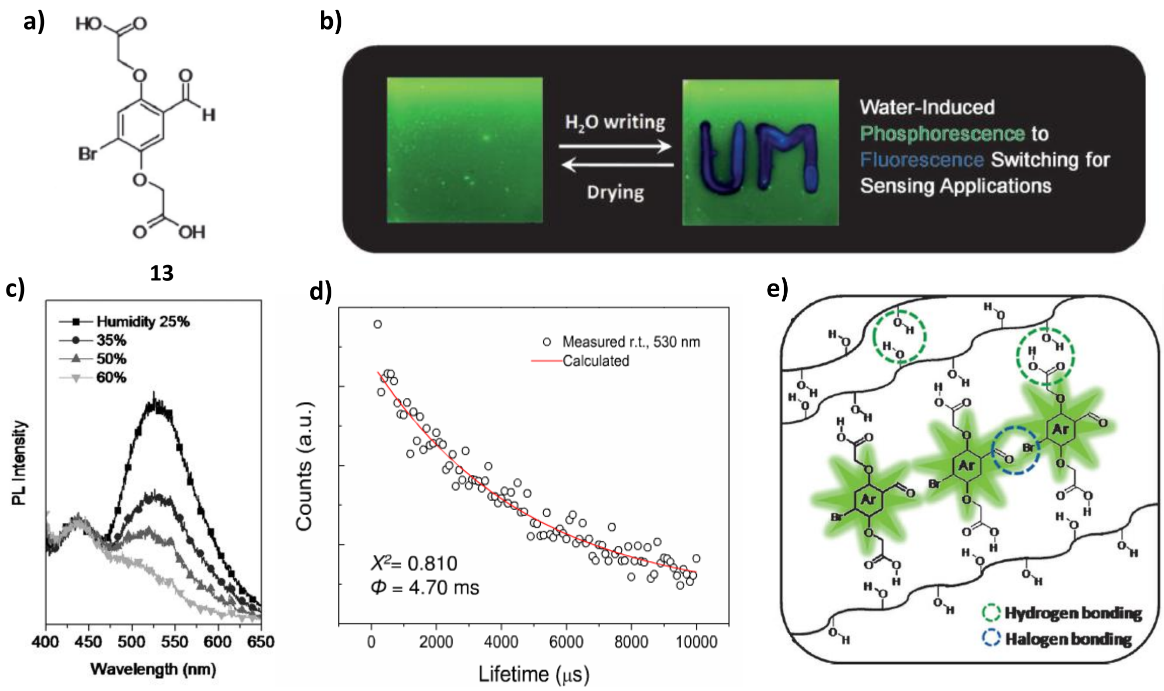

Figure 1.12. a) Chemical structure of **13**. b) Photographs of fluorescent water-mark written using water soaked pen over the PVA film embedded with molecule **13,** under UV light. c) Fluorescence spectra of 1 wt% of **13**-PVA film with different humidities. d) Emission decay profile of **13**-PVA film monitored at 530 nm. e) Schematic representation of Halogen- and Hydrogen-bonding in the **13**-PVA composite. (Adapted with permission from ref. 15. Copyright 2014 Wiley-VCH.)

Two different crystals were obtained based on the nature of the solvent and condition used for the crystallization. Crystal **1** was obtained by slow evaporation of anhydrous methanol solution in a desiccator at room temperature. On the other hand, crystal **2** was obtained by slow evaporation of the methanol/water solution under ambient conditions. The crystal of **1** emits yellow-green fluorescence while the crystal of **2** showed blue-green fluorescence (Figure 1.12c). In the crystal of **1**, hypophosphate ions formed hydrogen bonds with the amino groups of 9,10-*bis*(4-aminophenyl)anthracene, which led to a face-to-face slipped column geometry of the anthracene moieties, whereas in the crystal **2** the hydrogen bonds between 9,10-*bis*(4-aminophenyl)anthracene and hypophosphate ions were effectively prevented by the incorporated water molecules resulting in the weakening of π-π interaction of anthracene moieties (Figure 1.12d). This work provides a new strategy for better solid-state optical materials and sensing system capable of memorizing chemical stimuli such as wetting.

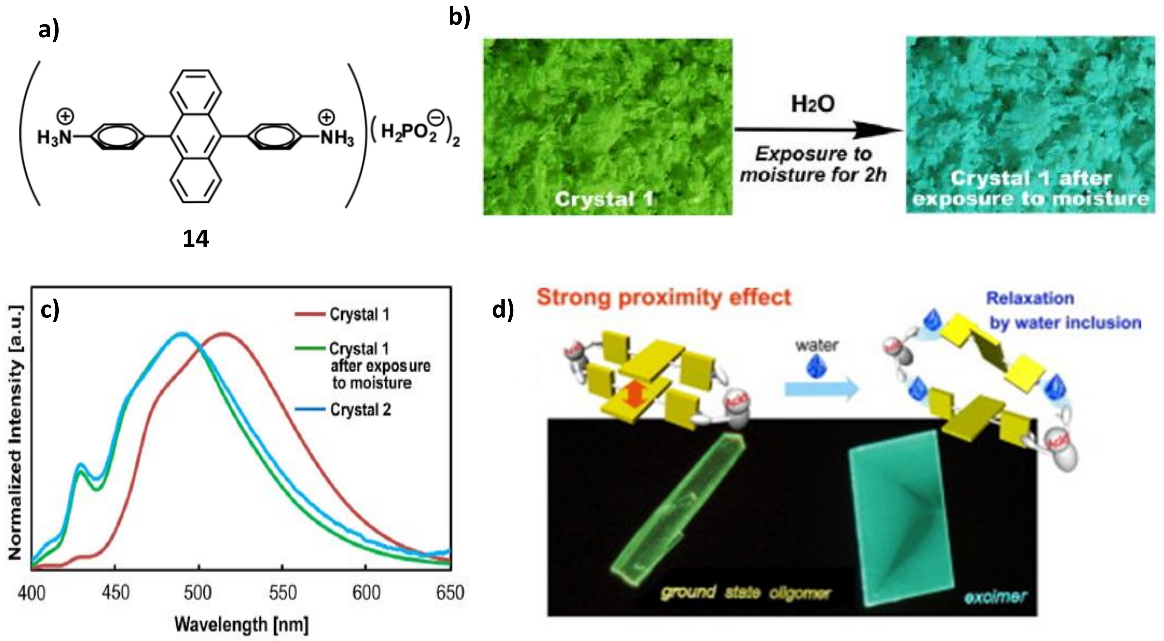

Figure 1.12. a) Chemical structure of **14**. b) Photographs of crystals under UV light before and after exposing to moisture. c) Fluorescence spectra of crystals. d) Schematic representation of water triggered modulation of fluorescence emission. (Adapted with permission from ref. 15. Copyright 2014 Elsevier.)

Qu and Shen have introduced a new type of smart carbon nanodots (CDs) for which luminescence properties can be modulated by controlling their self-assembly behavior using water as external stimulus.[16] Authors expanded the scope of CDs to smart supra-CD (Figure 1.13a) by partially functionalizing the surface of raw carbon nanodots[17] (CD-R) with alkyl chains to get partially functionalized carbon nanodots (CD-Ps). The functionalized CD-Ps can self-assemble to form supra-CDs in toluene. These smart supra-CDs exhibited water-induced enhancement of luminescence by disassembly of the supra-CDs (Figure 1.13b). In toluene, the functionalized carbon nanodots (CD-Ps) self-assemble to supra-CDs through amphiphilic interactions. The supra-CDs have very weak luminescence in toluene due to aggregation caused quenching of luminescence (Figure 1.13c). This was clear from the strong green luminescence CD-Ps dispersed well in dimethyl sulfoxide (DMSO). Drop casting of the toluene solution containing supra-CDs on a paper substrate also showed weak luminescence, indicating that supra-CDs are stable even after coating (Figure 1.13d). When water was sprayed, the luminescence of the supra-CD drop-cast paper enhanced to a quantum yield of 40% from the initial quantum yield of < 1%. The coated paper retained its enhanced luminescence even after drying, indicating an irreversible process.

The fluorescence decay profiles (Figure 1.13e) of the supra-CDs coated paper after water-spraying treatment is nearly the same as that of CD-Ps in DMSO solution, indicating that the enhanced luminescence is due to the disintegration of supra-CDs.

The water induced luminescent character of 'C' over the supra-CD coated paper exhibits superior photostability when compared to that of commercially available highlighter pen (Figure 1.14). The luminescent character written using commercial pen was quickly erased and disappeared after 1.5 h of UV irradiation. In contrast, the water-induced luminescent character written using supra-CDs in toluene can be clearly observed even after 1.5 h of UV irradiation. It is important to mention that such modulation of optical properties of CDs through self-assembly process is particularly interesting for exploring novel carbon-based nanomaterials for smart applications.

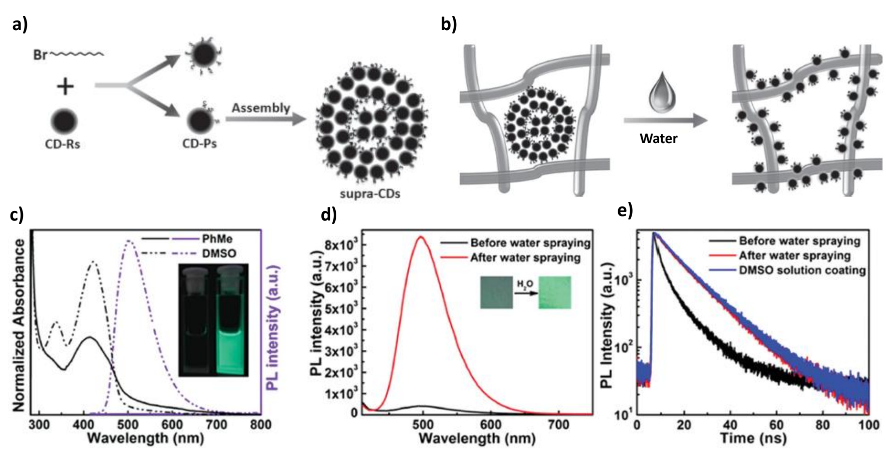

Figure 1.13. a) Schematic representation for preparation of supra-CDs from CD-Ps. b) Schematic representation for the mechanism of the water-induced enhancement of emission. c) Absorption (black line) and emission spectra (violet line) of supra-CDs in toluene and CD-Ps in DMSO. Inset: Photographs of supra-CDs in toluene (left) and CD-Ps in DMSO (right) under UV light. d) Water-induced changes in the emission spectra of supra-CDs in toluene coated over the paper. Inset: Photographs showing water-induced enhancement of green emission. e) Fluorescence decay profiles of paper coated with supra-CD in toluene before and after with spraying water and decay profiles of supra-CD coated paper made from DMSO solution. (Adapted with permission from ref. 16. Copyright 2015 Wiley-VCH.)

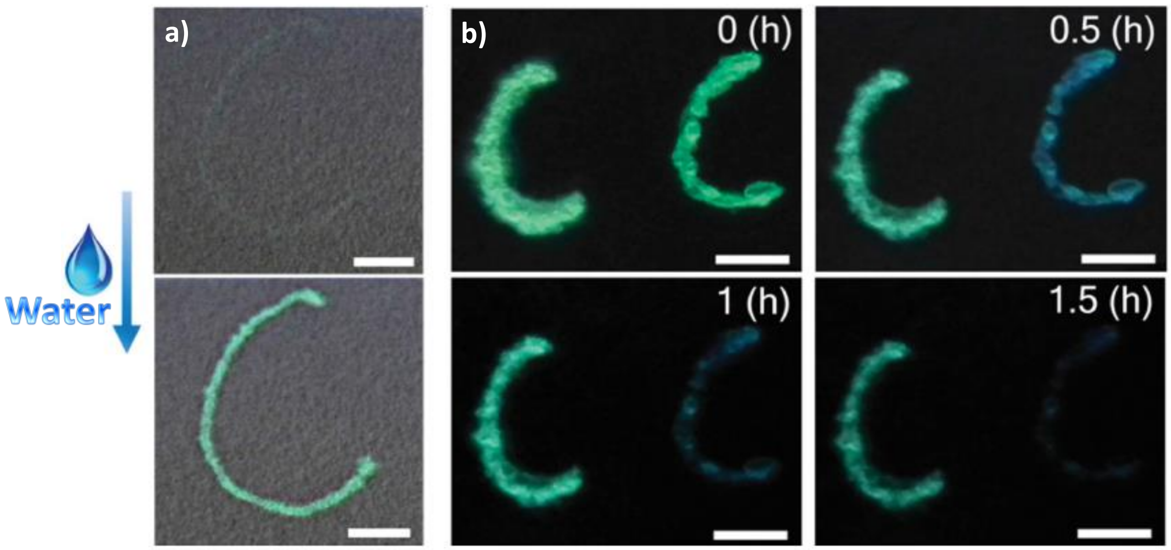

Figure 1.14. a) Photographs of handwritten image over the paper using a pen filled with a toluene solution of supra-CDs before and after spraying water under the UV light (scale bar = 5 mm). b) Photographs showing the photostability of image written using supra-CDs in toluene solution (left) and commercially available highlighter pen (right) with time under UV light (scale bar = 1 mm). (Adapted with permission from ref. 16. Copyright 2015 Wiley-VCH.)

Weder and co-workers have reported a new material that displayed an irreversible fluorescence color change upon exposure to moisture which could be used for sensory application to track humidity content in the environment (Figure 1.15).[18] This new material was prepared by incorporating the molecule **15** into hygroscopic polyamide matrix by melt-mixing process. The color change of polyamide blend film of **15** upon exposure to water can be readily detected by both UV and ambient lights (Figure 1.15b-e). The polyamide matrix gets plasticized in presence of water and trigger the self-assembly of sensor molecules. The Fluorescence spectra of polyamide blend film of **15** showed that the intensity of monomer band at 541 nm decreases with increase in intensity of excimer band at 644 nm as a function of moisture exposure time (Figure 1.15f). The isosbestic point at 610 nm indicated the presence of two components such as monomers and excimers and also confirms that the fluorescence color change is due to aggregation of the molecules. Figure 1.15g shows the ratios of monomer to excimer emission intensity as a function of time.

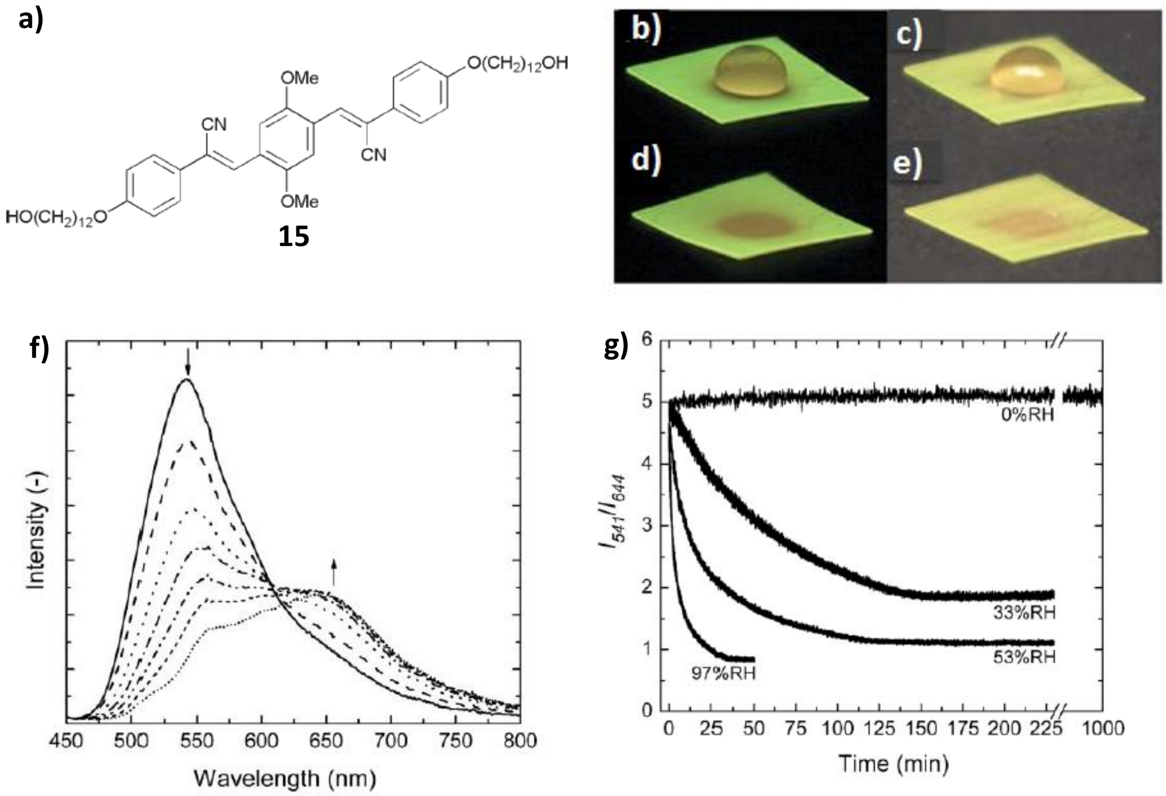

Figure 1.15. a) Chemical structure of **15**. Photographs of polyamide blend film of **15** exposed to water droplet taken upon illumination under b) UV light and c) ambient light. Photographs of same sample after removal of water under illumination with d) UV light and e) ambient light. f) Fluorescence spectra of polyamide blend film of **15** at 97% relative humidity with varying time. g) Plot of ratio of monomer/excimer intensity (I_{541}/I_{644}) versus time for the same material at different relative humidity. (Adapted with permission from ref. 18. Copyright 2007 The Royal Society of Chemistry.)

1.5. Thermoresponsive Fluorescent Molecular Assemblies

Molecular assemblies that exhibit thermoresponsive fluorescence color switching between two phases have potential use in thermo-sensory applications. Wang and co-workers have reported the trifluoromethyl substituted aromatic amine compounds **16** and **17** showing reversible thermally induced phase transformations with varying emission colors (Figure 1.16).[19] In these compounds, the phenyl rings can rotate freely between the nitrogen atoms that results in a different molecular conformation that leads to a change in optoelectronic properties. Besides, the presence of strong electron withdrawing CF_3 group can also affect the aggregation and luminescence properties of the molecules.

a)

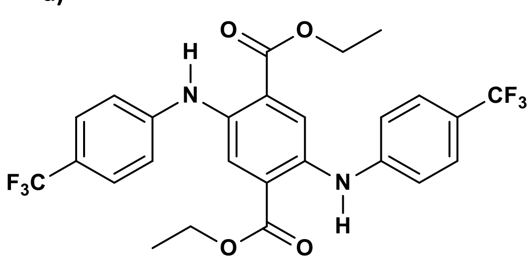

16

b)

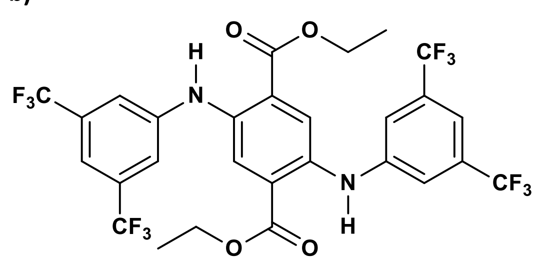

17

Figure 1.16. Chemical structures of trifluoromethyl substituted aromatic amine compounds **16** and **17**.

Compound **16** after recrystallization from chloroform solution showed a weak red emission. When it is heated to melt and rapidly cooled down to room temperature, a yellow solid with intense yellow emission was formed. On the contrary, if the cooling rate is slowed down to 0.5 K min^{-1}, the cooled material exhibited the emissive property that is same as that of the pristine compound **16**. The compound **17** also showed thermally induced reversible phase transformation along with emission switching from red to green. It was observed that the red solid of compound **16** changed to yellow solid by annealing at 150 °C for 3 min before melting (Figure 1.17a) and the compound **17** also showed the same property when it is annealed at 130 °C for 3 min (Figure 1.17b). The presence of an exothermic peak in differential scanning calorimetry (DSC) analysis of compound **16** and **17** confirms the thermally induced phase transformation (Figure 1.17e). The relationship between solid-state emission and molecular packing of the compound in different phase was studied by single-crystal structures. From the crystallographic data, it was found that the emission switching involves the transformation of π-stacked *H*-aggregates to cross-stacked *J*-type. These types of molecules have potential applications in fabrication of display, sensing and memory devices.

Recently, Das and co-workers have reported a thermally induced polymorphism by a pyridine appended butadiene derivative **18** (Figure 1.18a).[20] The different polymorphs showed different fluorescence colors. The pristine solid exhibited blue fluorescence and after melt-cooling showed a yellow emission. The difference in fluorescence is due to the thermal phase transformation and concomitant change in molecular packing from herringbone to a brick-stone arrangement (Figure 1.18b). The emission spectrum of a thin film formed by slow cooling (2 °C/min) of the melt showed a structured band with blue emission centered at 480 nm (Figure 1.18c). In contrary, when the melt was rapidly cooled to room temperature, the film displayed a broad yellow emission with maxima at 573 nm.

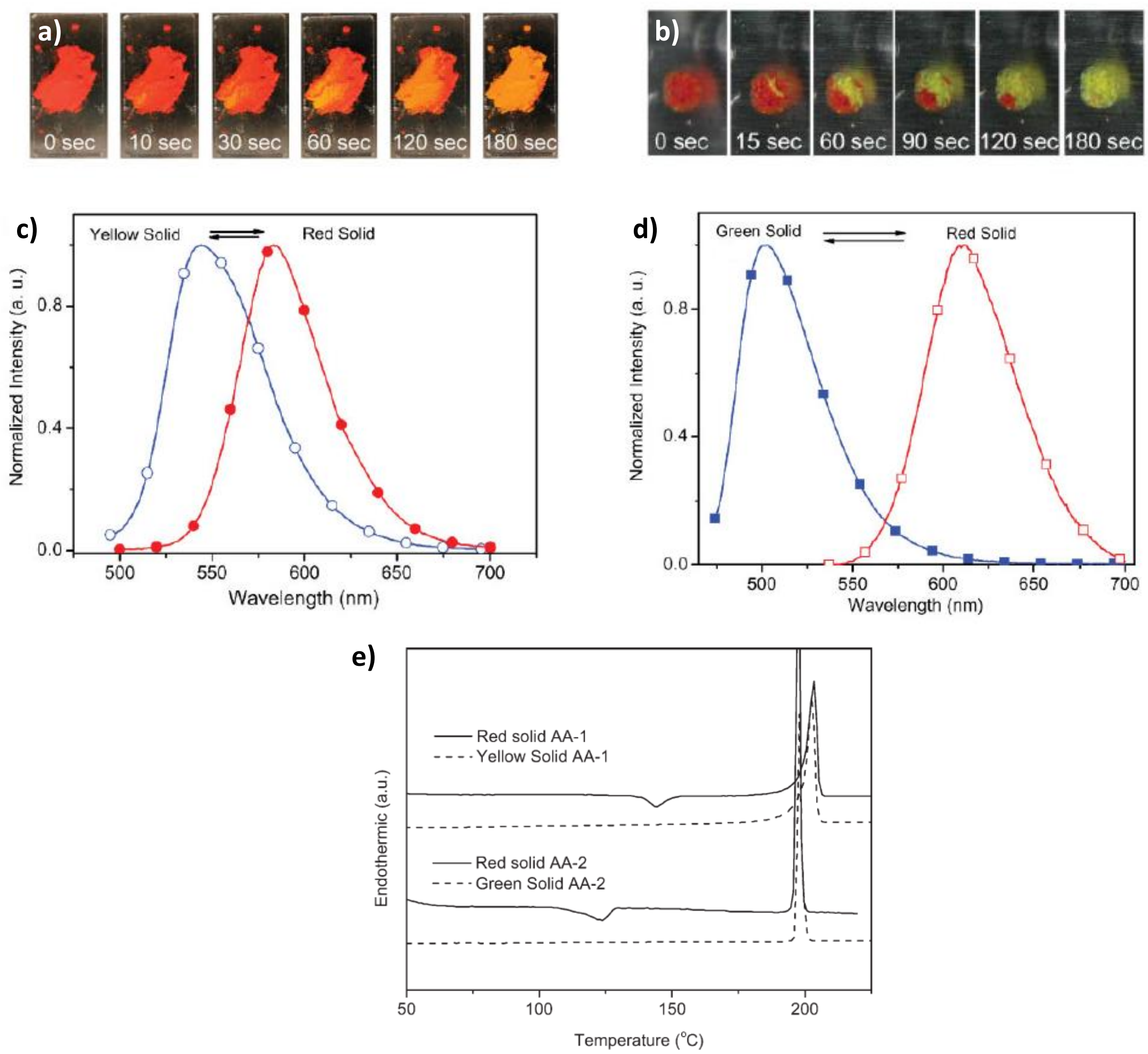

Figure 1.17. Photographs of solids taken under UV light with varying time a) red to yellow phase of **16** at 150 °C and b) red to green phase of **17** at 130 °C. c) and d) Emission spectra of solid samples. e) DSC curves of solids. (Adapted with permission from ref. 19a. Copyright 2009 Wiley-VCH.)

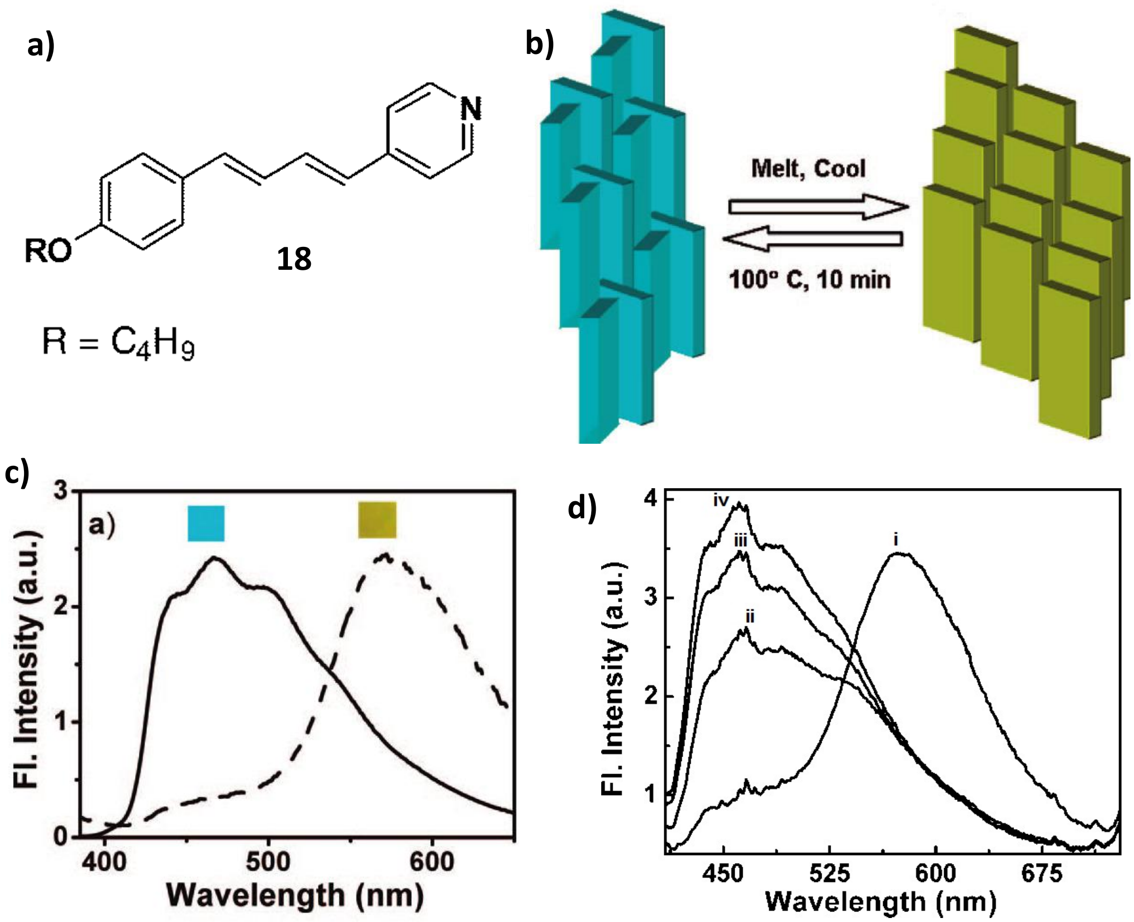

Figure 1.18. a) Chemical structure of **18**. b) Schematic representation of molecular arrangement in different phases. c) Emission spectra of **18** in film state formed by slow cooling (solid line) and rapid cooling (dashed line) from its melt. d) Emission spectra of rapidly cooled solid kept at 100 °C with varying time: i) 0 s, ii) 42 s, iii) 2 min and iv) 8 min. (Adapted with permission from ref. 20. Copyright 2009 American Chemical Society.)

From this observation, it can be interpreted that the slow cooling leads to a thermodynamically stable blue polymorph while rapid cooling leads to a kinetically trapped yellow polymorph. The polymorph exhibiting yellow fluorescence was fairly stable (>6 months) but could be converted back to the original form by keeping the film at 100 °C for a short period of time (~8–10 min) before slowly cooling to room temperature (Figure 1.18d).

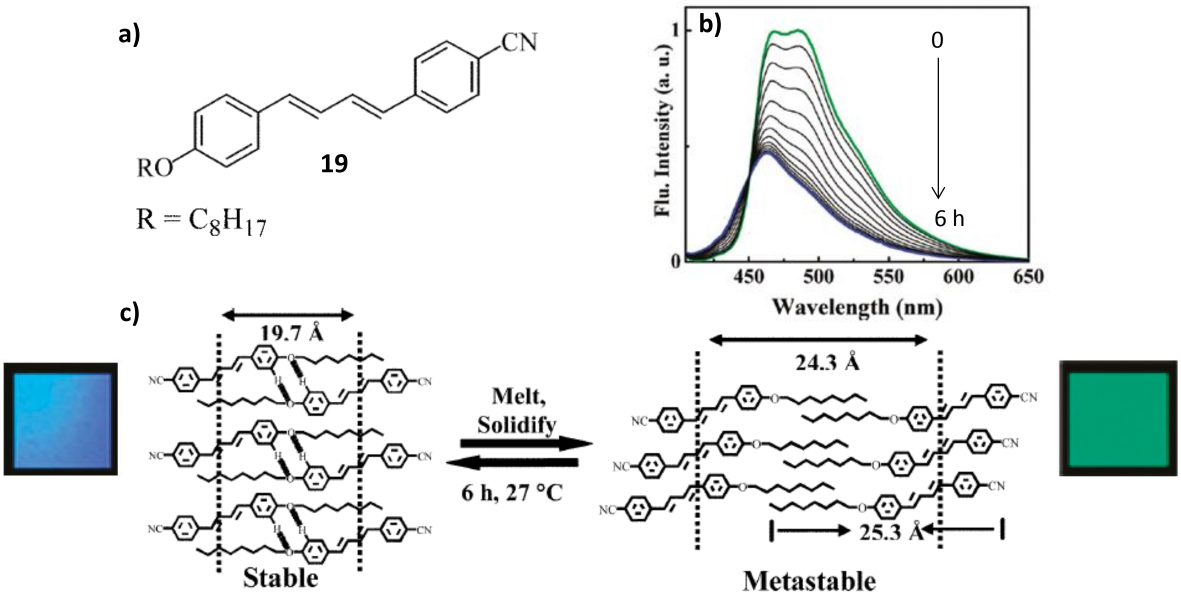

Figure 1.19. a) Chemical structure of **19**. b) Changes in emission spectra of **19** from metastable to stable state with time. c) Schematic representation of the molecular arrangement in two different states. Inset: photographs showing the solid-state fluorescence. (Adapted with permission from ref. 21a. Copyright 2004 The Royal Society of Chemistry.)

In blue phase, the π-π interaction between the neighboring molecules is less, which leads to decrease in excitonic coupling between the molecules. But in the green phase, planarization and rigidification of the molecules produce a red shift and enhancement in fluorescence intensity. The thermally induced fluorescence change of this material can be repeated for several cycles, which support their suitability for thermal imaging application.

In another report, the same group demonstrated the thermally reversible fluorescence of octyloxy-cyano-substituted diphenylbutadiene **19** that switches between two polymorphic states (Figure 1.19).[21] The difference in the fluorescence of two polymorphic states can be due to the variations in their monomer–*J*-aggregate ratio, which in fact is controlled by the molecular packing. The two polymorphic states are interconvertible. While the polymorph with blue fluorescence is stable, the green fluorescent form is metastable and can be reverted to stable blue form by keeping at 27 °C for 6 h (Figure 1.19b). The differences in the fluorescence behavior of the two polymorphic forms of **19** are explained on the basis of the crystal structures. The single crystal X-ray analysis indicates an extended π-stacked structure with intermolecular C–H···O hydrogen-bonds between aromatic hydrogen and oxygen atoms of adjacent molecules (Figure 1.19c). When thermal stimulus was applied, the weak interactions break and allow rearrangement of the aromatic units close to each other like *J*-type aggregates that resulted in green fluorescence.

Tong *et al*. have shown that the molecule **20** exhibited aggregation induced emission (AIE)[23] and tunable solid-state fluorescence upon alternate annealing and melting thermal treatments (Figure 1.20).[22,23] The reason for the tunability of emission was due to the conformational flexibility of rotary phenyl rings and changes in the tightness of packing upon thermal treatments. The molecule **20** in its pristine state showed yellowish green emission with maximum centered at 541 nm, upon melting followed by cooling to room temperature; the emission was shifted to 522 nm. The green emission at 522 nm can be reverted back to the yellowish green emission by annealing at 231 °C. The tunable fluorescence behavior showed good reproducibility for a number of cycles (Figure 1.20d). The appearance of a small endothermic peak at 231 °C before melting point at 236 °C in DSC analysis supports the phase transition behavior. Single crystal X-ray analysis confirmed the two different polymorphic structures. The single crystals with two different emissions were obtained simultaneously by the slow evaporation of concentrated ethyl acetate solution of **20** (Figure 1.20c). According to X-ray crystallographic analysis, the two-salicylaldimine moieties in compound **20** were structurally similar, but they were asymmetric in the crystalline state. This asymmetry was created due to the different torsion angles between the phenyl ring and attached Schiff base ring in each molecule. This conformational difference was responsible for the molecular packing in two polymorphic structures.

In another report, Park and co-workers investigated a thermally induced fluorescence switching properties of cyano-distyryl benzene derivative **21** (Figure 1.21).[24] The molecule **21** forms highly fluorescent ‘molecular sheets’ with the help of C–H···N and C–H···O hydrogen bonding interactions. Photophysical and computational studies have revealed the presence of two different phases, in which the green emitting G-phase is metastable when compared to the blue emitting B-phase. Figure 1.21b shows the images of single crystals grown from ethyl acetate solution. In the pristine state, the crystals showed yellow color with green emission (G-phase). Heating these crystals to 125 °C for an hour resulted in the change of color from yellow to pale green with blue in emission (B-phase) and the appearance of the crystal also changed from transparent to opaque. The two distinctive crystal phases are promoted by different modes of local dipole coupling, which leads to alteration in π-π overlap.

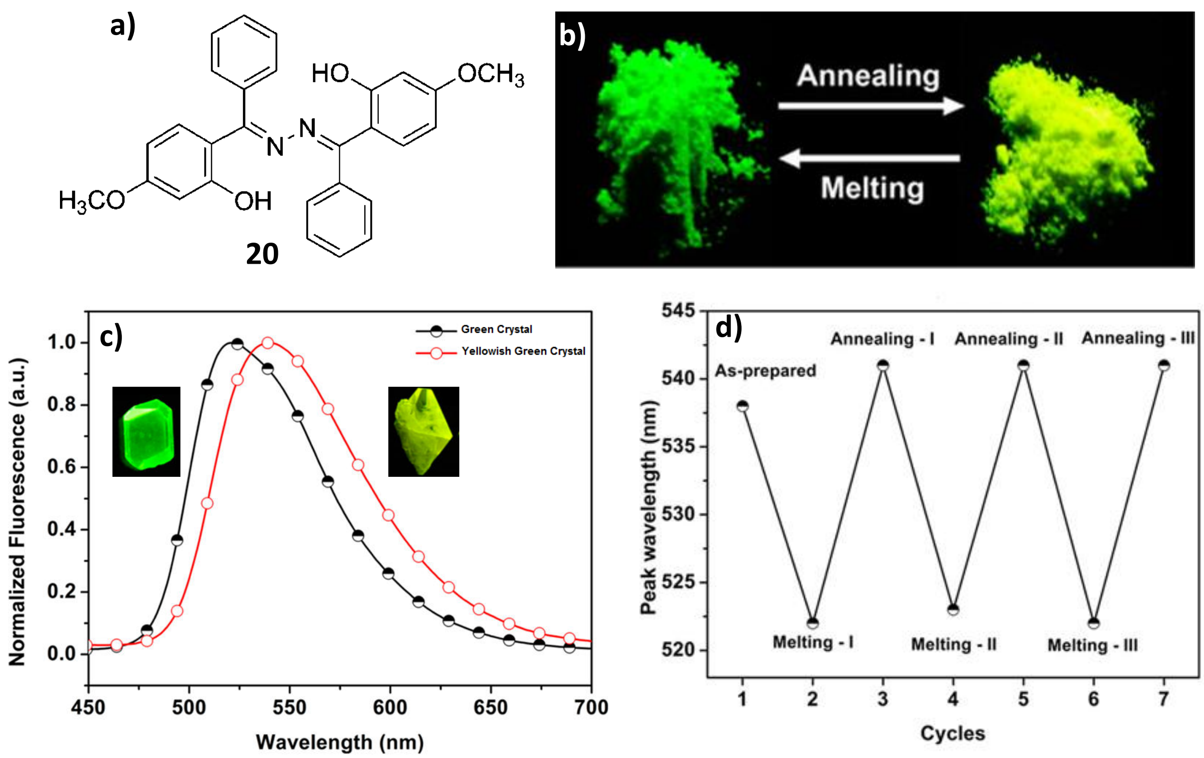

Figure 1.20. a) Chemical structure of **20**. b) Photographs taken under UV light showing reversible thermochromic phase transition in solid-state. c) Emission spectra of crystals. Inset: Photographs of crystals taken under UV light. d) The plot showing reversible fluorescence change upon thermal treatments. (Adapted with permission from ref. 22. Copyright 2013 American Chemical Society.)

These changes can be directly correlated with intermolecular excitonic and excimer coupling in both phases. The metastable G-phase was attributed to a kinetically trapped structure that was stabilized by antiparallel coupling of the local dipoles. This structure was observed to have a moderate excitonic coupling with the efficient excimer formation. Upon annealing, a smooth slip of the molecular sheets made the B-phase with a head to tail arrangement of the local dipoles. Here the excimer formation is diminished with substantial increase in excitonic coupling. The two different phases are also observed in thin films made on quartz substrates (Figure 1.21c). The phase formation selectively depends on the substrate temperature during deposition, where the B-phase formed at 100 °C and the G-phase at 25 °C substrate temperature.

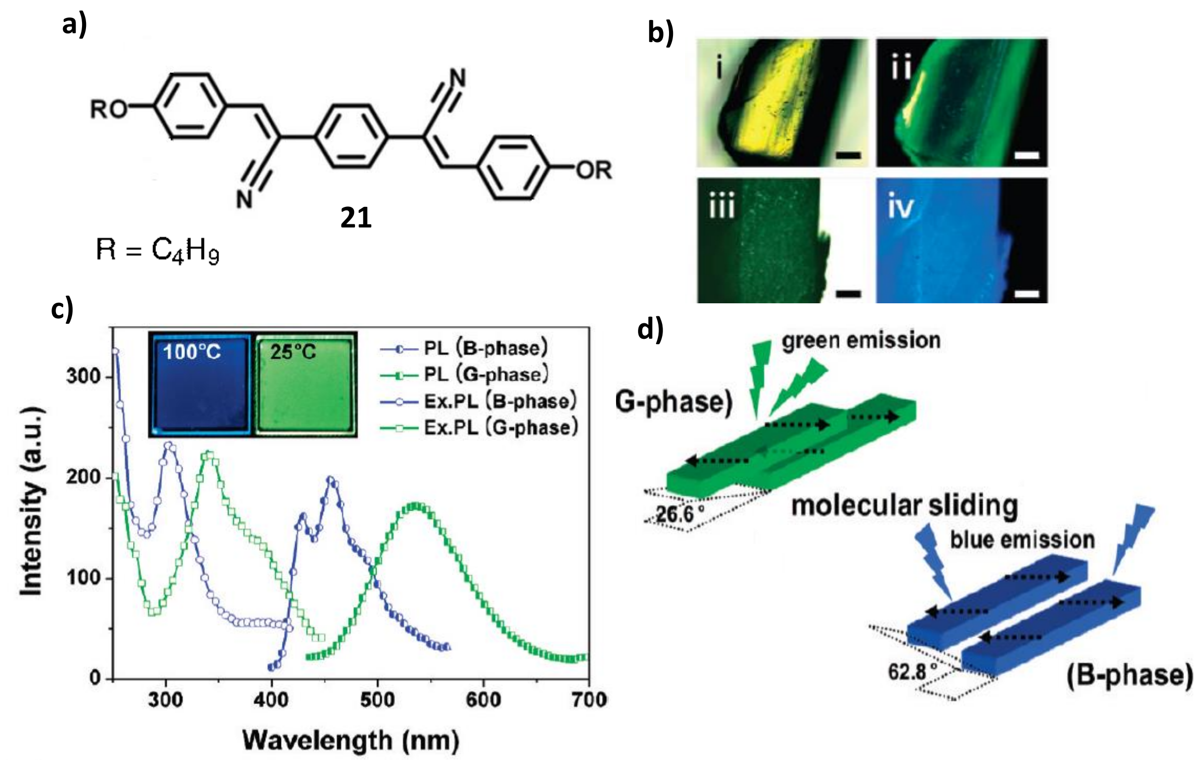

Figure 1.21. a) Chemical structure of **21**. b) Photographs of a single crystal: Before annealing under i) room light, ii) UV light and after annealing under iii) room light and iv) UV light (scale bar 0.2 mm). c) Excitation and emission spectra of thin films. Inset: Photographs of thin films taken under UV light with substrate temperature of 100 and 25 °C. d) Schematic representation of two different modes of slip-stacking arrangement. (Adapted with permission from ref. 24. Copyright 2010 American Chemical Society.)

1.6. Mechano Responsive Fluorescent Molecular Assemblies

Mechanochromism is a phenomenon of color change of solid materials caused by mechanical grinding, crushing or rubbing, whereas, mechanofluorochromism is the phenomenon in which materials change their fluorescence emission colors due to the formation of metastable form upon application of mechanical stimuli. It is generally a reversible process and can be reverted back to the original emissive material by heating or exposing to solvent vapor. The mechanofluorochromic behavior of these compounds are rooted to reversible switching between crystalline and amorphous states or stable and metastable liquid crystalline phases, or two different crystalline phases with changes in intermolecular interactions, such as π–π interaction, dipole-dipole interaction, and hydrogen bonding before and after the mechanical grinding of solids. These smart materials possessing mechano responsive behavior have potential application in fluorescence switches, mechanosensors, indicators for mechano-history, security papers, optoelectronic and data storage devices.[26]

The mechanofluorochromic behavior of the liquid crystalline molecule **22** was investigated by the research group of Kato (Figure 1.22).[27] When the shear mechanical pressure was applied to liquid crystalline material, the yellow emission of the metastable cubic phase changed to a stable columnar phase with blue-green emission. Annealing the stable columnar sample leads to the initial metastable cubic phase again. These self-assembled structures are driven by hydrogen bonding and π-π interactions. In the cubic phase molecules are arranged like disordered stacks in the segmented columns (Figure 1.22d), which on mechanical shearing converted to non-segmented columns (columnar phase) having more linear hydrogen-bonded structure. A thin film obtained by casting *n*-hexane solution of **22** over a glass substrate showed a change in luminescence from yellow to blue-green upon rubbing (Figure 1.22c).

Nagano *et al*. reported a water-soluble mechanofluorochromic pyrene derivative **23** that contained two dendritic groups attached with pyrene skeleton through an amide linker (Figure 1.23).[28] The hydroxyl groups incorporated into the dendrons ensured the solubility of **23** in water. The compound **23** was obtained as a yellow solid (Y-form) after purification by gel permeation chromatography. In the solid-state, mechanical grinding induced a luminescence color change from yellow to green (Figure 1.23b and 1.23c). The initial yellow photoluminescence was recovered by exposing ground sample to water vapor. The switching of photoluminescence color by mechanical grinding and exposure to water vapor can be repeated at least ten times. The mechanism can be explained as a grinding induced change in the arrangement of the molecules resulting in the conversion of normal excimers (Y-form) to partial overlaped excimers (G-form). This type of compounds can be potentially used for developing mechanosensor and humidity sensors.

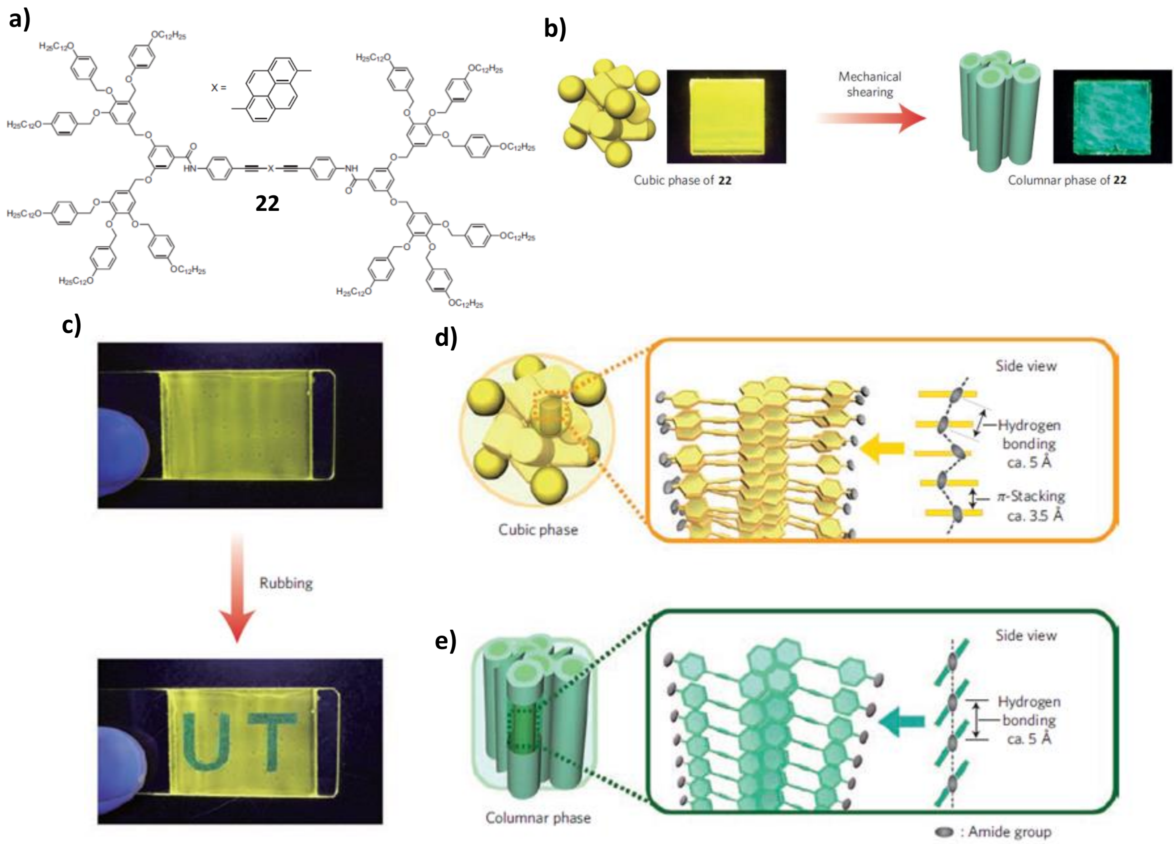

Figure 1.22. a) Chemical structure of **22**. b) Change of luminescent color and molecular assemblies of **22** on mechanical shearing. c) Thin film of compound **22** coated on a glass substrate from *n*-hexane solution (top), and the text 'UT' (below) was formed by rubbing the substrate with a glass rod. Photographs were taken under UV light. Schematic representations of molecular assemblies for **22** in d) the cubic and e) columnar phases. (Adapted with permission from ref. 26. Copyright 2009 NPG.)

Isothermally reversible and bistable fluorescence switching of a mechanochromic perylene bisimide (PBI) **24** was reported by Mizoshita and co-workers (Figure 1.24).[29] The molecule **24** contains fluorescent PBI core with siloxane-based bulky and flexible substituents at the 2,5,8,11 positions to diminish intermolecular interactions. A film was prepared by smearing the compound **24** on a glass or quartz substrate by annealing at 100 °C and then cooling to room temperature. The film exhibited green fluorescence (G-form) initially, which on applying mechanical shearing showed a fluorescence color change to orange (O-form). The orange color fluorescence returned to green by annealing at 100 °C or exposing to solvent vapors. The pattern drawn on the film can be self-erased by adding a small amount of silicone oil. The orange fluorescence pattern developed on the film without silicone oil showed no change for at least a week. The lifetime of metastable O-form depends on the amount of silicone oil present in the film. Higher the amount of silicone oil present in the film faster is the conversion from O-form to G-form (Figure 1.25). The fluorescence color change by mechanical shearing can be explained through the molecular rearrangement of PBI core. In the crystalline G-form the molecules are isolated by the bulky siloxane-based shells, which exhibit monomer-like green emission. On the other hand, in the amorphous O-form the molecules interact with one another because of the loss in the periodic molecular arrangement, which leads to the formation of excimers.

Tian *et al*. observed a piezochromic luminescence of molecule **25** by grinding and the exertion of external pressure on the powder (Figure 1.26).[30] The solid powder upon grinding changes its luminescence color from green to yellow and the recovery of the initial state was made by heating above 160 °C (Figure 1.26b). The inter conversion of the two states with their distinct emission colors is completely reversible through grinding and heating. When the applied pressure was varied from 0 to 8 GPa the corresponding photoluminescence spectra displayed a shift from lower to higher wavelength region (Figure 1.26d). The maximum red shift in the emission was observed at 7.92 Gpa pressure. Comparing with applied pressure the grinding method is not apparently strong enough to cause a better piezochromic effect.

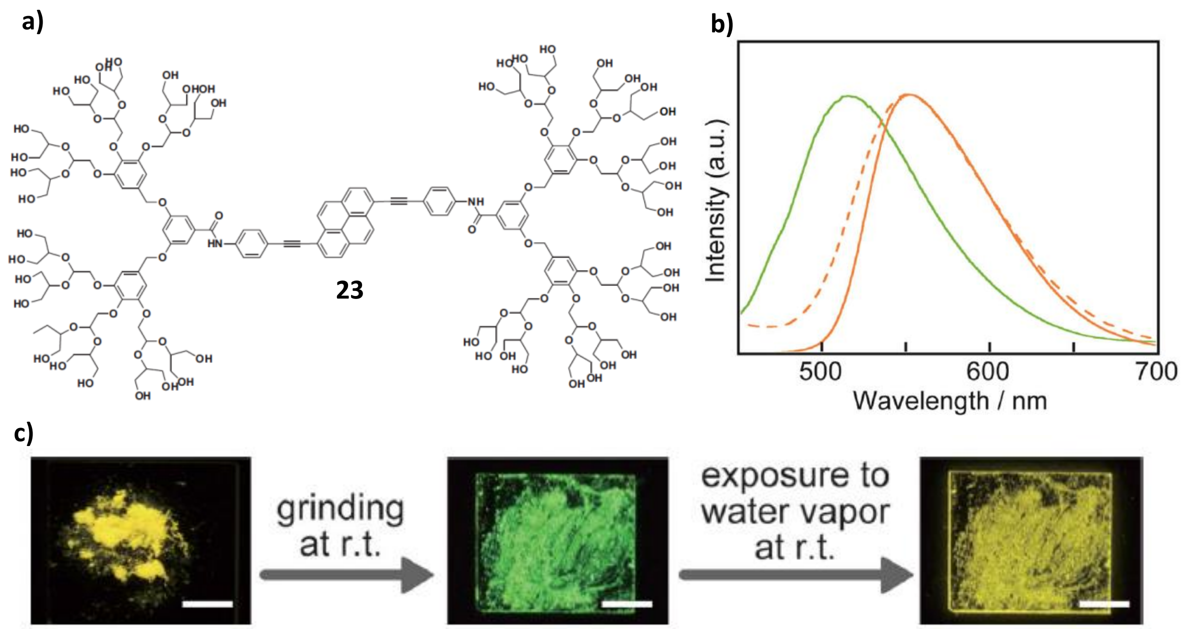

Figure 1.23. a) Chemical structure of **23**. b) Emission spectra of **23** in the Y-form (orange solid line), after mechanical grinding (G-form, green solid line) and exposed to water vapor after mechanical grinding (orange dotted line). c) Photographs of change in the luminescence color of compound **23** in the solid-state under UV light. Scale bar 5 mm. (Adapted with permission from ref. 28. Copyright 2013 Wiley-VCH.)

The photoluminescence spectrum under an applied pressure of 2.43 GPa was quite similar to that of the powder ground with a pestle. Single crystals with three polymorphs having distinguished luminescence color green, yellow and red were obtained by solvent diffusion method. On the basis of single-crystal structures, photophysical, and computational studies, it is proposed that enhanced π-π interaction between adjacent anthracene planes in the crystal and increased excitonic coupling and orbital overlap between neighboring molecules induced the shift in fluorescence emission from green to red.

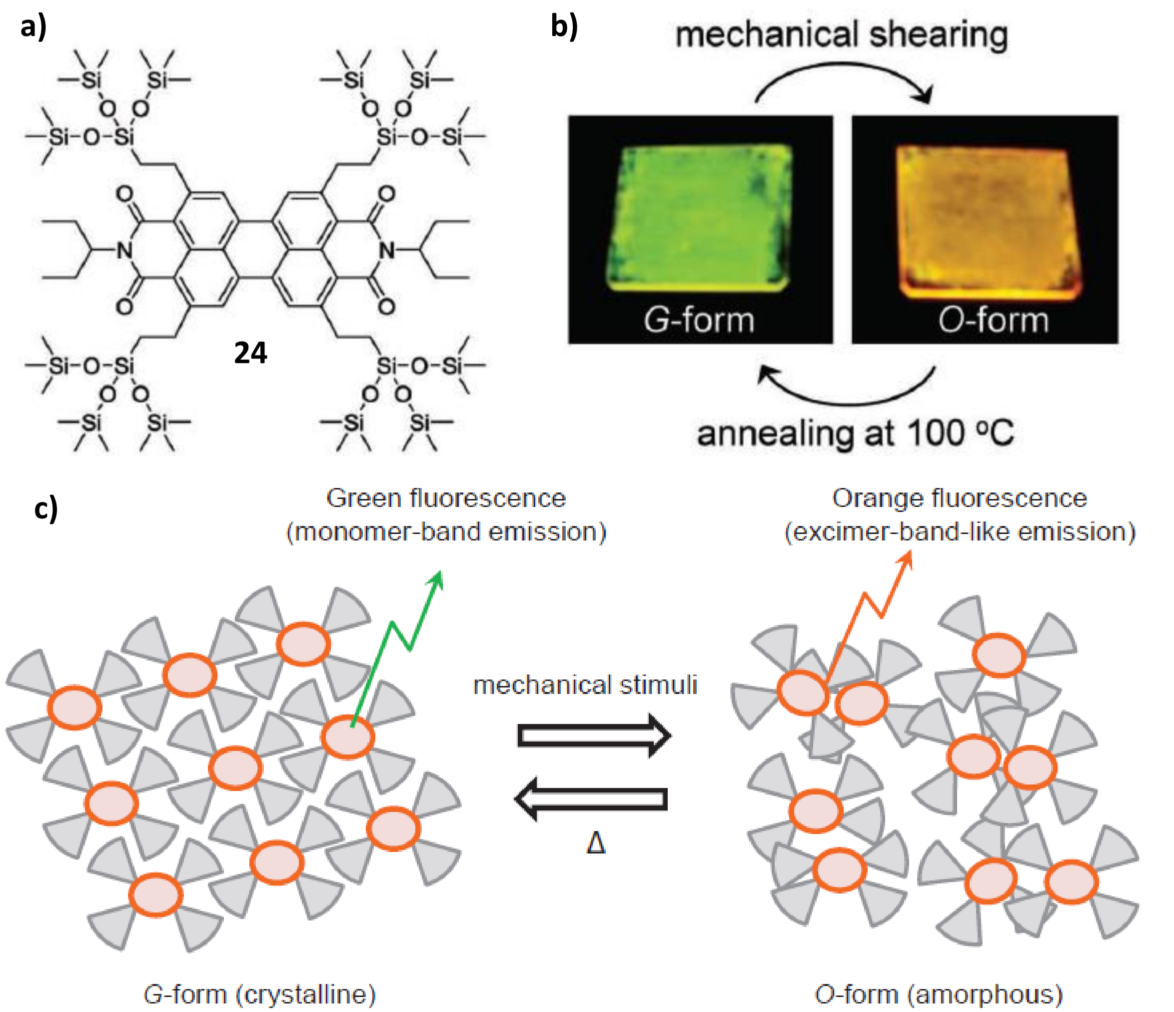

Figure 1.24. a) Chemical structure of **24**. b) Photograph of an annealed film (left, *G* -form) and a mechanically sheared film (right, *O* -form) of **24** under UV light. c) Schematic representation of the structural transition of **24** in the solid-state. (Adapted with permission from ref. 29. Copyright 2012 Wiley-VCH.)

Applying external pressure leads to a transformation from *J*-type aggregation (green) to *H*-type aggregation (yellow) and further to aggregated dimers stacked in a more tightly bound face-to-face arrangement (red). The color-switchable feature of this material may have potential application in optical recording and sensors for temperature and pressure.

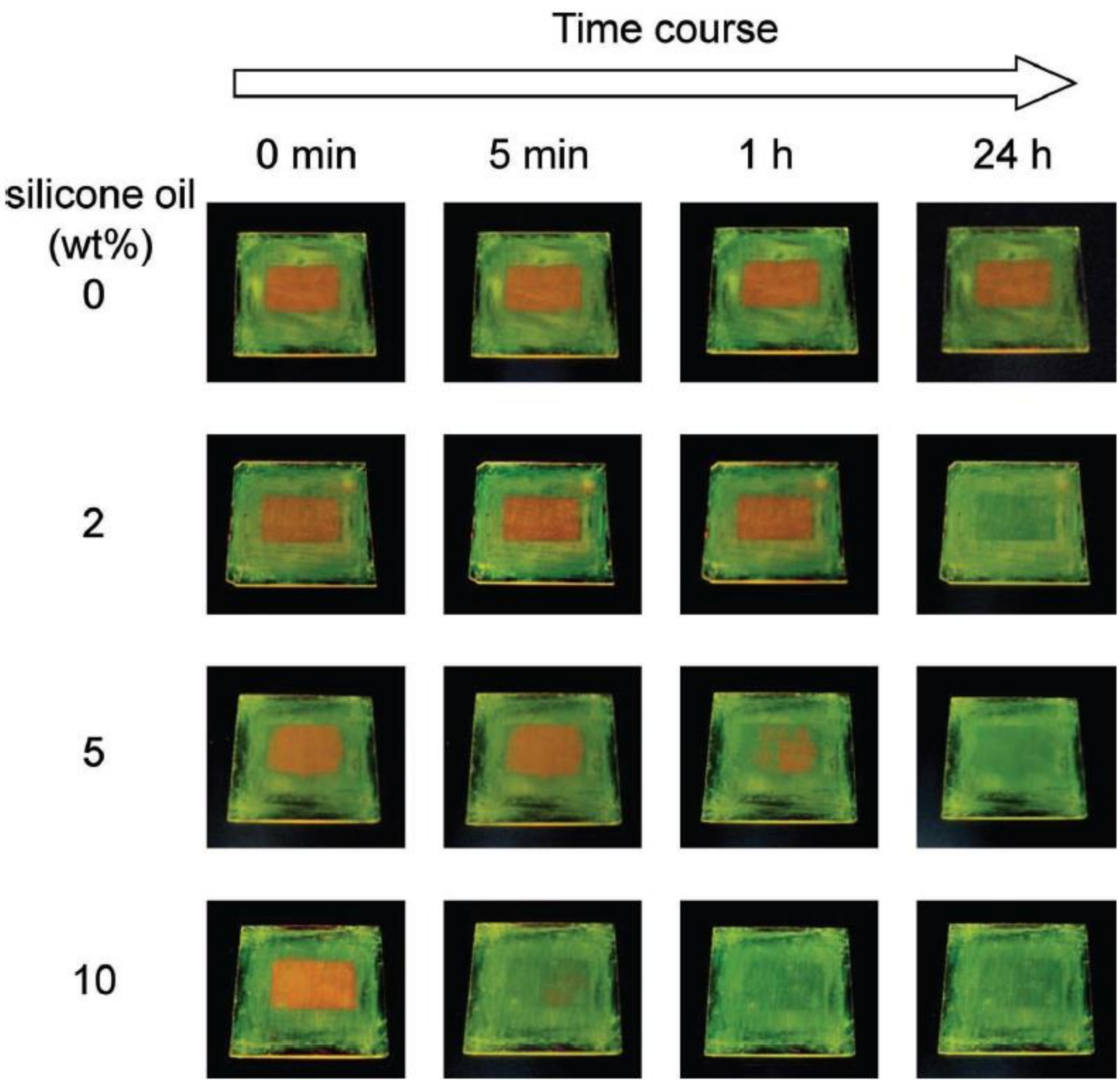

Figure 1.25. Self-erasing behavior of fluorescent films of **24** containing 0–10 wt% of silicone oil. (Adapted with permission from ref. 29. Copyright 2012 Wiley-VCH.)

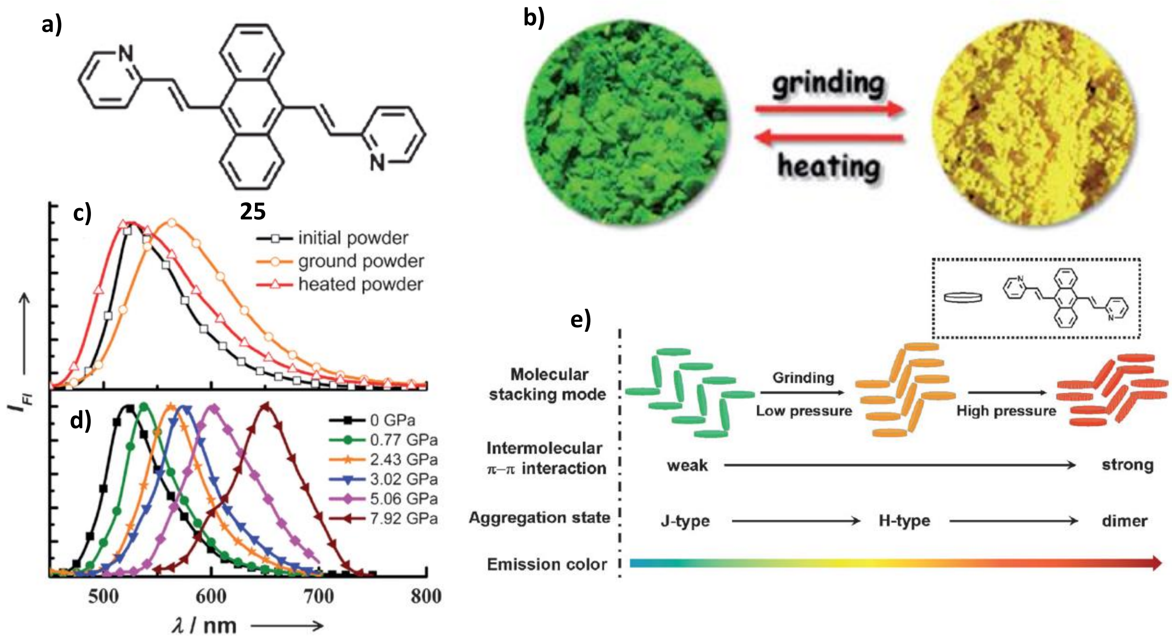

Figure 1.26. a) Chemical structure of **25**. b) Photographs of ground powder (right) and heated powder (left) under UV light. c) Photoluminescence spectra of **25** with different stimuli. d) Photoluminescence spectra of **25** under different external pressure. e) Schematic representation of stacking modes and corresponding emission colors for the various molecular aggregation states of **25**. (Adapted with permission from ref. 30. Copyright 2012 Wiley-VCH.)

1.7. Origin, Objectives and Approaches to the Thesis

Self-assembly is an important tool to construct well organized supramolecular assemblies of linear π-conjugated molecules. The optoelectronic properties of these molecules are strongly influenced by the alignment of the chromophores within the self-assembly. The main objective of the present study is to provide a detailed investigation on tuning the emission properties of small π-conjugated oligomers. Among the various classes of π-conjugated systems, phenyleneethynylenes (PEs) have received considerable attention due to their unique optical and morphological properties. Recent studies from our group revealed many interesting morphological and chiroptical properties of self-assembled organogels of OPEs.[8,9] Even though more number of reports are available in the literature on the self-assembly and optical properties of PEs, studies pertaining to tuning the emission behaviors are still limited.

The present work is a systematic investigation on the design, synthesis, morphological and stimuli responsive emission properties of PEs. The design principle involves the derivatization of PEs with amide H-bonding and substitution of alkyl chains at the end. In order to fulfil the above objectives, three different approaches were planned. In the first approach, PE molecule with alkoxy side chain was synthesized and their stimuli responsive fluorescence behaviour was investigated. In this case, water acts as an external stimulus to tune the emission of this molecular assembly. In the second approach, heat acts as a stimulus for tuning the emission of the molecular assembly having long hydrocarbon chain. In the final approach, molecular assembly having chiral side chains were synthesized and its emission and chiroptical properties were investigated. The present thesis is a detailed and systematic approach to the above objectives which are presented in the subsequent three chapters.

1. 8. References

[1] (*a*) J.-M. Lehn, *Supramolecular Chemistry - Concepts and Perspectives*, Wiley-VCH, Weinheim, **1995**; (*b*) J. L. Atwood, J. E. D. Davies, D. D. MacNicol, F. Vögtle, J.-M. Lehn, *Comprehensive Supramolecular Chemistry*, Pergamon, Oxford, **1996**; (*c*) K. Ariga, T. Kunitake, *Supramolecular Chemistry – Fundamentals and Applications*, Springer, Heidelberg, **2006**; (*d*) J. Steed, J. L. Atwood, *Supramolecular Chemistry*, 2nd ed., Wiley, Chichester, **2009**.

[2] (*a*) U. H. F. Bunz, *Chem. Rev*. **2000**, *100*, 1606–1644; (*b*) L. Kloppenburg, D. Song, U. H. F. Bunz, *J. Am. Chem. Soc*. **1998**, *120*, 7973–7974; (*c*) I. A. Levitsky, J. Kim, T. M. Swager, *J. Am. Chem. Soc.* **1999**, *121*, 1466–1472; (*d*) T. Sato, D.-L. Jiang, T. Aida, *J. Am. Chem. Soc.* **1999**, *121*, 10658–10659; (*e*) P. Samori, V. Francke, K. Müllen, J. P. Rabe, *Chem. Eur. J.* **1999**, *5*, 2312–2317.

[3] (*a*) T. M. Swager, *Acc. Chem. Res.* **1998**, *31*, 201–207; (*b*) D. T. McQuade, A. E Pullen, T. M. Swager, *Chem. Rev*. **2000**, *100*, 2537–2574.

[4] (*a*) M. Levitus, K. Schmieder, H. Ricks, K. D. Shimizu, U. H. F. Bunz, M. A. Garcia-Garibay, *J. Am. Chem. Soc.* **2001**, *123*, 4259–4265; (*b*) K. Schmieder, M. Levitus, H. Dang, M. A. Garcia-Garibay, *J. Phys. Chem. A* **2002**, *106*, 1551–1556; (*c*) M. Levitus, G. Zepeda, H. Dang, C. Godinez, T. A. Khuong, K. Schmieder, M. A. Garcia-Garibay, *J. Org. Chem*. **2001**, *66*, 3188–3195.

[5] (*a*) R. Thomas, S. Varghese, G. U. Kulkarni, *J. Mater. Chem.* **2009**, *19*, 4401–4406; (*b*) S. Varghese, S. Das, *J. Phys. Chem. Lett.* **2011**, *2*, 863–873.

[6] P. V. James, P. K. Sudeep, C. H. Suresh, K. G. Thomas, *J. Phys. Chem. A* **2006**, *110*, 4329–4337.

[7] K. Yoosaf, P. V. James, A. R. Ramesh, C. H. Suresh, K. G. Thomas, *J. Phys. Chem. C* **2007**, *111*, 14933–14936.

[8] (*a*) A. Ajayaghosh, R. Varghese, V. K. Praveen, S. Mahesh, *Angew. Chem.Int.*

Ed. **2006**, *45*, 3261–3264; (*b*) A. Gopal, R. Varghese, A. Ajayaghosh, *Chem. Asian J.* **2012**, *7*, 2061–2067.

[9] A. Ajayaghosh, R. Varghese, S. Mahesh, V. K. Praveen, *Angew. Chem., Int. Ed.* **2006**, *45*, 7729–7732.

[10] R. Gupta, R. Thomas, G. U. Kulkarni, *J. Mater. Chem.* **2012**, *22*, 19139–19145.

[11] R. H. Pawle, T. E. Haas, P. Müller, S. W. Thomas, *Chem. Sci.* **2014**, *5*, 4184–4188.

[12] (*a*) Y. Sagara, T. Kato, *Nat. Chem.* **2009**, *1*, 605–610; (*b*) Z. Chi, X. Zhang, B. Xu, X. Zhou, C. Ma, Y. Zhang, S. Liu, J. Xu, *Chem. Soc. Rev.* **2012**, *41*, 3878–3896.

[13] M. S. Kwon, D. Lee, S. Seo, J. Jung, J. Kim, *Angew. Chem. Int. Ed.* **2014**, *53*, 11177–11181.

[14] (*a*) D. R. Kearns, W. A. Case, *J. Am. Chem. Soc*. **1966**, *88*, 5087–5097; (*b*) W. D. K. Clark, A. D. Litt, C. Steel, *J. Am. Chem. Soc.* **1969**, *91*, 5413–5415; (*c*) J. Xu, A. Takai, Y. Kobayashi, M. Takeuchi, *Chem. Commun*. **2013**, *49*, 8447–8449.

[15] M. Sugino, K. Hatanaka, T. Miyano, I. Hisaki, M. Miyata, A. Sakon, H. Uekusa, N. Tohnai, *Tetrahedron Lett.* **2014**, *55*, 732–736.

[16] Q. Lou, S. Qu, P. Jing, W. Ji, D. Li, J. Cao, H. Zhang, L. Liu, J. Zhao, D. Shen, *Adv. Mater.* **2015**, *27*, 1389–1394.

[17] (*a*) A. Zhu, Q. Qu, X. Shao, B. Kong, Y. Tian, *Angew. Chem., Int. Ed.* **2012**, *51*, 7185–7189; (*b*) S. Qu, X. Liu, X. Guo, M. Chu, L. Zhang, D. Shen, *Adv. Funct. Mater*. **2014**, *24*, 2689–2695; (*c*) S. Qu, H. Chen, X. Zheng, J. Cao, X. Liu, *Nanoscale* **2013**, *5*, 5514–5518.

[18] J. Kunzelman, B. R. Crenshaw, C. Weder, *J. Mater. Chem.* **2007**, *17*, 2989–2991.

[19] (*a*) Y. Zhao, H. Gao, Y. Fan, T. Zhou, Z. Su, Y. Liu, Y. Wang, *Adv. Mater*. **2009**, *21*, 3165–3169; (*b*) S. Varughese, *J. Mater. Chem. C* **2014**, *2*, 3499–3516.

[20] N. S. S. Kumar, S. Varghese, N. P. Rath, S. Das, *J. Phys. Chem. C* **2008**, *112*, 8429–8437.

[21] (*a*) R. Davis, N. P. Rath, S. Das, *Chem. Commun*. **2004**, 74–75; (*b*) R. Davis, N. S. S. Kumar, S. Abraham, C. H. Suresh, N. P. Rath, N. Tamaoki, S. Das, *J. Phys. Chem. C* **2008**, *112*, 2137–2146.

[22] (*a*) Y. Hong, J. W. Y. Lam, B. Z. Tang, *Chem. Soc. Rev*. **2011**, *40*, 5361–5388; (*b*) J. Mei, Y. Hong, J. W. Y. Lam, A. Qin, Y. Tang, B. Z. Tang, *Adv. Mater*. **2014**, *26*, 5429–5479.

[23] R. Wei, P. Song, A. Tong, *J. Phys. Chem. C* **2013**, *117*, 3467–3474.

[24] S.-J. Yoon, J. W. Chung, J. Gierschner, K. S. Kim, M.-G. Choi, D. Kim, S. Y. Park, *J. Am. Chem. Soc*. **2010**, *132*, 13675–13683.

[25] (*a*) Z. G. Chi, X. Q. Zhang, B. J. Xu, X. Zhou, C. P. Ma, Y. Zhang, S. W. Liu and J. R. Xu, *Chem. Soc. Rev*. **2012**, *41*, 3878–3896; (*b*) A. Pucci and G. Ruggeri, *J. Mater. Chem*. **2011**, *21*, 8282–8291; (*c*) K. Ariga, T. Mori and J. P. Hill, *Adv. Mater*. **2012**, *24*, 158–176.

[26] Y. Sagara and T. Kato, *Nat. Chem*., **2009**, *1*, 605–610.

[27] (*a*) Y. Sagara, T. Kato, *Angew. Chem., Int. Ed*. **2008**, *47*, 5175–5178; (*b*) Y. Sagara, S. Yamane, T. Mutai, K. Araki, T. Kato, *Adv. Funct. Mater*. **2009**, *19*, 1869–1875.

[28] Y. Sagara, T. Komatsu, T. Ueno, K. Hanaoka, T. Kato and T. Nagano, *Adv. Funct. Mater*. **2013**, *23*, 5277–5284.

[29] N. Mizoshita, T. Tani, S. Inagaki, *Adv. Mater*. **2012**, *24*, 3350–3355.

[30] Y. Dong, B. Xu, J. Zhang, X. Tan, L. Wang, J. Chen, H. Lv, S. Wen, B. Li, L. Ye, B. Zou and W. J. Tian, *Angew. Chem. In. Ed*. **2012**, *51*, 10782–10785.

Chapter 2

Molecular Assembly for Self-erasable Writing Using Water as Ink and Its Application as Security Marker for Currency and Documents

Abstract

Stimuli responsive fluorescent materials are important in sensing and security applications. Herein we report the synthesis and properties of a p-phenyleneethynylene based fluorescent molecule that changes its emission color from blue to cyan when in contact with Water. The original emission can be retrieved by evaporation of the water. A practical application of the molecule is demonstrated by making security labels on currency and documents. Temporary marking or writing could be done on the security label using water as ink which produced reversible color change. Interaction of the molecular assembly with water molecules facilitates breaking of the hydrogen bonds and the stretching of the hydrophilic ethoxy chains, which pushes the nearby molecules to the opposite directions along the inward direction to cause the fluorescence change.

2.1. Introduction

Water is the gift of Nature to the mankind and is required for everything in life. Therefore, finding a new use for water is practically impossible without an out-of-box thinking.[1] One such innovative thinking is whether a drop of water can secure the authenticity of a valuable document/currency or whether water can be used as environmentally benign ink for writing. Thoughts in this direction have resulted in a few reports on the use of water as marker/ink for writing.[2] These reports describe specially coated papers on which water induces a visible color change due to the structural changes of the coated chemical. Self-erasable, writing or printing is a novel concept of temporary communication, which allows the use of the writing medium for a certain period of time.[3] Self-erasable printing inks reduce the usage of papers for printing and save millions of trees, help in reducing the green gas emission. Even though Xerox company came up with such an idea, the technology could not be successfully launched [4] and only very few reports are available using the concept of self-erasable writing on fluorescent medium.[5]

Recently, Kim and co-workers demonstrated inkjet printing of polymerizable diacetylene (DA) **1** on banknotes for anti-counterfeit purposes.[6] An ink suspension composed of a complex formed using the molecule **1** and the commercial non-ionic surfactant Brij 78 was printed on a Korean banknote using a computer controlled conventional thermal inkjet printer. Figure 2.1b shows the letters “Bank of Korea” printed on banknotes. Under normal day light the printed letters were not visible, because DA molecules do not absorb visible light when it is in the monomer state (Figure 2.1b, left). However, UV irradiation (254 nm, 1 mW cm^{-2}, 30 s) resulted in the appearance of blue-colored letters (Figure 2.1b, middle), which confirms the formation of polydiacetylene (PDA). When the note was placed on a hot plate, blue to red color transition occurred (Figure 2.1b, right). A completely reversible color transition from red to blue was observed by cooling the note to room temperature. The reversible color change of the letters on the banknote is attributed to the thermal stability of **1**. The reversible thermochromic image was stable for a number of thermal cycles and can be used to control the currency counterfeit.

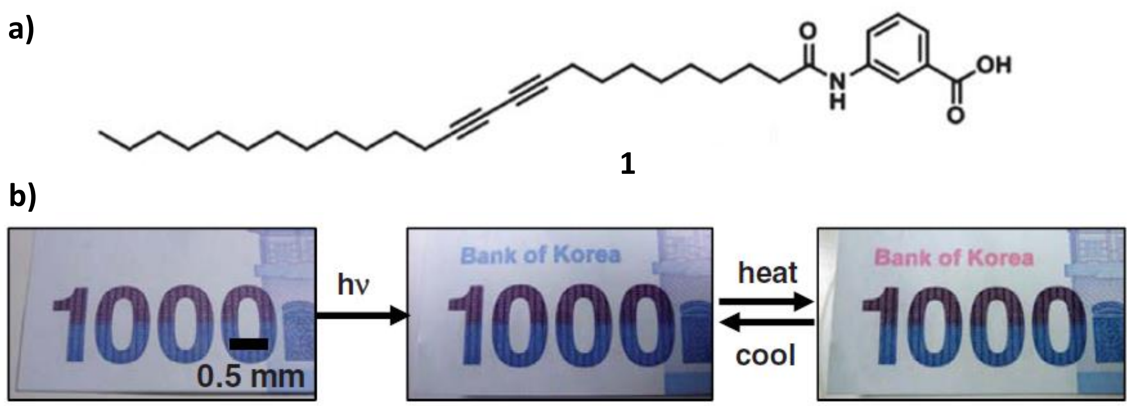

Figure 2.1. a) Molecular structure of **1**. b) Photographs of printed images on bank notes using polymeric complex of **1** before irradiation (left), after irradiation (middle) and after heating (right). (Adapted with permission from ref. 6a. Copyright 2011 Wiley-VCH.)

In a different study, the same authors have developed a stable microemulsion ink system using a proper combination of DA monomer **2**, organic solvent, surfactant and co-surfactant.[7] Due to the lack of amphiphilic character, the molecule **2** is not suitable for the preparation of surfactant-assisted aqueous ink system. However, the high solubility of **2** in organic solvents allowed successful preparation of microemulsion based ink system in combination with the surfactant Sodium dodecylsulfate. The diacetylene containing microemulsion can be readily transferred to a paper substrate by utilizing inkjet printing with a conventional thermal inkjet printer.

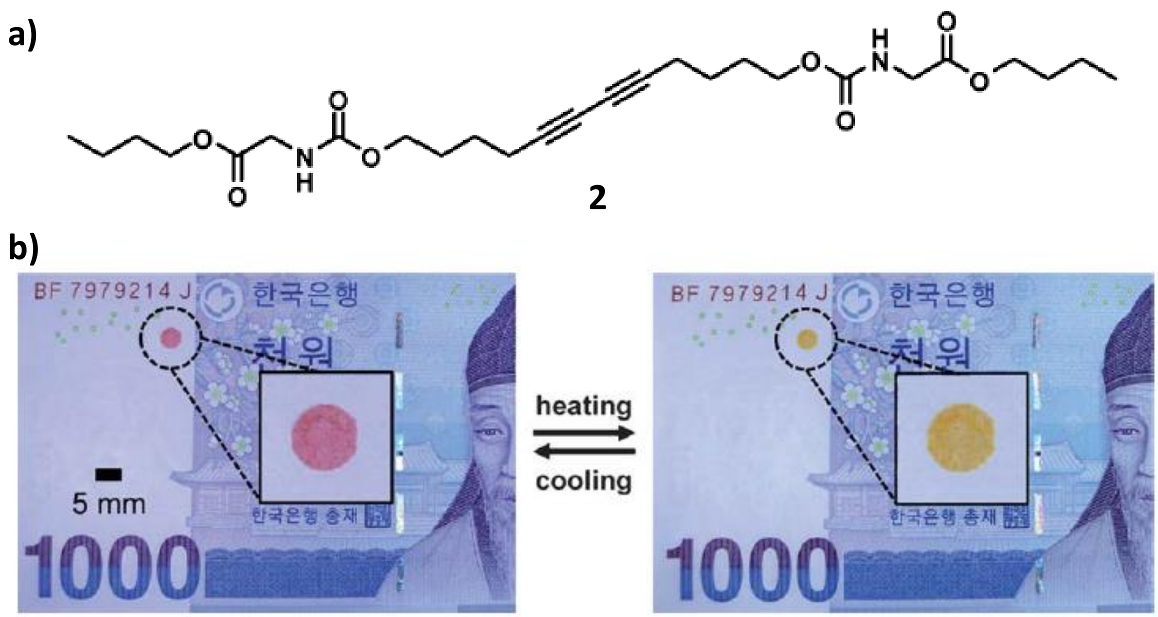

Figure 2.2. a) Molecular structure of **2**. b) Photographs of printed images of polymerized **2** on banknotes upon thermal cycles. (Adapted with permission from ref. 7. Copyright 2012 The Royal Society of Chemistry.)

UV induced polymerization afforded the formation of PDA on the ink-coated paper. The printed PDA supramolecules displayed a blue-to-red-to-yellow color transition upon heating. Initially, the blue colored PDA was converted to red by heating to 100 °C and further heating to 180 °C lead to generation of yellow colored PDA. Upon cooling to room temperature, the yellow colored PDA became red and a complete colorimetric reversibility was observed between red (30 °C) and yellow (180 °C). The color change of the PDA was expected to be related to the crystallization and melting of the alkyl chains. [8] During the thermochromic transition, the polymer undergoes a volume expansion. As a result of this expansion and the ample energy available for segmental motions, the packing of the side groups becomes less rigid and they are free to explore many different conformations via torsional motions about their side-chain axes.[9] The reversible red to yellow thermochromic property of PDA printed on banknote may find application in counterfeit prevention.

Gupta and co-workers have demonstrated a novel multi-stage excitable (379, 980 and 1550 nm) and highly luminescent Y_2O_3:Yb^{3+}/Er^{3+} nanorod based transparent security ink for currency counterfeit prevention.[10] The luminescent nanorods were synthesized using hydrothermal method, and exhibited both hypersensitive green (562 nm) and strong red (660 nm) emission in a single host lattice (Figure 2.3a). Moreover, these luminescent nanorods also showed down-shifted (1127 nm) emission as well as upconverted (562 nm) emission at a single excitation near infrared wavelength of 980 nm. Furthermore, these luminescent nanorods exhibited emission color shift from red to green upon controlling the sintering temperature. The integration of luminescent nanorods with a suitable polymer matrix such as polyvinyl chloride (PVC) gold medium offers multi-wavelength excitable transparent security ink that are useful for the protection of currency and documents from counterfeiting (Figure 2.3b).

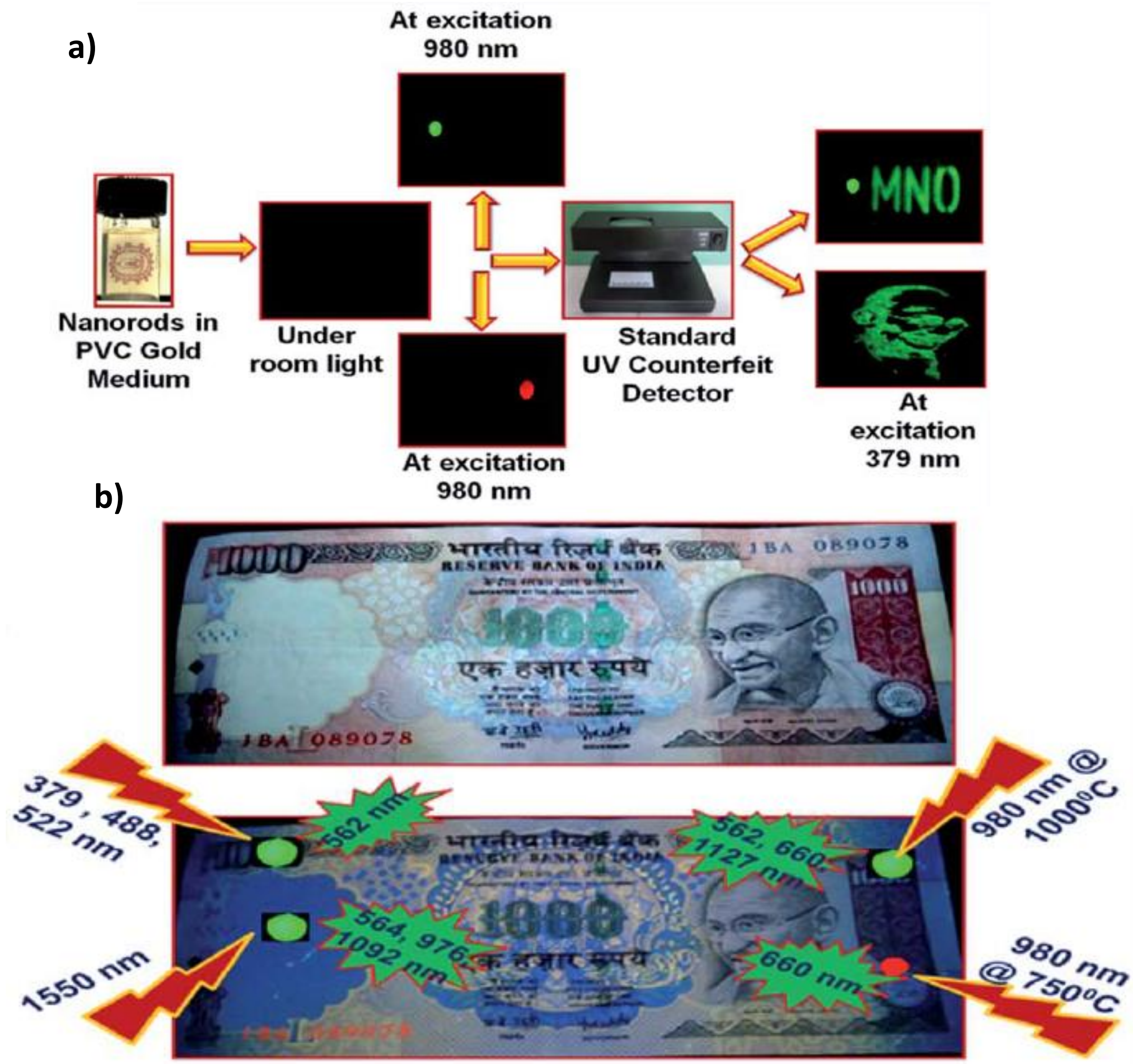

Figure 2.3. a) Scheme showing the photographs of printed pattern under different excitation wavelengths (379 and 980 nm). The pattern is printed on black paper using transparent security ink. b) Proposed scheme for high-end protection of Indian currencies to protect counterfeiting. (Adapted with permission from ref. 8. Copyright 2014 The Royal Society of Chemistry.)

Currency counterfeiting has become a nightmare for government and private agencies all over the world and causes huge loss of economy every year.[11] Although several security features[12] have already been employed to protect currency notes, counterfeiting has not been completely stopped. This is mainly because of the lack of safety features that are difficult to hack by the counterfeiters. Thus, developing a security marker having unique safety features to prevent such counterfeiting activity is always demanding and has been a subject of intense research. Along this line, a research group from Korea came up with the idea of using colorimetric indicators for providing security features to currency notes.[6,7] When compared to visible color change composite materials, luminescent materials provide improved security because of their unique optical properties. Therefore, the development of simple and specific luminescent materials for anti-counterfeiting is of great importance. In this chapter, we describe the use of fluorescent molecular assembly made up of oligo(*p*-phenyleneethynylene)s (OPEs) molecule which acts as a self-erasable security marker for currency and documents.

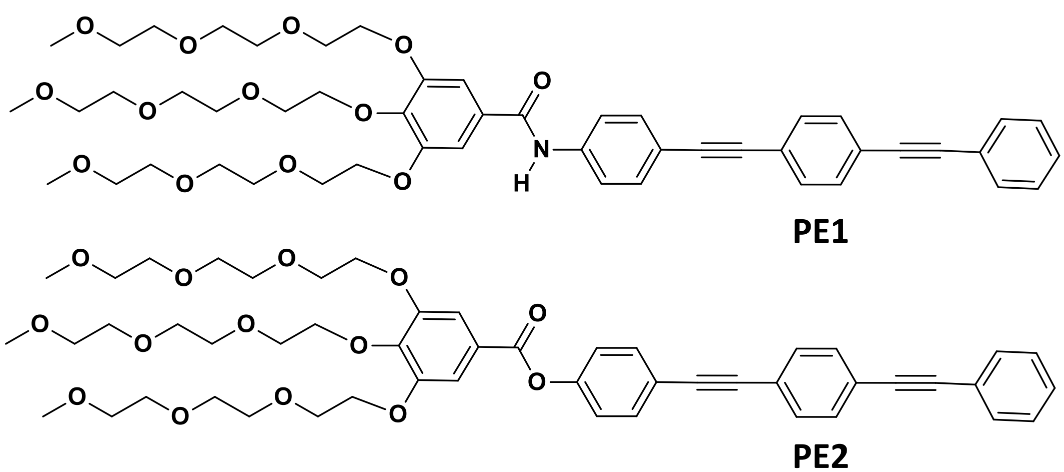

Figure 2.4. Structure of molecules under investigation.

For the above-mentioned purpose, we have designed two tailor-made molecular systems, **PE1** and **PE2** having structures as shown in Figure 2.4. In these molecules, the triple bonded linear aromatic π-backbone (phenyleneethynylene, PE) is the fluorescent core, which is connected to a bulky end group through an amide or ester bond. The terminal bulky group is composed of flexible oxyethylene chains. The amide linkage provides hydrogen bonds that control the molecular assembly whereas the ester linkage cannot provide such a control. These molecules were synthesized by multistep synthetic procedures using palladium-catalyzed Sonogashira–Hagihara[13] cross coupling reactions. Chemical structures of these molecules were characterized by FT-IR, ^{1}H and ^{13}C NMR spectroscopy as well as by high-resolution mass spectrometry. The molecules synthesized were readily soluble in common organic solvents such as chloroform, toluene and tetrahydrofuran (THF). Detailed self-assembly, morphological, optical and X-ray diffraction studies of **PE1** and **PE2** were carried out.

2.2. Results and Discussion

2.2.1. Synthesis of PEs

The synthesis of precursors **6** and **8** (Scheme 2.1) starts from methyl 3,4,5-trihydroxybenzoate **1** which on reaction with 2-(2-(2-methoxyethoxy)ethoxy)ethyl 4-methylbenzenesulfonate in the presence of potassium carbonate gave methyl 3,4,5-tris(2-(2-(2-methoxyethoxy)ethoxy)ethoxy)benzoate **2**, which upon hydrolysis in the presence of potassium hydroxide gave 3,4,5-tris(2-(2-(2-methoxyethoxy)ethoxy)ethoxy)benzoic acid **3**. The compound 3,4,5-tris(2-(2-(2-

methoxyethoxy)ethoxy)ethoxy) benzoyl chloride **4** was prepared by reaction of **3** with thionyl chloride. Reaction of 4-iodoaniline with compound **4** gave the amide derivative **6** and the ester derivative **8** was synthesized by reaction of **4** with 4-iodophenol.

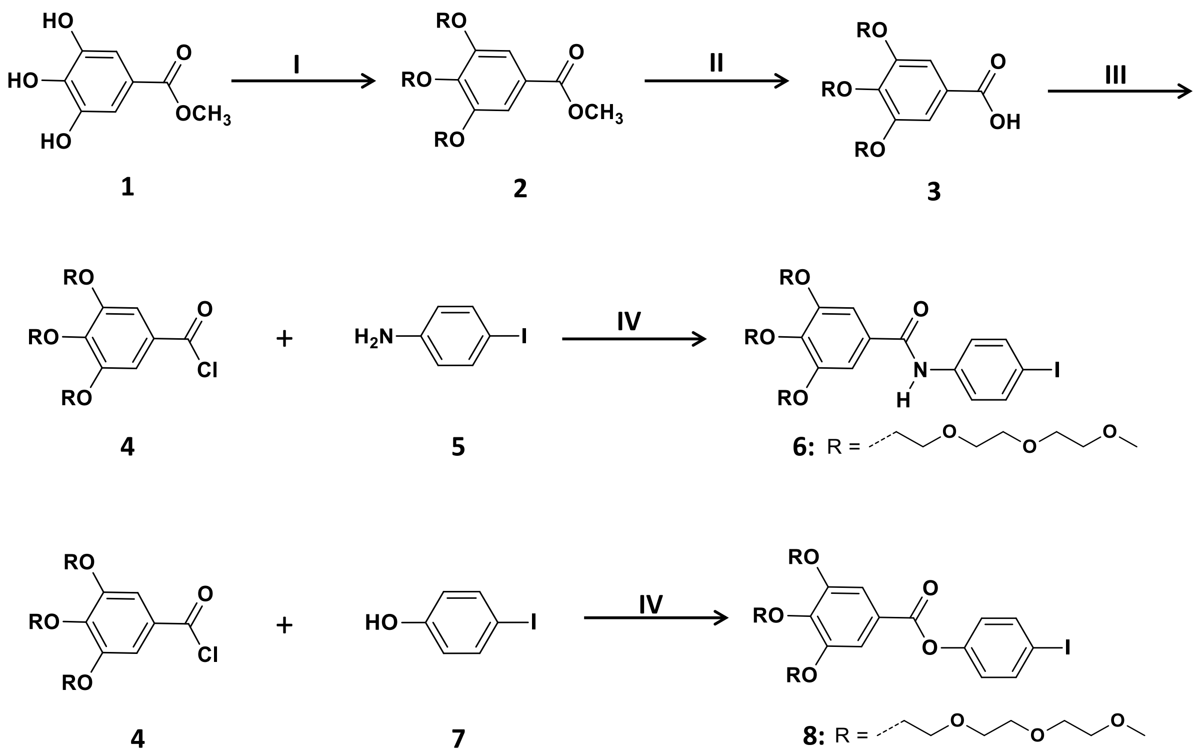

Scheme 2.1. Synthesis of compounds **2-8**. Reagents and conditions: I) 2-(2-(2-methoxyethoxy)ethoxy)ethyl 4-methylbenzenesulfonate, K_2CO_3, CH_3CN, 80 °C, 48 h; II) KOH, EtOH, 80 °C, 12 h; III) $SOCl_2$, CH_2Cl_2 , rt., 5 h; IV) toluene, Et_3N, rt., 12 h.

Synthesis of 1-ethynyl-4-(phenylethynyl)benzene **12** starts from ethynylbenzene **9** which on Sonogashira-Hagihara cross coupling with ((4-iodophenyl)ethynyl)trimethyl silane **10** in presence of $[PdCl_2(PPh_3)_2]$ catalyst and CuI as co-catalysts gave trimethyl((4-(phenylethynyl)phenyl)ethynyl)silane **11**. Desilylation of **11** in the presence of potassium fluoride gave **12** in 93% yield

(Scheme 2.2). The Sonogashira-Hagihara coupling between amide derivative **6** and 1-ethynyl-4-(phenylethynyl)benzene **12** using [Pd(PPh_3)$_2$(Cl_2)$_2$] and CuI as the catalysts gave **PE1** in 57% yield and the coupling of ester derivative **8** with **12** gave **PE2** in 60% yield. All the molecules were purified by column chromatography using silica gel (100-200 mesh) and characterized by ^{1}H-NMR, and HRMS-FAB spectroscopic techniques.

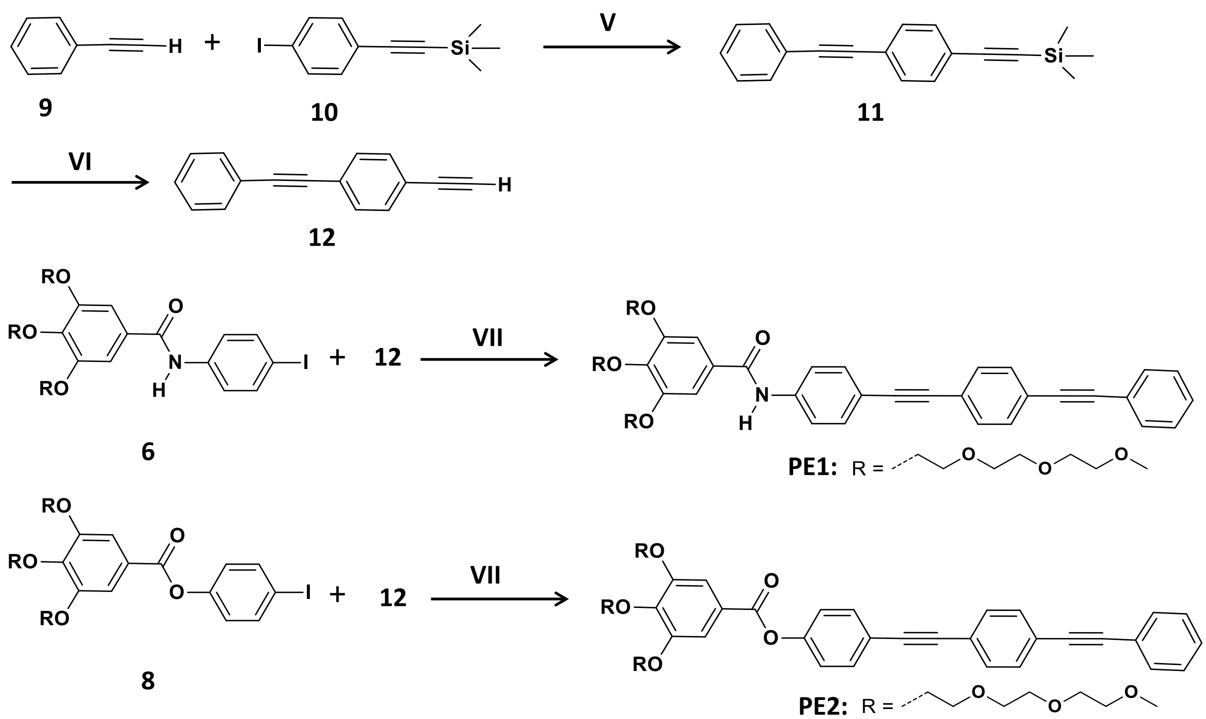

Scheme 2.2. Synthesis of **PE1** and **PE2**. Reagents and conditions: V) [$PdCl_2(PPh_3)_2$], CuI, THF, Et_3N, rt., 12 h; VI) KF, CH_2Cl_2, CH_3OH, rt., 6 h; VII) [$PdCl_2(PPh_3)_2$], CuI, THF, Et_3N, rt., 24 h**.**

2.2.2. Photophysical Studies

The UV/Vis absorption spectrum of **PE1** in THF ($c = 1 \times 10^{-5}$ M) at 25°C showed an absorption band with λ_{max} at 336 nm (Figure 2.5a). However, in THF-water mixture

(1:9 v/v), the intensity of the absorption band is decreased with a small shift of the λ_{max} to 324 nm with a weak shoulder band at 388 nm. Similarly, the absorption spectra of **PE2** in THF and THF-water mixture (1:9 v/v) are shown in the Figure 2.5b. In THF(c = 1 × 10^{-5} M) at 25 °C, **PE2** showed a strong π-π* absorption band at 322 nm and in THF-water mixture the absorption maximum was blue shifted to 308 nm. Both **PE1** and **PE2** showed blue shift in the absorption maximum upon aggregation and they are able to aggregate efficiently in THF-water mixture.

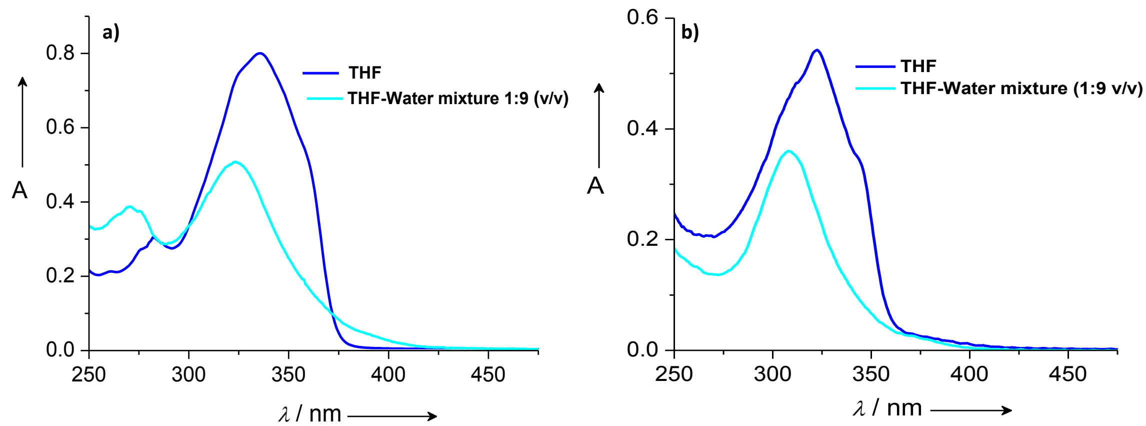

Figure 2.5. Absorption spectra of a) **PE1** and b) **PE2** in THF and THF-water mixture (1:9 v/v) at (c = 1 × 10^{-5} M).

The emission spectrum of **PE1** in THF (c = 1 × 10^{-5} M) exhibited a maximum at 395 nm when excited at 340 nm (Figure 2.6a). The fluorescence quantum yield (Φ_f) was estimated as 0.02 (± 0.002) using quinine sulphate as a standard. Interestingly, in THF-water mixture (1:9 v/v), a significant red shift of the emission maximum (λ_{em} = 488 nm) with increased intensity (3.2 times) and quantum yield (Φ_f = 0.14 ± 0.05) were observed. This shift in the emission wavelength is obvious by the color change from blue to intense cyan (Figure 2.6d). This observation is an indication of aggregation induced enhanced emission (AIEE), which is a phenomenon associated with the aggregation of certain organic molecules.[14] Usually, AIEE is observed at the same wavelength position or with a slight shift with respect to the original emission of the molecule. Therefore, the large red shift of 93 nm ($\Delta\nu$ = 107527 cm^{-1}) with enhanced fluorescent intensity [15] observed in the case of the self-assembled **PE1** is unique and hence of great potential for applications.

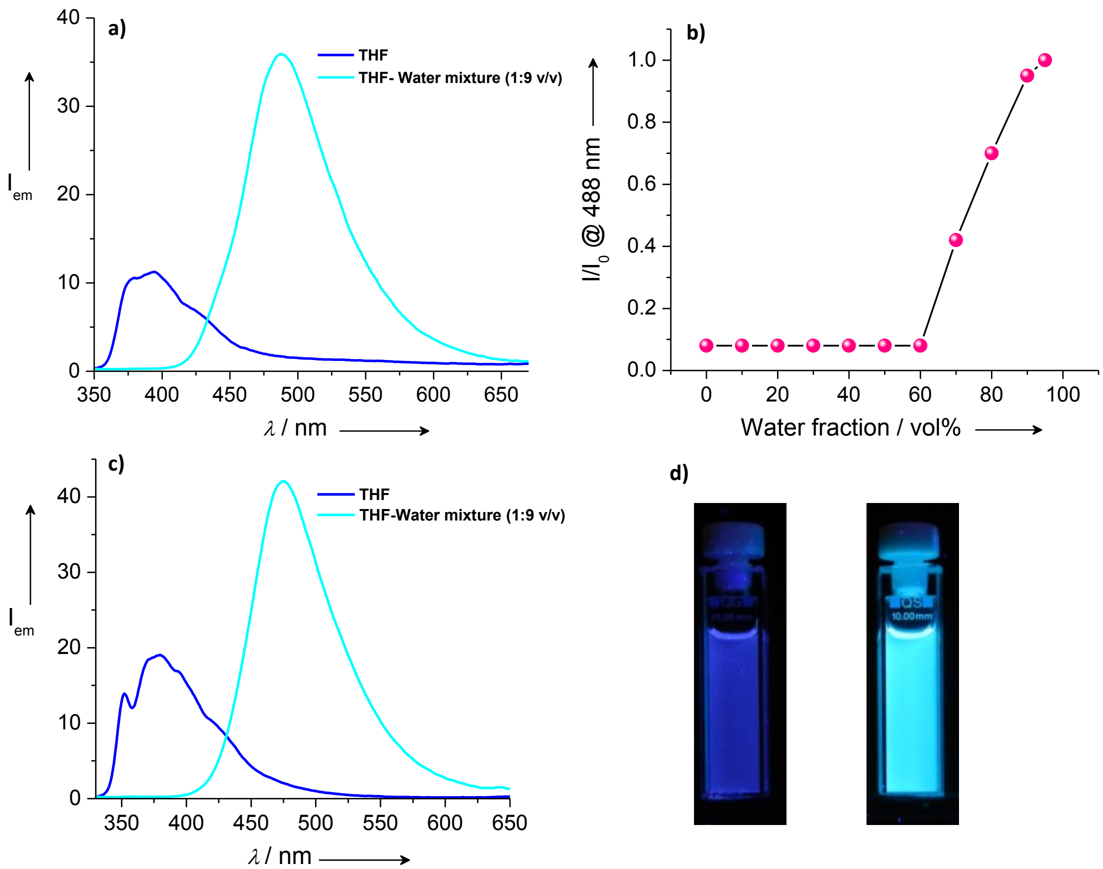

Figure 2.6. Emission spectra (λ_{ex} = 340 nm) of a) **PE1** and c) **PE2** in THF and THF-water mixture (1:9 v/v) at concentration 1 × 10^{-5} M. b) Changes in fluorescence intensities of **PE1** with different water fractions in the THF-water mixtures. d) Shows photographs of **PE1** in THF (left) and THF-water mixture 1:9 v/v (right) under illumination at 365 nm.

This enhanced emission at 488 nm occurs at above 60% water in THF as shown in the Figure 2.6b. We then compared the fluorescence emission properties of **PE1** with those of **PE2**. The emission property of **PE2** in THF-water mixture was similar to that of **PE1** (Figure 2.6c). It shows 2.2 times increased emission intensity in the aggregated state with 95 nm red shift when compared to the monomer emission.

The absorption and emission spectra of **PE1** (1×10^{-5} M) in different solvents indicate that the molecule exists as monomers in methanol with high absorption and low emission intensities (Figure 2.7). In all other solvents, it shows aggregation tendency with slight red shift and decreased absorption intensities. The emission intensities get enhanced due to AIEE character of the molecule.

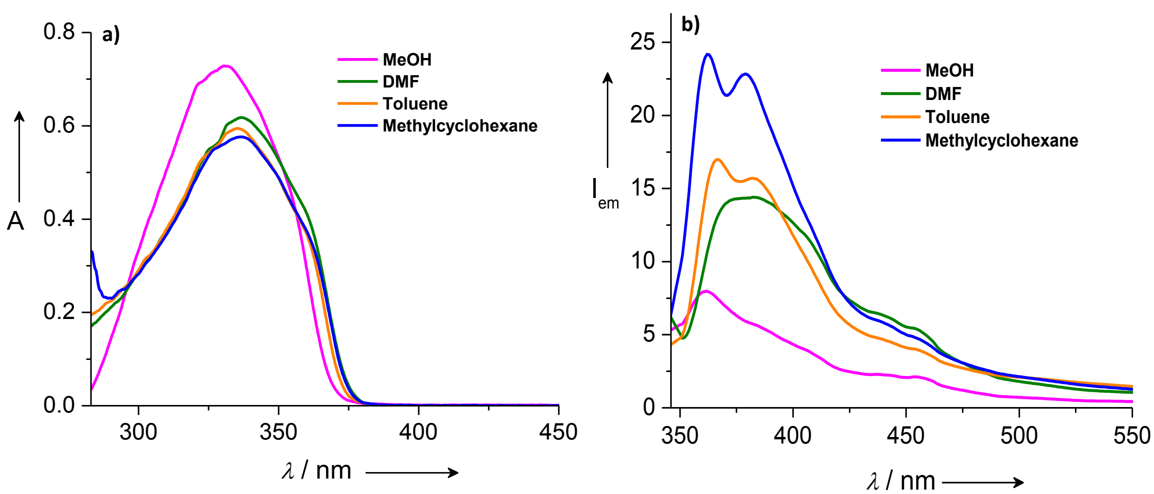

Figure 2.7. a) Absorption and b) emission spectra (λ_{ex} = 340 nm) of **PE1** (1×10^{-5} M) in different solvents.

2.2.3. Morphological Characterization

The scanning electron microscopy (SEM) and transmission electron microscopy (TEM) analyses of the **PE1** in THF-water (1:9 v/v, $c = 5 \times 10^{-5}$ M), drop cast on aluminium substrate and carbon coated copper grids exhibited spherical particles with average diameter of 100 nm (Figure 2.8). The spherical particle formation is further confirmed by dynamic light scattering (DLS) analysis (Figure 2.9b) of the samples ($c = 5 \times 10^{-5}$ M), which showed average hydrodynamic radius (R_H) of 122 nm. Fluorescence microscopy experiment also revealed the formation of fluorescent spherical particles (Figure 2.9a). The spherical particles are stable enough without adding any stabilizers or surfactants.

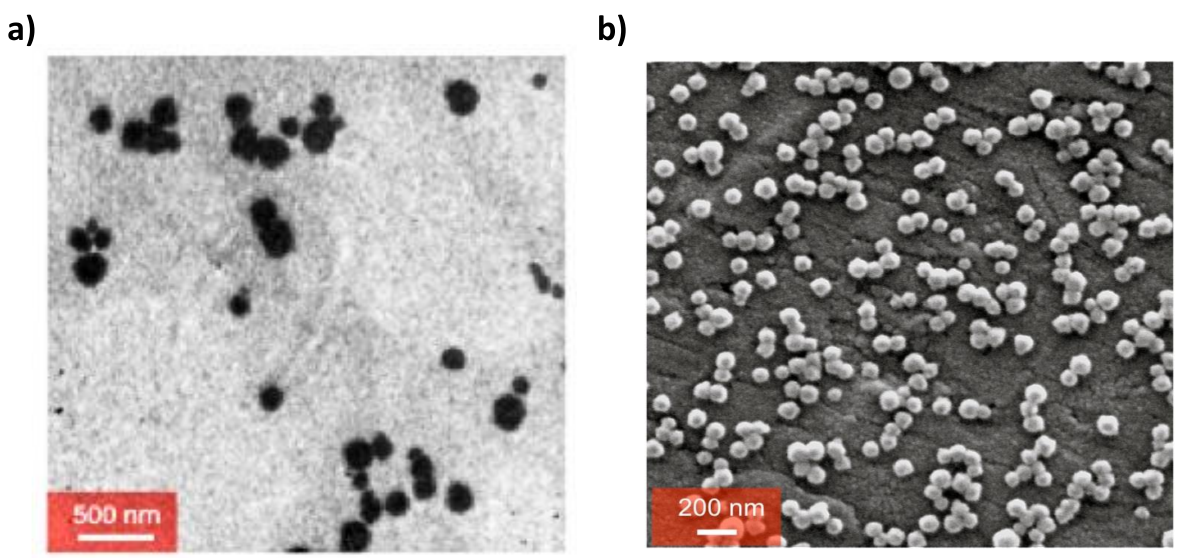

Figure 2.8. a) TEM and b) SEM images of **PE1** ($c = 5 \times 10^{-5}$ M) aggregates prepared from THF-water mixture (1:9 v/v) displaying spherical particles.

2.2.4. Stability of Aggregates

In order to know the stability of spherical aggregates present in solution variable temperature emission study of **PE1** in 1:9 v/v THF-water mixture ($c = 5 \times 10^{-5}$ M) was carried out. The aggregates show green emission with a maximum at 488 nm and they were heated from 20 to 80 °C at a heating rate of 1 °C per minute with constant stirring. Above 40 °C the aggregates start breaking which is confirmed by change in emission intensity and at 70 °C, the aggregates were completely dissociated which is clear from the plot of emission intensity monitored at 488 nm versus temperature (Figure 2.10).

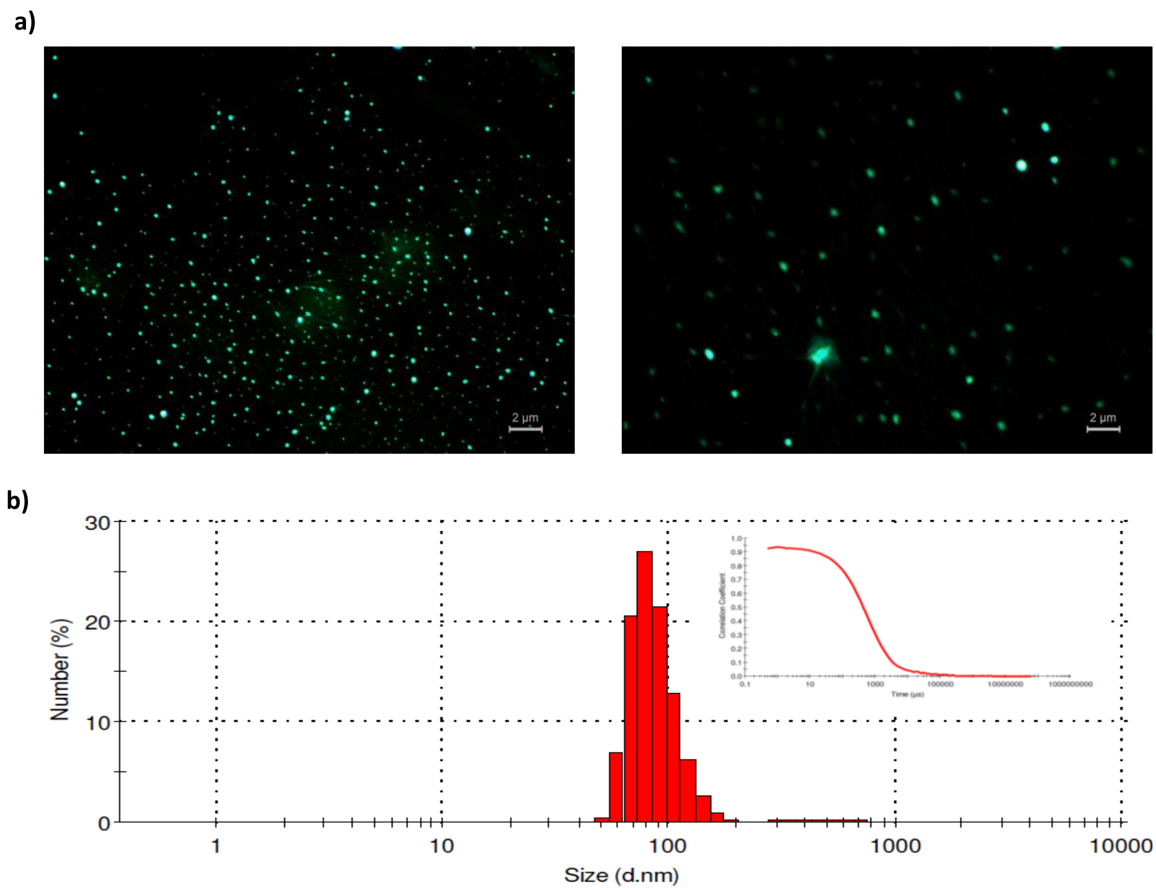

Figure 2.9. a) Fluorescent images of the particles formed from **PE1** ($c = 5 \times 10^{-5}$ M) in THF-Water (1:9 v/v). The samples were prepared by drop casting the solution over glass plate and drying at ambient temperature. Scale bar is 2 µm. b) DLS in THF-water mixture (1:9 v/v) at 5×10^{-5} M concentration. Inset shows the correlogram data.

2.2.5. Fluorescence Modulation Studies with Water

The molecules **PE1** and **PE2** appear as pasty pale yellow solid in its pristine state. The emission spectra of these molecules in the pristine state are shown in the Figure 2.11. **PE1** emission is blue in color and **PE2** shows cyan emission under UV excitation. These molecules in their pristine state are difficult in handling, because of their pasty nature. Hence we decided to make a film out of them by dissolving them in chloroform solution.

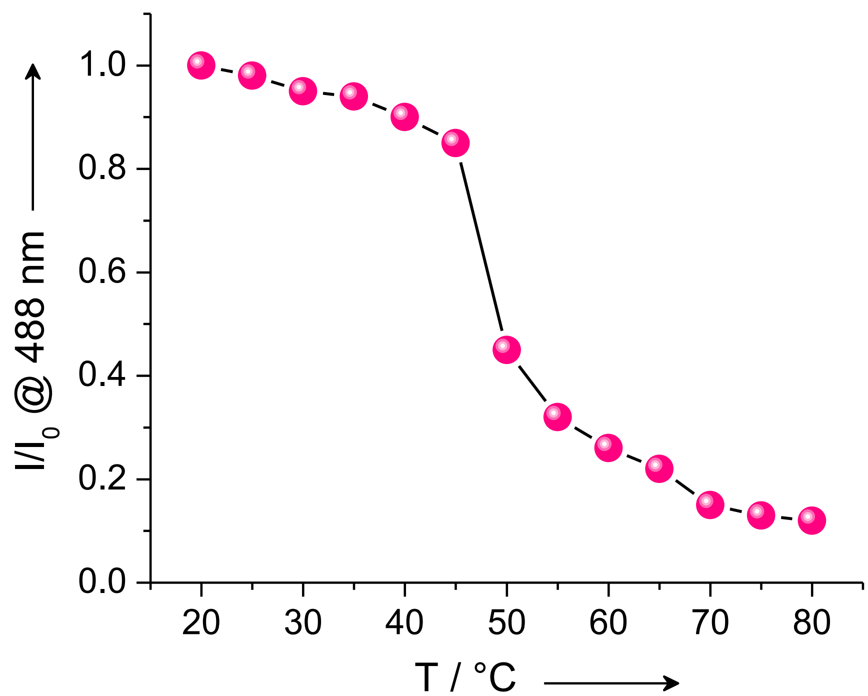

Figure 2.10. The plot of fluorescence intensity versus temperature shows the stability of spherical particles formed from **PE1** ($c = 5.0 \times 10^{-5}$ M) in THF-water mixture (1:9 v/v).

In chloroform ($c = 1 \times 10^{-3}$ M) **PE1** showed an absorption maximum at 334 nm and an emission maximum at 395 nm (Figure 2.12). When this solution was coated on a paper and excited with a UV lamp (λ_{ex} = 365 nm), a blue emission with a maximum at 425 nm was observed. When brought in contact with water, the fluorescence color of the paper changed from blue to intense cyan (λ_{em} = 488 nm) as shown in Figure 2.13a. The cyan color was returned to the original blue (Figure 2.13b) when the water was dried off. This process could be repeated a number of times (Figure 2.14b). The fluorescence color change occurs only when the paper comes in contact with water or when the humidity (Figure 2.14c) of the surrounding reaches above 95 percentage.[16] Interestingly, the blue fluorescing chloroform solution of **PE2** ($c = 1 \times 10^{-3}$ M) when coated on a paper immediately showed a cyan emission. The cyan emission of **PE2** did not show any change when brought in contact with water. These experiments revealed the fact that only **PE1** is capable of exhibiting the fluorescence color change with water for which the presence of the hydrophilic oxyethylene chains and the amide hydrogen-bonding moiety are essential.

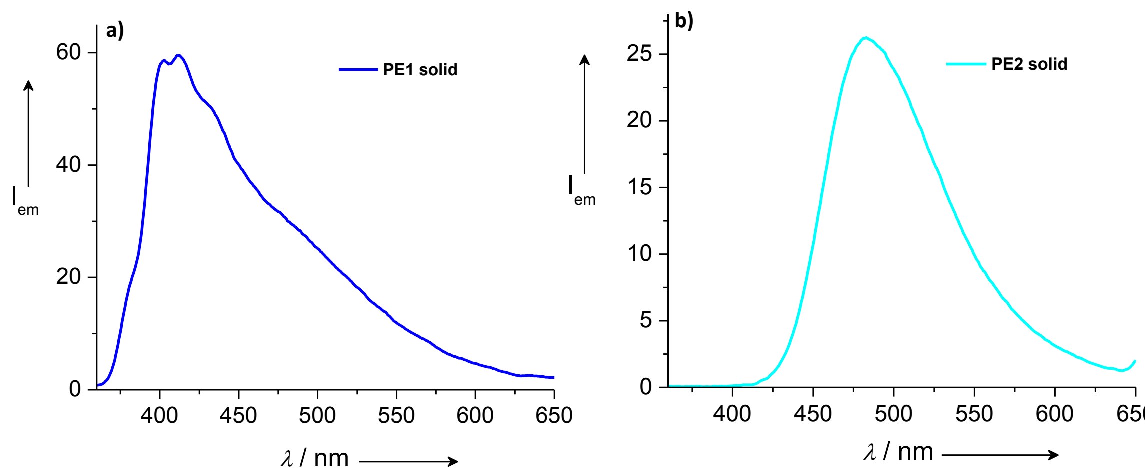

Figure 2.11. Emission spectra a) **PE1** and b) **PE2** in the solid state.

Having known the above water induced reversible fluorescence color change of **PE1**, our next attempt was to explore the potential application of this molecule for self-erasable writing. For this purpose, ordinary writing papers (7.0 cm × 5.0 cm) were coated with a solution of **PE1** in chloroform (c = 1 × 10^{-3} M) and dried under vacuum for 30 min. The blue emission of the molecule remained intact on the paper, which was confirmed by illuminating with a UV lamp (λ_{ex} = 365 nm), however under daylight it looked like normal white paper. Upon writing on this paper using a pen filled with water under a UV light (365 nm) illumination, cyan letters were visible (Figure 2.13).

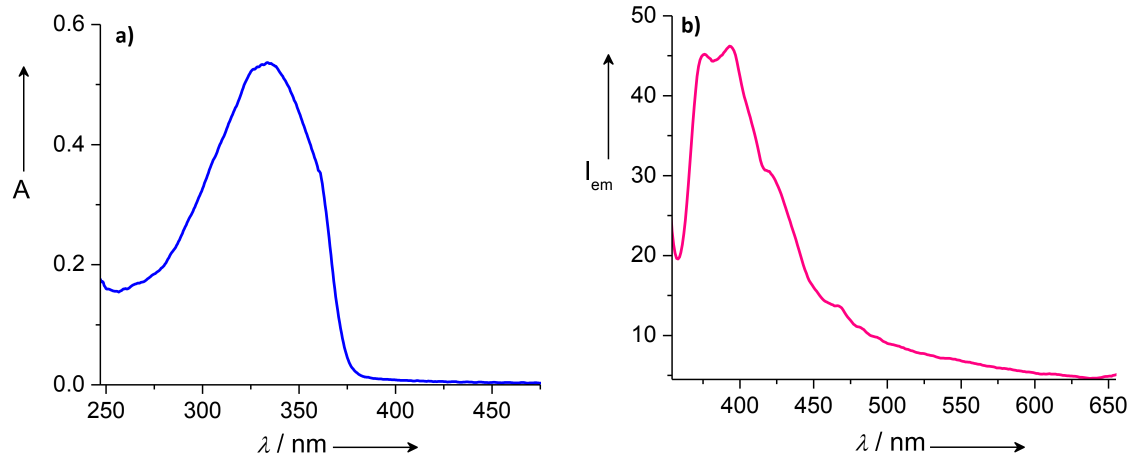

Figure 2.12. a) Absorption and b) emission spectra (λ_{ex} = 340 nm) of **PE1** (1 × 10^{-3} M) in chloroform.

The written paper after different time intervals is shown in the Figure 2.14a. The writing was clear to read up to 1h on keeping under ambient condition in an atmosphere having 80 – 85% humidity. The complete erasing of the writing occurred within 4 h, which is clear from the plot of the intensity of emission at 488 nm with time (Figure 2.14a, solid circles). However, when the same experiment was performed on a glass plate coated with **PE1**, fast erasing was observed and complete disappearance of the letters happened within 20 – 25 min (Figure 2.14a, open circles). The slow disappearance of the letters on paper substrates could be due to the better adherence of water molecules when compared to glass substrate. However, exposure to a hot air gun immediately erased the written letters on the paper substrate. These findings can be easily utilized to demonstrate free hand reversible writing on the **PE1** coated fluorescent paper using water as ink. Figure 2.13c shows the handwritten image "CSIR" on **PE1** coated fluorescent paper using a water filled pen. Snap shots of video images taken while writing are shown in the Figure 2.15.

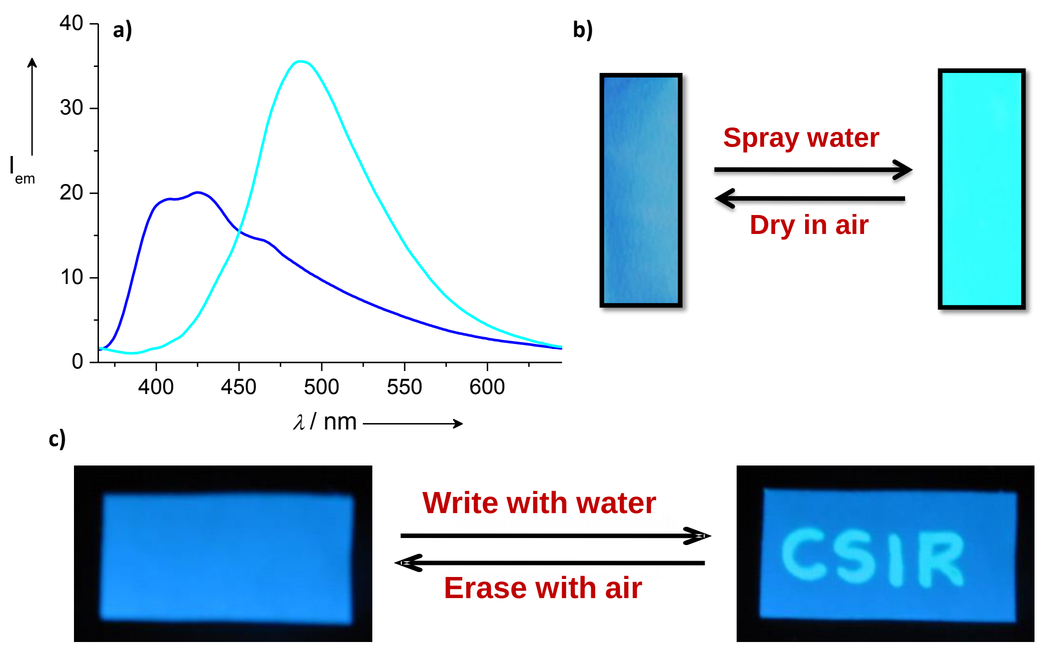

Figure 2.13. a) Emission spectra (λ_{ex} = 340 nm) of **PE1** coated paper in the absence (blue) and presence of (cyan) water. b) Photographs of the paper before (left) and after (right) spraying with water under 365 nm UV light. c) Photographs of **PE1** coated fluorescent paper after writing with water (right) and erasing with air (left) under illumination at 365 nm.

In order to understand the stability and fluorescence modulation of **PE1** coated paper with water a detailed study has been carried out. For this purpose, the emission of **PE1** in water at different pH and having different ions were recorded (Figure 2.17a and b). The fluorescence intensity remained more or less the same at different pH except a small decrease in the highly acidic pH. In the case of water containing different ions the fluorescence showed a slight decrease in Zn^{2+} and Fe^{3+}. These studies reveal have reveal that the purity of water (presence of metal ions as well as different pH) has no substantial effect on the fluorescence response of the system.

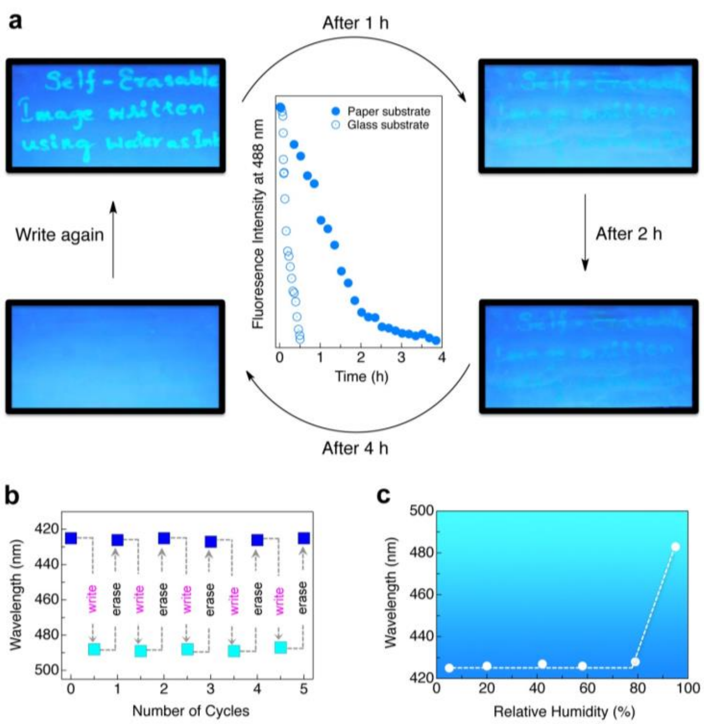

Figure 2.14. a) Photographs of hand written images on a **PE1** coated fluorescent paper under illumination at 365 nm over a period of 4 h. A secondary plot of the corresponding changes in the fluorescence spectra is shown in the middle. b) Changes in the fluorescence color of paper upon repeated cycles of writing with water and erasing with hot air. c) Changes in the photoluminescence color of paper upon exposure to different relative humidity.

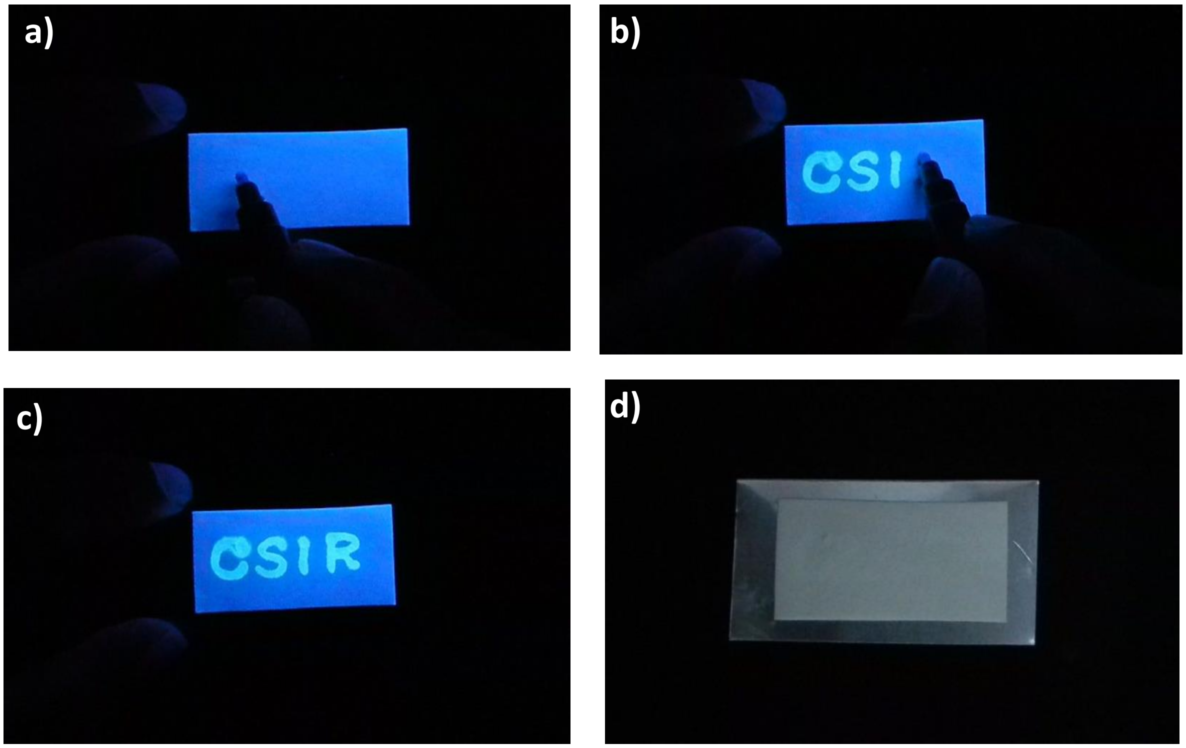

Figure 2.15. Snap shots of the self-erasable writing on **PE1** coated fluorescent paper under UV light 365 nm. a) Film before writing b) and c) after writing. d) The written image under normal daylight (note that the letters are not visible).

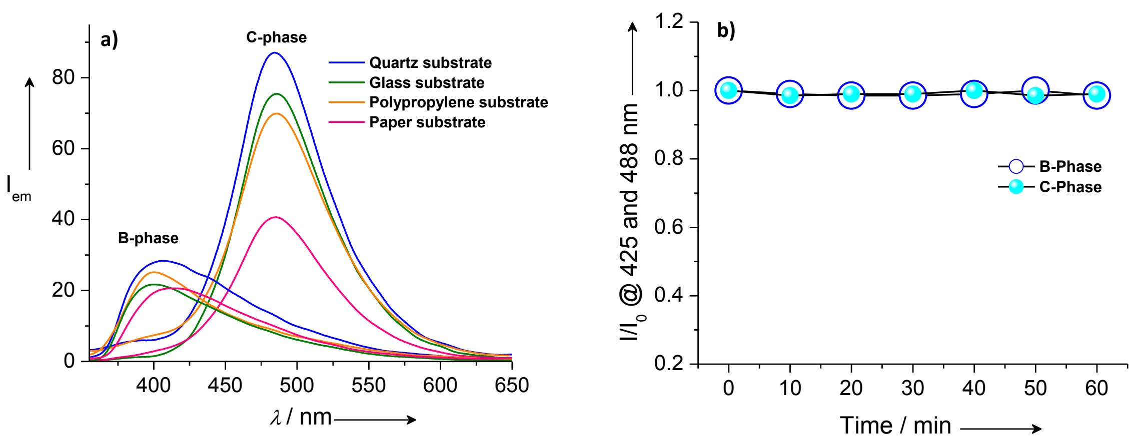

Figure 2.16. a) Emission spectra (λ_{ex} = 340 nm) of **PE1** in B-phase and C-phase drop cast over different solid substrates. b) Comparison of variation of emission in the B-Phase and C-Phase of **PE1** coated over a quartz plate under ambient light with time.

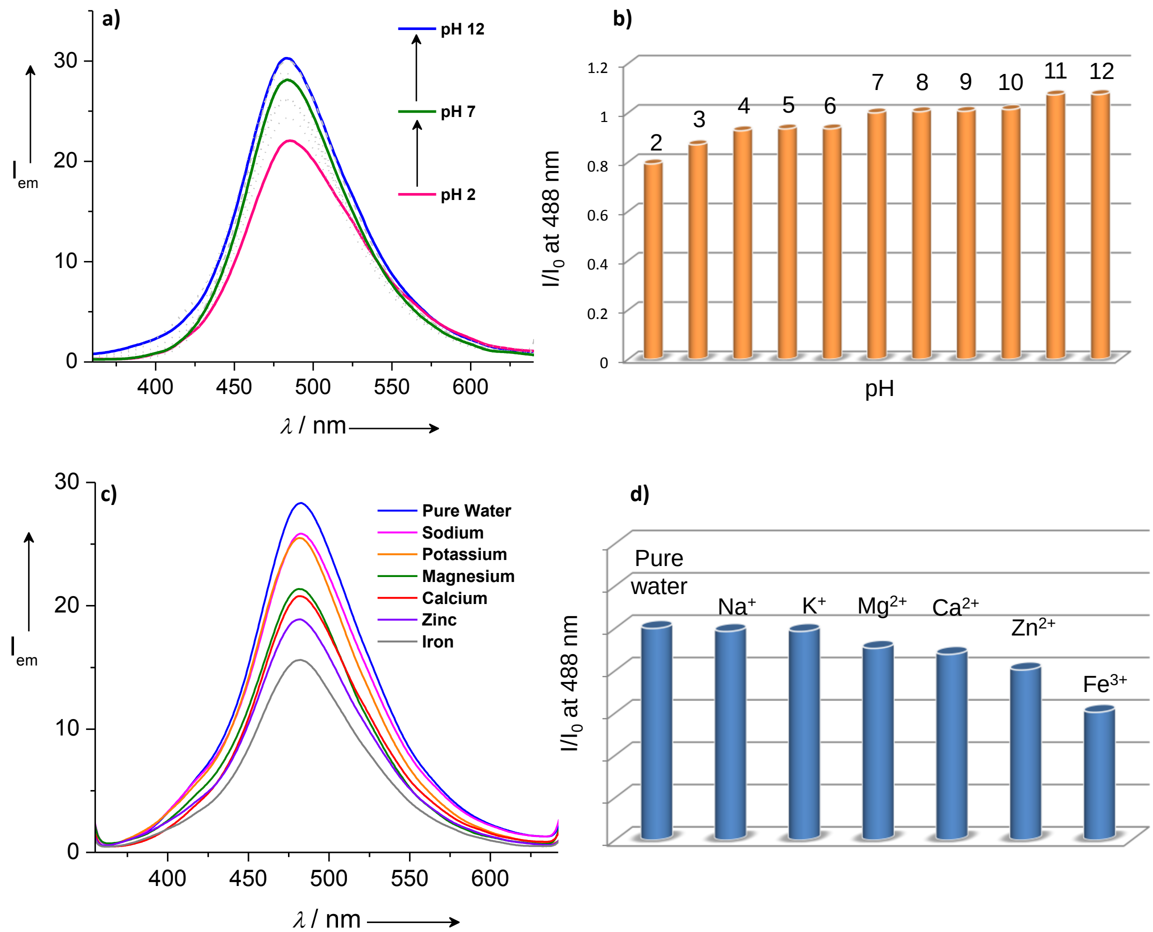

Figure 2.17. a) Fluorescence changes of **PE1** coated paper substrate with water having different pH. b) Bar diagram of fluorescence intensity changes monitored at 488 nm. Fluorescence intensity obtained with application of water at pH 7 is taken as I_0. c) Fluorescence changes of **PE1** coated paper substrate with water having different metal ions (c = 1 × 10^{-3} M). d) Bar diagram of fluorescence intensity changes monitored at 488 nm. Fluorescence intensity obtained with application of deionised water is taken as I_0.

The water-induced fluorescence switching property of **PE1** was observed by films prepared using different substrates without any considerable change in the emission (Figure 2.16a). The emission intensity in both phases is quite stable for several hours (Figure 2.16b). The quantum yield and fluorescence lifetime characteristics of PE derivatives in different states are presented in Table 1. The fluorescence decay profiles of **PE1** in different conditions are shown in Figure 2.18.

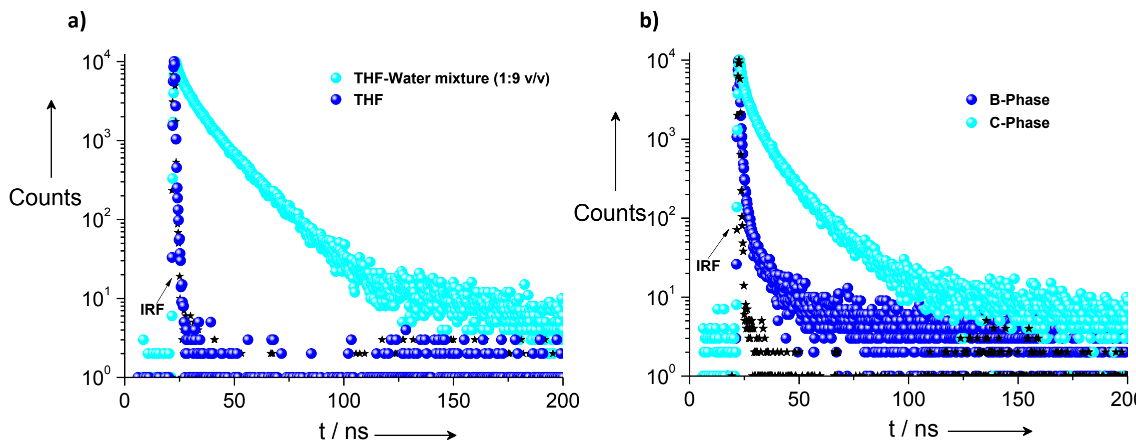

Figure 2.18. Emission decay profiles of **PE1** in a) THF (blue) and THF-Water mixture (1:9 v/v) (cyan), b) blue-emitting film (blue) and cyan-emitting film (cyan). Fluorescence decay profiles were recorded by excitation at 375 nm, emission monitored at the emission maximum.

Table 1. Quantum yield and fluorescence lifetime characteristics of **PE** derivatives.

Molecule	Solution state	Aggregated state	Blue film	Cyan film
PE1	$\Phi_f = 0.02$	$\Phi_f = 0.14$	$\Phi_f = 0.13$	$\Phi_f = 0.18$
	τ= 0.29 ns	τ_1 = 14.95 ns (68%) τ_2 = 5.52 ns (29%) τ_3 = 1.10 ns (3%)	τ_1 = 1.04 ns (72%) τ_2 = 5.29 ns (18%) τ_3 = 2.92 ns (10%)	τ_1 = 15.25 ns (47%) τ_2 = 5.84 ns (44%) τ_3 = 1.68 ns (9%)
PE2	$\Phi_f = 0.02$	$\Phi_f = 0.18$	---	$\Phi_f = 0.22$
	τ = 0.78 ns	τ_1 = 23.35 ns (60%) τ_2 = 8.55 ns (34%) τ_3 = 1.68 ns (6%)	---	τ_1 = 21.54 ns (52%) τ_2 = 8.23 ns (41%) τ_3 = 1.44 ns (7%)

In THF, the emission arises from excitation of the monomer band at the 310-350 nm regions as shown in the Figure 2.19a. In the case of the film state, a strong blue shift in the excitation with red shift in emission was observed (Figure 2.19d) indicating the formation of fluorescent H-type aggregates.

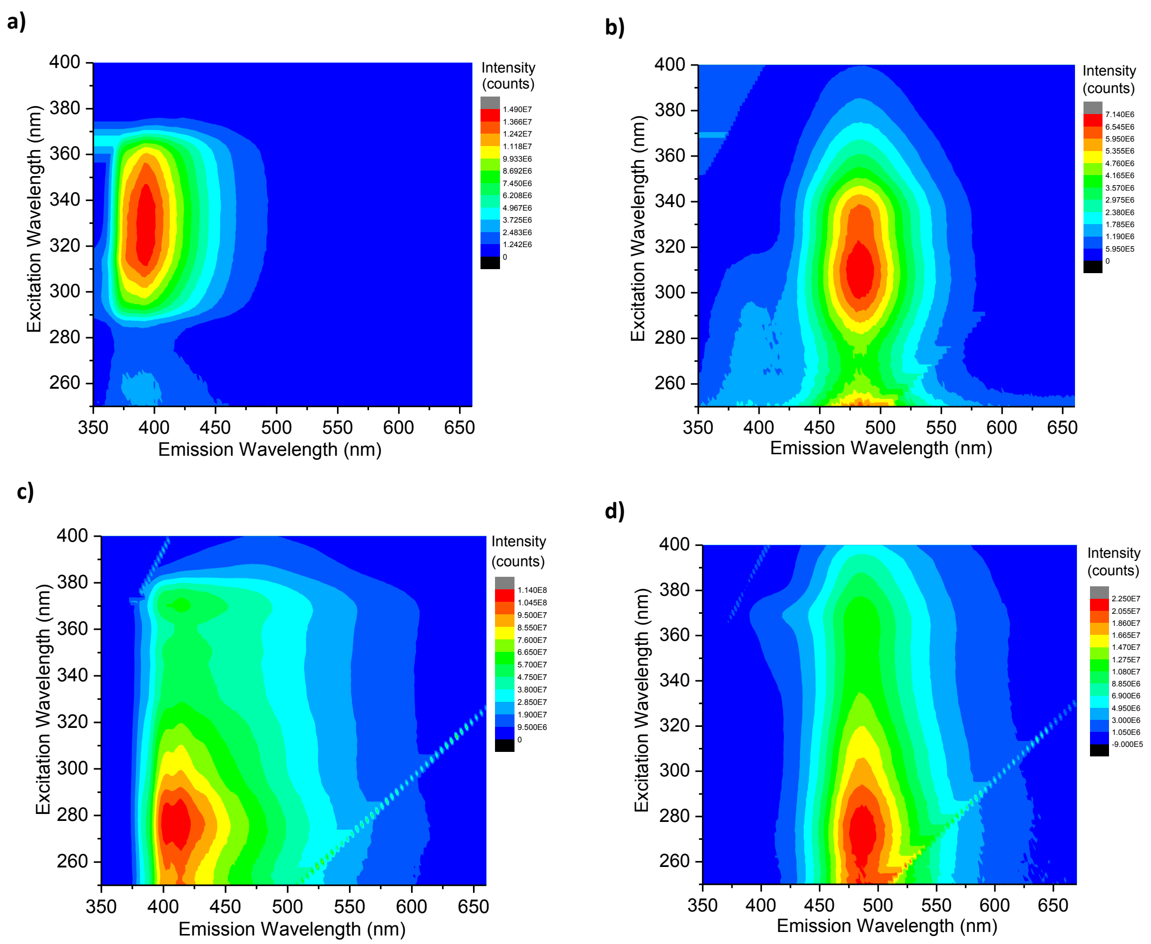

Figure 2.19. The figures show contour map of the observed fluorescence intensity as a function of the fluorescence emission and excitation wavelength for **PE1**. a) THF ($c = 1 \times 10^{-5}$ M), b) THF-water (1:9 v/v) mixture ($c = 1 \times 10^{-5}$ M), c) blue emitting film and d) cyan emitting film.

2.2.6. Application of PE1 as Security Labels

A practical application of the water responsive fluorescent molecular assembly of **PE1** is as a security label for checking the authenticity of currency and documents. Preventing currency counterfeit and document duplication are equally important as war against terrorism. Therefore, point of care authentication of currency and valuable documents has of great importance.[17] The currently used fluorescent labels on currency bills are reproducible and non-responsive to moisture or other stimuli. Therefore, water induced fluorescence color change from blue to cyan with **PE1** assembly is a unique property that can be exploited for making security labels. The fluorescent assembly can be positioned on an appropriate place in the currency, which can be read as a blue emission. To check the authenticity, the blue fluorescent area needs to be touched with a wet finger or a mark should be made with water filled pen. At the point of contact with water, a bright cyan image appears which can be instantly erased with a hot air gun. This blue to cyan color change and its instant reversal to the original blue fluorescence is the signature of the authenticity (Figure 2.20a-c).

We further demonstrated the use of our fluorescent molecular assembly for securing a hundred rupees Indian non-judicial document paper (Figure 2.20d-f). We made a stamp impression with letter written as “GOVT OF INDIA - ORIGINAL” over the document paper. The letters in the stamp impression shows a blue fluorescence under a UV lamp, which upon contact with moisture changed to cyan. The original blue fluorescence is regained after exposing to hot air. This simple, easy to use security system is difficult to duplicate since it is based on a subtle change in the molecular assembly on interaction with water, resulting the fluorescence modulation.

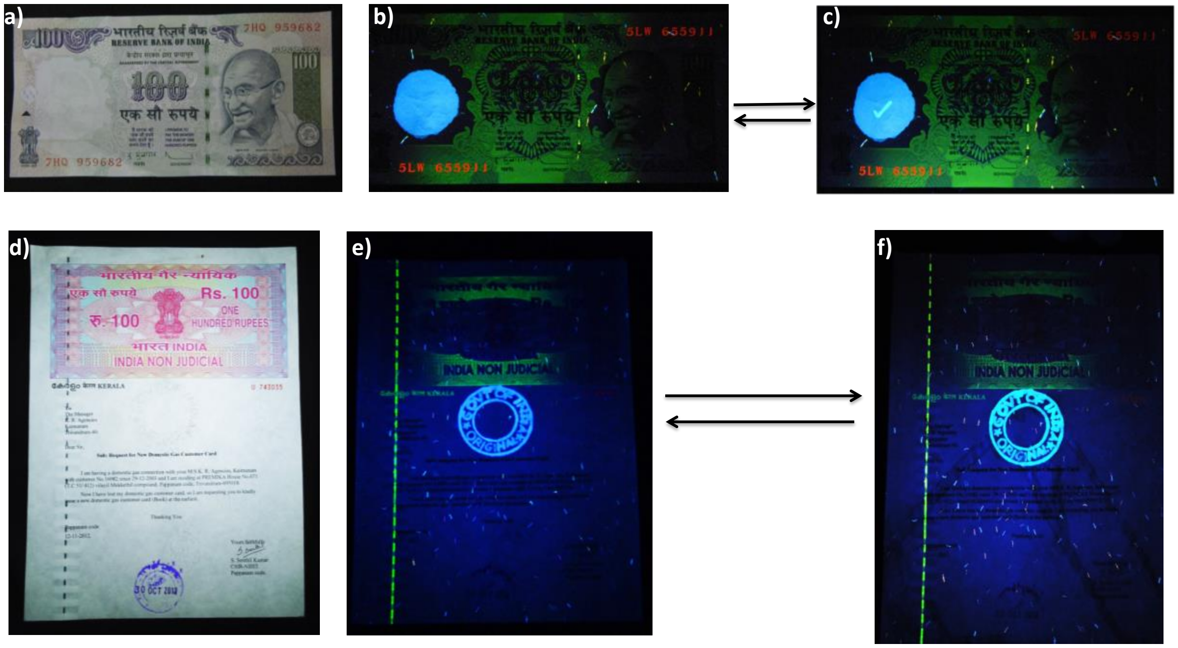

Figure 2.20. Photographs of Indian currency note and a stamp paper a) and d) under day light. b) **PE1** coated currency note. c) Tick mark made using water pen. e) Letters stamped over the stamp paper using **PE1**. f) Fluorescence color change after spraying water (illuminating at 365 nm).

2.2.7. Mechanism of Fluorescence Color Change

In order to obtain a deeper insight on the mechanism of the water induced fluorescence color change, we performed small angle film X-ray analysis (SAXS) of the **PE1** molecular assembly before and after exposing to water. These data are compared with X-ray diffraction pattern of **PE2**. The initial blue emitting film of **PE1** (Figure 2.21a) showed two sharp diffraction patterns at 42.5 and 21.6 Å, which are assigned to an H-type molecular arrangement. The 42.5Å peak corresponds to the width of a single one-dimensional (1-D) layer of the molecules and the 21.6 Å peak corresponds to the rigid rod **PE** moiety. After spraying water, the cyan emitting film showed four sharp diffractions 41.3, 37.5, 24.8 and 21.8 Å of varying intensities

(Figure 2.21b). These peaks indicate the sliding of the molecules in the presence of water.[18] The diffraction peak corresponding 24.8 Å may be associated with the slipped packing of the rigid **PE** moiety and 41.3 Å can be assigned to the total width of the 1-D assembly. The 21.8 and 37.5 Å peaks are assigned to the rigid **PE** part and the total length of the **PE1** molecule respectively. After complete removal of water, the regenerated blue emitting film exhibited the original X-ray pattern revealing the sliding back of the assembly to its original form. The X-ray diffraction pattern of **PE2** film (Figure 2.21c) showed four different peaks (42.6, 35.2, 26.6 and 22.5 Å) almost similar to that of the **PE1** film after water treatment, indicating identical slipped molecular packing. This slipped packing is formed due to the absence of hydrogen bonding amide groups in **PE2**.

A comparison of the diffraction patterns of **PE1** and **PE2** helped us in arriving at a plausible mechanistic pathway for the observed fluorescence variation of **PE1** when it comes in contact with water molecules as depicted in Figure 2.22. Our experimental data suggest a molecular slipping mechanism for the reversible fluorescence modulation. Interaction with water molecules facilitates breaking of the hydrogen bonds and the stretching of the hydrophilic ethoxy chains, which pushes the nearby molecules to the opposite directions along the inward direction. The presence of an amide bond as in **PE1** is essential for the observed reversible fluorescence color change. In the blue phase (B-phase) each molecule is expected to form hydrogen bonds with the adjacent molecules through the amide groups as evident from the FT-

IR spectral data (Figure 2.23). The absence of hydrogen bonding groups makes the molecules to pack in the slipped manner as observed in the case of **PE2** resulting in the cyan (C-phase) emission.

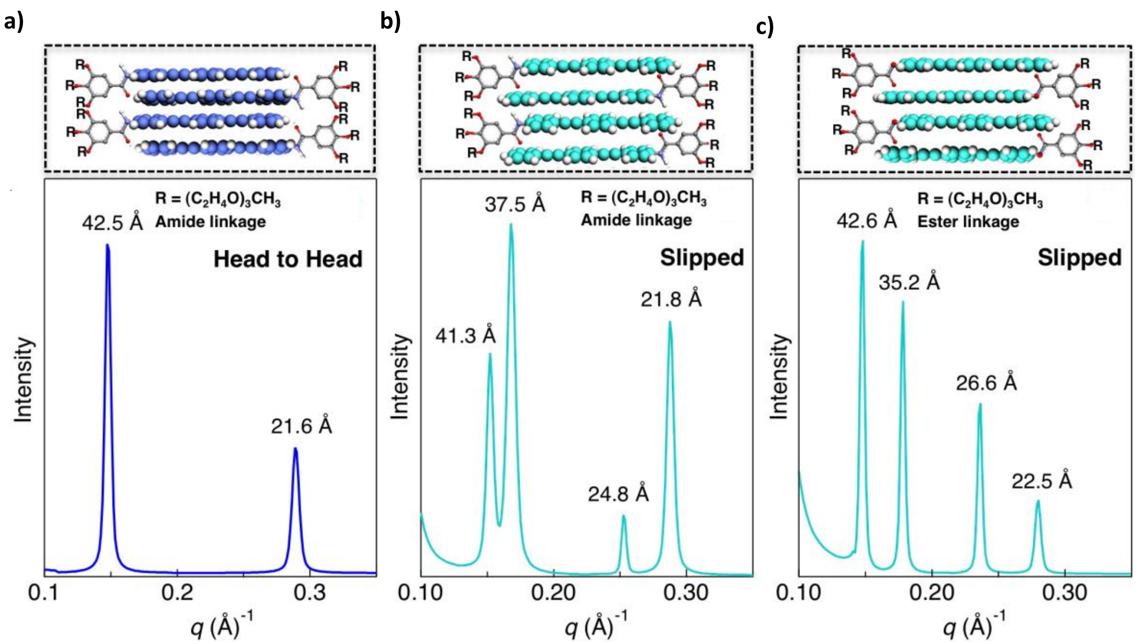

Figure 2.21. SAXS pattern of **PE1** in the a) absence, b) presence of water and c) SAXS pattern of **PE2**. The corresponding molecular arrangements are shown on the top of the SAXS patterns.

FT-IR spectra showed C=O stretching frequency of the B-phase and the C-phase respectively at 1670 cm^{-1} and 1661 cm^{-1}. When compared to the B-phase, C=O stretching frequency of the C-phase is shifted to a lower frequency, suggesting that the initial hydrogen bonds with amide groups weaken and the carbonyl groups enter into hydrogen bond with water molecules,[19] allowing the **PE1** molecules to pack in a slipped manner. Peaks corresponding to amide N-H stretching are not observed;

because the peak corresponding to the O-H stretching of the water molecules are intense enough to hide the N-H stretching peaks.

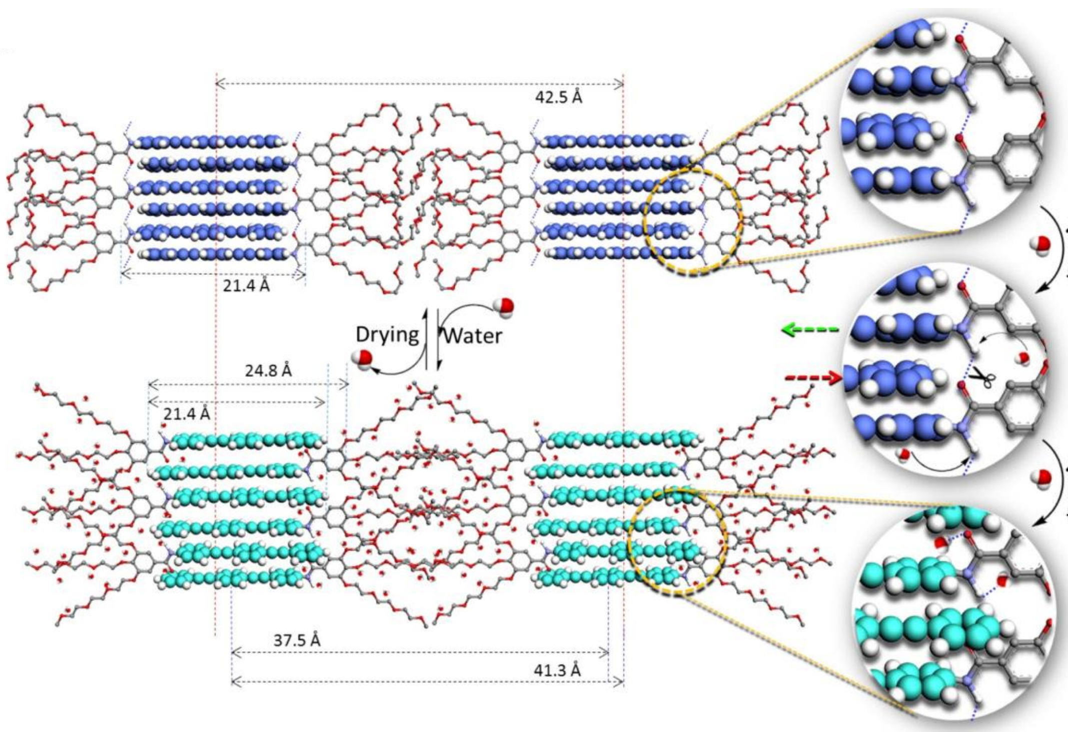

Figure 2.22. Schematic illustration of sliding of the **PE1** molecule in the absence and presence of water on paper surface. Disruption of H-bonds and the breathing of the oxyethylene chains in presence of water experience an inward pushing of the molecules resulting in the change of an H-type (B-phase) to J-type (C-phase) packing. The images in circular panel (right) show the zoomed portion of the molecular arrangement illustrating the H-bond breaking and molecular sliding (arrows show the direction of sliding).

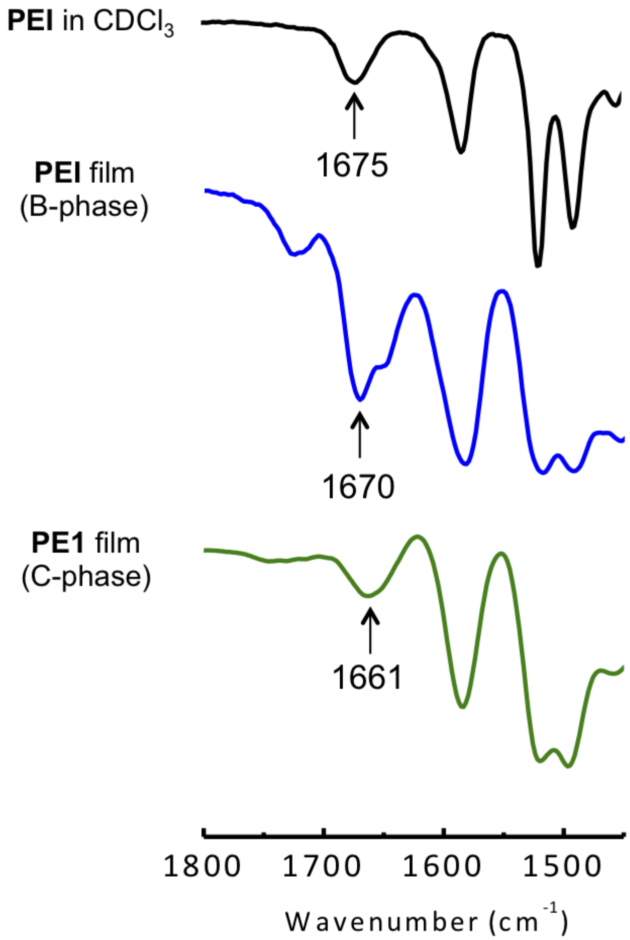

Figure 2.23. FT-IR spectra of dilute solution of **PE1** in $CDCl_3$ (top), blue emitting film (middle) and cyan emitting film (bottom). Arrows indicate amide carbonyl IR bands.

2.3. Conclusions

The present fluorescent molecular assembly has several unique features required for an ideal security system. The “holy grail” of **PE1** is the initial blue fluorescence color of the self-assembly since most of the blue emitting molecules either significantly quenches the fluorescence or shift the color to longer wavelength upon self-assembly. This molecular system not only possess good fluorescence quantum yield but also maintain its initial fluorescence color in the film state. The fluorescence color variation from blue to cyan occurs only with water on contact, and not with moist air, pressure or temperature. It has good photo and thermal stability, well suited for long-term application. Other structural variants of **PE1** do not exhibit blue to cyan fluorescence color change when in contact with water and hence difficult to duplicate. Synthetic reproduction of the molecular system reported here involves several chemical steps, which can be repeated only with trained chemists in standard laboratory conditions. A molecular assembly having these features which can be used as a security label in combination with water induced slipping phenomenon is a unique example and not easily available. This system is needed only in small volumes for large area applications and adaptable to the protection of any paper based documents such as currencies, certificates, judicial stamp papers, and travel documents.

2.4. Experimental Section

2.4.1. Synthesis: General Procedure

Unless otherwise stated, all starting materials and reagents were purchased from commercial suppliers and used without further purification. The solvents were purified and dried by standard methods prior to use. The reactions were monitored using thin layer chromatography (TLC) on silica gel 60 F_{254} (0.2 mm; Merck). Visualization was accomplished using UV lamp (365 nm). Column chromatography was performed on glass columns of different sizes hand packed with silica gel 60 (particle size 0.040–0.063 mm, Merck).

2.4.2. Synthesis: Characterization Techniques

Melting points were determined with MEL-Temp-II melting point apparatus and are uncorrected. ^{1}H (300 and 500 MHz) and ^{13}C NMR (125 MHz) spectra were measured on a Bruker Avance DPX spectrometer. Chemical shifts are reported in parts per million (ppm) using tetramethylsilane (TMS) (δ_H = 0 ppm) or the solvent residual signal ($CDCl_3$: δ_C = 77.00 ppm) as an internal reference. The resonance multiplicity is described as s (singlet), d (doublet), t (triplet) and m (multiplet). IR spectra were recorded on a Perkin-Elmer Spectrum One FT-IR spectrometer using KBr sealed cell and plate for solution and film samples respectively. Mass spectra (MS) were recorded on a Thermo Scientific Q Exactive Hybrid Quadrupole-Orbitrap electrospray ionization mass spectrometer (ESI-MS) or a JEOL JSM 600 fast atom bombardment (FAB) high-resolution mass spectrometer.

2.4.3. Synthesis: Experimental Procedures

Synthesis of methyl 3,4,5-tris(2-(2-(2-methoxyethoxy)ethoxy)ethoxy)benzoate (2): Compound **1** (1.0 g, 5.4 mmol) and K_2CO_3 (3.8 g, 27.0 mmol) were taken in a 250 mL two-neck round bottom flask containing 40 mL dry acetonitrile. The mixture was stirred at room temperature for 30 minutes and 2-(2-(2-methoxyethoxy)ethoxy)ethyl 4-methylbenzenesulfonate (6.0 g, 19.0 mmol) was added dropwise. The reaction mixture was stirred at 80 °C for 48 h. After cooling the reaction mixture to room temperature, the solvent was evaporated under reduced pressure. The residue thus obtained was extracted using chloroform, washed with water, brine and dried over anhydrous sodium sulphate. The crude product was subjected to column chromatography (2% methanol/chloroform) over silica gel that gave the pure product.

Yield: 90%; ^{1}H NMR (500 MHz, $CDCl_3$): δ = 7.26 (s, 2H), 4.20-4.15 (m, 6H), 3.85 (s, 3H), 3.83-3.77 (m, 6H), 3.76-3.70 (m, 6H), 3.69-3.62 (m, 12H), 3.61-3.58 (m, 6H), 3.50 (s, 3H), 3.34 (s, 6H) ppm; HRMS-FAB (m/z): $[M+Na]^+$ calcd. for $C_{29}H_{50}O_{14}$, 645.32; found, 645.70.

Synthesis of 3,4,5-tris(2-(2-(2-methoxyethoxy)ethoxy)ethoxy)benzoic acid (3): Compound **2** (3 g, 4.8 mmol) was taken in a 250 mL round bottom flask containing 50 mL ethanol and 10 mL 0.5 M KOH in ethanol was added to it. The reaction mixture was heated to 80 °C for 12 h and after cooling to room temperature the solvent was evaporated. The residue was extracted using chloroform and shaken well with 10% HCl. The organic layer was washed with water, brine, dried over anhydrous sodium sulphate and then solvent was evaporated under reduced pressure to get the crude product. This was used for next step without further purification.

Yield: 90%; ^{1}H NMR (500 MHz, $CDCl_3$): δ = 7.33 (s, 2H), 4.26-4.19 (m, 6H), 3.89-3.81 (m, 6H), 3.76-3.72 (m, 6H), 3.69-3.63 (m, 12H), 3.57-3.54 (m, 6H), 3.38 (s, 9H) ppm; HRMS-FAB (m/z): $[M+Na]^+$ calcd. for $C_{28}H_{48}O_{14}$, 631.67; found, 631.62.

Synthesis of 3,4,5-tris(2-(2-(2-methoxyethoxy)ethoxy)ethoxy)benzoyl chloride (4): Compound **3** (1 g, 1.64 mmol) was taken in a two-neck round bottom flask containing 20 mL dry dichloromethane under nitrogen atmosphere. $SOCl_2$ (0.5 g, 5.0 mmol) was added dropwise through a syringe. The reaction mixture was stirred at room temperature for 5 h and then purged with nitrogen to remove the solvent and unreacted $SOCl_2$. The residue obtained was used for the next step without purification and characterization.

Synthesis of *N*-(4-iodophenyl)-3,4,5-tris(2-(2-(2-methoxyethoxy)ethoxy)ethoxy) benzamide (6): Iodoaniline **5** (0.44 g, 2.0 mmol) was dissolved in 20 mL dry toluene in a two neck round bottom flask under nitrogen atmosphere. Dry triethylamine (2 mL) was added to the flask and the reaction mixture was stirred to stir at room temperature for 15 min. Compound **4** was dissolved in 10 mL dry toluene separately and added to the reaction flask dropwise followed by stirring at room temperature for 12 h. After completion of reaction, the solvent toluene was evaporated and the residue was extracted using chloroform. The organic layer was washed with water, brine and then dried over anhydrous sodium sulphate. After the removal of solvent, residue was purified on a silica gel column using 5% methanol/chloroform as an eluent.

Yield: 75%; ^{1}H NMR (500 MHz, $CDCl_3$): δ = 8.74 (s, 1H), 7.64 (d, J = 8.5 Hz, 2H), 7.51 (d, J = 9.0 Hz, 2H), 7.22 (s, 2H), 4.21-4.19 (m, 6H), 3.83-3.79 (m, 6H), 3.76-3.72 (m, 6H), 3.69-3.63 (m, 12H), 3.53-3.50 (m, 6H), 3.37 (s, 3H), 3.32 (s, 6H) ppm; HRMS-FAB (m/z): $[M+Na]^+$ calcd. for $C_{34}H_{52}INO_{13}$,832.25; found, 832.75.

Synthesis of 4-iodophenyl 3,4,5-tris(2-(2-(2-methoxyethoxy)ethoxy)ethoxy) benzoate (8): Iodophenol **7** (0.44 g, 2.0 mmol) was dissolved in 20 mL dry toluene in 250 mL two neck round bottom flask under nitrogen atmosphere. Dry triethylamine (2 mL) was added to the flask and the reaction mixture stirred at room temperature for 15 min. Compound **4** was dissolved in 10 mL dry toluene separately and added to the reaction flask dropwise. The reaction mixture was continued to stir at room temperature for 12 h. After completion of the reaction, solvent toluene was evaporated under reduced pressure and the residue was extracted using chloroform. The organic layer was washed with water, brine and then dried over anhydrous sodium sulphate. After the removal of solvent, residue was purified by silica gel column chromatography using 5% methanol/chloroform as an eluent.

Yield: 75%; ^{1}H NMR (500 MHz, $CDCl_3$): δ = 7.74 (d, J = 8.5 Hz, 2H), 7.43 (s, 2H), 6.98 (d, J = 8.5 Hz, 2H), 4.28-4.22 (m, 6H), 3.89-3.82 (m, 6H), 3.76-3.72 (m, 6H), 3.69-3.63 (m, 12H), 3.56-3.53 (m, 6H), 3.38 (s, 3H), 3.37 (s, 6H) ppm; HRMS-FAB (m/z): $[M+Na]^+$ calcd. for $C_{34}H_{51}IO_{14}$,833.23; found, 833.22.

Synthesis of trimethyl((4-(phenylethynyl)phenyl)ethynyl)silane (11): In a two neck round bottom flask purged with argon, ((4-iodophenyl)ethynyl)trimethylsilane **10** (0.5 g, 1.67 mmol), $Pd(PPh_3)_2Cl_2$ (0.1 g, 0.17 mmol) and CuI (0.03 g, 0.1 mmol) were dissolved in a degassed 20 mL (1:1) mixture of triethylamine and THF. Phenylacetylene **9** (0.2 g, 2.0 mmol) was added to the reaction mixture and stirred at room temperature under argon atmosphere for 12 h. After completion of reaction, chloroform (50 mL) was added to the reaction mixture and then stirred well with 10% HCl to neutralize triethylamine. The organic layer was washed with water, brine and then dried over anhydrous sodium sulphate. After the removal of solvent, the residue was purified by silica gel column chromatography using 2% ethylacetate/hexane as an eluent.

Yield: 92%; ^{1}H NMR (500 MHz, $CDCl_3$): δ = 7.53-7.51 (m, 2H), 7.47-7.43 (m, 4H), 7.36-7.34 (m, 3H), 0.26 (s, 9H) ppm; HRMS-FAB (m/z): $[M]^+$ calcd. for $C_{19}H_{18}Si$, 274.12; found, 274.71.

Synthesis of 1-ethynyl-4-(phenylethynyl)benzene (12): To a solution of **11** (0.42 g, 1.71 mmol) in 5 mL dichloromethane, KF (1.0 g, 17.0 mmol) in 15 mL methanol was added to it and allowed to stir at room temperature for 6 h. After completion of the reaction, the reaction mixture was extracted using chloroform, washed with water, brine and then dried over anhydrous sodium sulphate. Solvent was evaporated under reduced pressure and the residue was used for the next step without further purification.

Yield: 93%; ^{1}H NMR (500 MHz, $CDCl_3$): δ =7.54-7.52 (m, 2H), 7.50-7.46 (m, 4H), 7.37-7.35 (m, 3H), 3.17 (s, 1H) ppm; HRMS-FAB (m/z): $[M]^+$ calcd. for C_6H_{10}, 202.08; found, 202.49.

Synthesis and characterization of PE derivatives. In a general synthetic procedure, the aryl halide (0.80 mmol), bis(triphenylphosphine)palladium (II) dichloride (10 mol%), and copper (I) iodide (10 mol%) were added to an oven-dried two neck round bottom flask equipped with a magnetic stirring bar. The round bottom flask was then sealed with a rubber septum, evacuated and backfilled with argon three times.

Degassed triethylamine (10 mL) was added followed by degassed THF (10 mL) to serve as the co-solvent. After stirring for 5 minutes at room temperature, the terminal alkyne 1-ethynyl-4-(phenylethynyl)benzene (0.96 mmol) dissolved in 10 mL (1:1) mixture of degassed triethylamine and THF was added. The reaction mixture was stirred at room temperature until complete reaction was noted by the TLC. The content was extracted using chloroform and washed with dilute hydrochloric acid. The organic layer was washed with brine and dried over anhydrous sodium sulphate and then evaporated under reduced pressure. The crude product was then purified by column chromatography using silica gel as adsorbent.

PE1: Yield, 57%; m.p.: 67-69 ^oC; TLC ($CHCl_3$:MeOH, 95:5 v/v): R_f = 0.48; ^1H NMR (500 MHz, $CDCl_3$): δ = 8.64 (s, 1H), 7.73 (d, J = 8.5 Hz, 2H), 7.55-7.7.51 (m, 8H), 7.36-7.35 (m, 3H), 7.25 (s, 2H), 4.25-4.23 (m, 6H), 3.85-3.80 (m, 6H), 3.73-3.71 (m, 6H), 3.68-3.63 (m, 12H), 3.53-3.51 (m, 6H), 3.38 (s, 3H), 3.32 (s, 6H) ppm; ^{13}C NMR (125 MHz, $CDCl_3$): δ = 165.5, 152.5, 142.2, 138.8, 132.3, 131.6, 131.5, 131.44, 129.9, 128.4, 128.3, 123.2, 123.1, 122.9, 120.1, 118.43, 107.9, 91.3, 91.2, 89.1, 88.8, 72.3, 71.9, 71.8, 70.7, 70.6, 70.6, 70.4, 69.82, 69.19, 58.9, 58.2 ppm; IR (KBr): 3240, 2874, 2208, 1667, 1585 cm^{-1}; ESI-MS (m/z): $[M+Na]^+$ calcd. For $C_{50}H_{61}NO_{13}$, 906.41; found, 906.40.

PE2: Yield, 60%; m.p.: 58-60 ^oC; TLC ($CHCl_3$:MeOH, 95:5 v/v): R_f = 0.52; ^1H NMR (500 MHz, $CDCl_3$): δ = 7.60 (d, J = 8.5 Hz, 2H), 7.55-7.52 (m, 6H), 7.45 (s, 2H), 7.37-7.35 (m, 3H), 7.21 (d, J = 8.5 Hz, 2H), 4.28-4.24 (m, 6H), 3.89-3.82 (m, 6H), 3.76-3.72 (m, 6H), 3.69-3.63 (m, 12H), 3.56-3.53 (m, 6H), 3.37 (s, 3H), 3.36 (s, 6H) ppm; ^{13}C NMR (125 MHz, $CDCl_3$): δ = 163.4, 151.5, 150.1, 142.4, 131.9, 130.6, 130.5, 127.5, 127.4, 122.9, 122.2, 122.1, 121.9, 121.0, 108.8, 98.9, 90.28, 89.5, 88.25, 88.1, 71.7, 71.2, 70.0, 69.8, 69.7, 68.8, 68.14, 58.18 ppm; IR (KBr): 2876, 2212, 1734, 1587 cm^{-1}; ESI-MS (m/z): $[M+Na]^+$ calcd. for $C_{50}H_{60}O_{14}$, 907.40; found, 907.39.

2.4.4. Preparation of Fluorescent Papers and Security Labels

A solution was prepared by dissolving **PE1** (2.7 mg) in chloroform (3 mL) at room temperature. 2 mL of this solution ($c = 1 \times 10^{-3}$ M) was coated on paper strips (7 cm × 5 cm) and dried over a period of 30 min under vacuum. These paper strips were used as self-healing writing pads using a pen filled with ordinary water. Security labels were created over documents such as banknotes or stamped papers by coating the **PE1** solutions followed by drying under vacuum for 30 min. Over this layer a tick mark was made with a pen filled with ordinary water. The marked area showed a cyan color whereas the untouched area appeared in blue upon illumination with a UV lamp (365 nm). After reading, the mark was erased on keeping for 3–4 h at room temperature or drying with hot air (maintained at ~ 70–80 °C) for 2 min. For printing over document papers, fluorescent ink was prepared by mixing 1 mL chloroform solution of **PE1** ($c = 1 \times 10^{-3}$ M) with 1.5 mL of polydimethylsiloxane (PDMS). This ink was used for creating impressions on documents using prefabricated stamps, which served as the security mark.

2.4.5. Description on Experimental Techniques

Optical Measurements: The solvents for the spectroscopic measurements are spectroscopic grade (99.8 %) and were used as received. The UV/Vis absorption spectra were recorded on a Shimadzu spectrophotometer UV-2100. The emission spectra were recorded on a SPEX-Flourolog-3 FL3-221 spectrofluorimeter using a front face sample holder. Fluorescence lifetimes were measured using IBH (FluoroCube) time-correlated picosecond single photon counting (TCSPC) system. The lifetime values were obtained using DAS6 decay analysis software. The quality of the fit has been judged by the fitting parameters such as χ^2 (< 1.1) as well as the visual inspection of the residuals.

Fluorescence Quantum Yield Measurements:

Fluorescence quantum yield (Φ_s) of **PE** derivatives were determined using quinine sulfate (Φ_r = 0.546 in 0.1 N H_2SO_4) as the reference standard. The experiments were done using optically matching solutions and the quantum yield was calculated using equation 1,

$$\Phi_s = \Phi_r \, (A_r F_s / A_s F_r) \, (\eta_s^2 / \eta_r^2) \qquad \text{--------} \ (1)$$

where, A_s and A_r are the absorbance of the sample and reference solutions respectively at the same excitation wavelength, F_s and F_r are the corresponding relative integrated fluorescence intensities and η is the refractive index of the solvent.

Fluorescence quantum yield in the film state were measured using a calibrated integrating sphere attached to a SPEX Fluorolog spectrofluorimeter. A Xe arc lamp was used to excite the sample placed in the sphere with λ = 340 nm as the excitation wavelength. The absolute fluorescence quantum yield was calculated based on the de Mello method by using Equation (2):

$$\Phi_{PL} = [E_i(\lambda) - (1\text{-}A)\, E_0(\lambda)] \,/\, L_e(\lambda)A \qquad \text{---------(2)}$$

For equation (2):

$$A = [L_0(\lambda) - L_i(\lambda)] \,/\, L_0(\lambda) \qquad \text{----------(3)}$$

where $E_i(\lambda)$ and $E_0(\lambda)$ are the integrated luminescence as a result of the direct excitation of sample and secondary excitation, respectively; A is the absorbance of the sample calculated using Equation (3); $L_i(\lambda)$ is the integrated excitation when the sample is directly excited; $L_0(\lambda)$ is the integrated excitation when the excitation light first hits the sphere and reflects into the sample; and $L_e(\lambda)$ is the integrated excitation profile for an empty sphere.

Transmission Electron Microscopy (TEM): Transmission Electron Microscopy was performed on a JEOL-JEM0310 microscope with an accelerating voltage of 100 kV. Samples were prepared by drop casting the aggregated solution from *n*-decane on carbon coated copper grids and the TEM pictures were obtained without staining.

Scanning Electron Microscopy (SEM): SEM images were obtained on a JEOL 5600 LV scanning electron microscope with an accelerating voltage of 12–15 kV after sputtering with gold.

Fluorescent Microscopic Studies: Fluorescent microscopic images were recorded on a Leica-DMIR2 Optical Microscope using UV light (340-380 nm) as the excitation source. Samples were prepared by drop casting aggregated solution of **PE** on a glass slide followed by slow evaporation.

Small Angle X-ray diffraction (SAXS): Small angle 2D-X-ray scattering were measured using Xeuss instruments. Cu-Kα (wavelength, λ = 1.54 Å) is the X-ray source with collimated area of 0.64 mm^2. Sample to detector distance is 221.75/1050 mm for SAXS measurements respectively; silver behenate is used for distances calibration. 2D-X-ray scattering data were azimuthally integrated using Fit-2D software.

2.5. References

[1] (*a*) Q. Wang, J. L. Mynar, M. Yoshida, E. Lee, M. Lee, K. Okuro, K. Kinbara, T. Aida, *Nature*, **2010**, *463*, 339–343; (*b*) P. H. Kouwer, M. Koepf, V. A. A. Le Sage, M. Jaspers, A. M. van Buul, Z. H. Eksteen-Akeroyd, T. Woltinge, E. Schwartz, H. J. Kitto, R. Hoogenboom, S. J. Picken, R. J. M. Nolte, E. Mendes, A. E. Rowan, *Nature*,**2013**, *493*, 651–655.

[2] (*a*) J. Lee, M. Pyo, S. Lee, J. Kim, M. Ra, W.-Y. Kim, B. Park, C. Lee, J.-M. Kim, *Nat. Commun.* **2014**, *5*, 3736; (*b*) L. Sheng, M. Li, S. Zhu, H. Li, G. Xi, Y.-G. G. Li, Y. Wang, Q. Li, S. Liang, K. Zhong, et al., *Nat. Commun.* **2014**, *5*, 3044.

[3] (*a*) A. Kishimura, T. Yamashita, K. Yamaguchi, T. Aida, *Nat. Mater.* **2005**, *4*, 546–549; (*b*) R. Klajn, P. J. Wesson, K. J. Bishop, B. A. Grzybowski, *Angew. Chem., Int. Ed.* **2009**, *48*, 7035–7039.

[4] G. Iftime, N. Chopra, P. M. Kazmaier, *Reimageable paper*, 2008, US 7381506 B2.

[5] (*a*) B. Hardwick, W. Jackson, G. Wilson, A. W. Mau, *Adv. Mater.* **2001**, *13*, 980–984; (*b*) E. L. Prime, D. H. Solomon, *Angew. Chem., Int. Ed.* **2010**, *49*,

3726–3736; (*c*) N. Mizoshita, T. Tani, S. Inagaki, *Adv. Mater.* **2012**, *24*, 3350–3355;

[6] (*a*) B. Yoon, D.-Y. Y. Ham, O. Yarimaga, H. An, C. W. Lee, J.-M. Kim, *Adv. Mater.* **2011**, *23*, 5492–5497; (*b*) B. Yoon, J. Lee, I. Park, S. Jeon, J. Lee, J.-M. Kim, *J. Mater. Chem. C,* **2013**, *1*, 2388–2403.

[7] B. Yoon, H. Shin, O. Yarimaga, D.-Y. Ham, J. Kim, I. Park, J.-M. Kim, *J. Mater. Chem.* **2012**, *22*, 8680–8686.

[8] S. Dei, A. Matsumoto, A. Matsumoto, *Macromolecules,* **2008**, *41*, 2467–2473.

[9] M. F. Rubner, D. J. Sandman, C. Velazquez, *Macromolecules*, **1987**, *20*, 1296–1300.

[10] P. Kumar, J. Dwivedi, B. K. Gupta, *J. Mater. Chem. C*, **2014**, ***2***, 10468–10475.

[11] (*a*) B. L. Volodin, B. Kippelen, K. Meerholz, B. Javidi, N. Peyghambarian, *Nature* **1996**, *83*, 58–60; (*b*) S. Armstrong, O. Graydon, D. Pile, R. Won, *Nat. Photonics* **2012**, *6*, 801; (*c*) J. M. Meruga, W. M. Cross, P. S. May, Q. Luu, G. A. Crawford, J. J. Kellar, *Nanotechnology* **2012**, *23*, 395201.

[12] (*a*) Y. Cui, R. S. Hegde, I. Y. Phang, H. K. Lee, X. Y. Ling, *Nanoscale* **2014**, *6*, 282–288; (*b*) R. Abargues, P. J. Rodriguez-Canto, S. Albert, I. Suarez, P. Martínez-Pastor, *J. Mater. Chem. C*, **2014**, *2*, 908–915.

[13] K. Sonogashira, Y. Tohda, N. Hagihara, *Tetrahedran Lett.* **1975**, *16*, 4467-4470.

[14] Y. Hong, J. W. Lam, B. Z. Tang, *Chem. Soc. Rev*, **2011**,*40*, 5361–5388.

[15] S.-J. J. Yoon, J. W. Chung, J. Gierschner, K. S. Kim, M.-G. G. Choi, D. Kim, S. Y. Park, *J. Am. Chem. Soc.* **2010**, *132*, 13675–13683.

[16] Y. Sagara, T. Komatsu, T. Ueno, K. Hanaoka, T. Kato, T. Nagano, *Adv. Funct. Mater.* **2013**, *23*, 5277–5284.

[17] (*a*) J. Andres, R. Hersch, J. Moser, A. Chauvin, *Adv. Funct. Mater.* **2014**, *24*, 5029–5036. (*b*) E. L. Prime, D. H. Solomon, *Angew. Chem., Int. Ed.* **2010**, *49*, 3726–3736.

[18] (*a*) Z. Huang, S.-K. Kang, M. Banno, T. Yamaguchi, D. Lee, C. Seok, E. Yashima, M. Lee, *Science* **2012**, *337*, 1521–1526; (*b*) W. Zhang, T. Aida, *Science* **2012**, *337*, 1462–1463.

[19] R. Iwamoto, *J. Phys. Chem. A* **2010**, *114*, 7398–7407.

Chapter 3

Two Stage Self-Assembly and Gelation of a π-Gelator

Abstract

Modulation of photophysical properties through different aggregation pathways has emerged as a promising approach to the design of responsive materials. Particularly, switching the emission properties by controlling the molecular packing mode instead of modifying the chemical structure is quite challenging. Herein we report a cyano substituted phenyleneethynylene ***PE-CN****, which in the gel state, depending on rate of cooling, exhibits transformation of highly ordered lamellar to columnar structure accompanied by emission shift from blue to green respectively. Similar luminescence switching and molecular packing variation were observed even by simply varying the concentration of the gelator. The nature of molecular assembly was established with the help of fluorescence spectroscopy, small-angle X-ray scattering (SAXS), FT-IR, SEM and TEM analyses. FP-TRMC study of the* ***PE-CN*** *xerogel revealed nearly 1000 times more of the charge carrier mobility half-life time for the green emitting gel than the blue one. The gelation allows the trapping of the green state for a sufficiently long duration with the tendency of reverting back to a thermodynamically stable blue state. The molecular assembly obtained by* ***PE*** *without a cyano group does not show any*

emission switching properties which highlights the role of the cyano group in the observed properties of ***PE-CN****.*

3.1. Introduction

Functional π-conjugated oligomers are able to organize into well-defined nanoarchitectures through noncovalent interactions many of which are useful for the fabrication of organic electronic devices.[1] Especially the bottom-up construction of one-dimensional (1D) nanostructures has received more attention due to their ability to create high charge carriers.[2] These nanostructures can be used as smart nanomaterials based on their stimuli responsive and well-controlled electronic properties.[3] Among various stimuli temperature is considered to be the most convenient to regulate well-defined nanostructures.

Yagai and co-workers have reported thermally interconvertible semiconductive nanorods and nanotapes comprising of oligothiophenes with high charge-carrier mobilities in their condensed state.[4] These authors have prepared a quaterthiophene and functionalized its one end with barbituric acid (BA) while the other end was functionalized by a tridodecyloxybenzyl tail (**QT-BA**, Figure 3.1). Atomic force microscopy (AFM) of the H-aggregated **QT-BA** exhibited uniform rod-like nanostructures. X-ray diffraction of **QT-BA** in the film state, revealed the formation of a hexagonally columnar assembly with a lattice constant of $a = 6.6$ nm. However, the addition of one equivalent of the bismelamine, **BM** to a solution of the H-aggregated **QT-BA** resulted in the disruption of the assembly leading to the formation of supramolecular copolymers of **QT-BA** and **BM** through complementary triple H-bonds. AFM images of the co-aggregates displayed flat, tape-like nanostructures. In addition, X-ray diffraction pattern of a solvent free film showed the formation of multilamellar superstructures with an interlayer spacing of 3.2 nm. Flash-photolysis time resolved microwave conductivity (FP-TRMC) measurements showed that the hole mobilities of the hexagonally-packed nanorods is higher than that of the multilamellar nanotapes. Interestingly, the nano-tapes can be changed to nanorods upon heating the solution of co-aggregates **QT-BA** and **BM** to 70 °C as revealed from the AFM analysis.

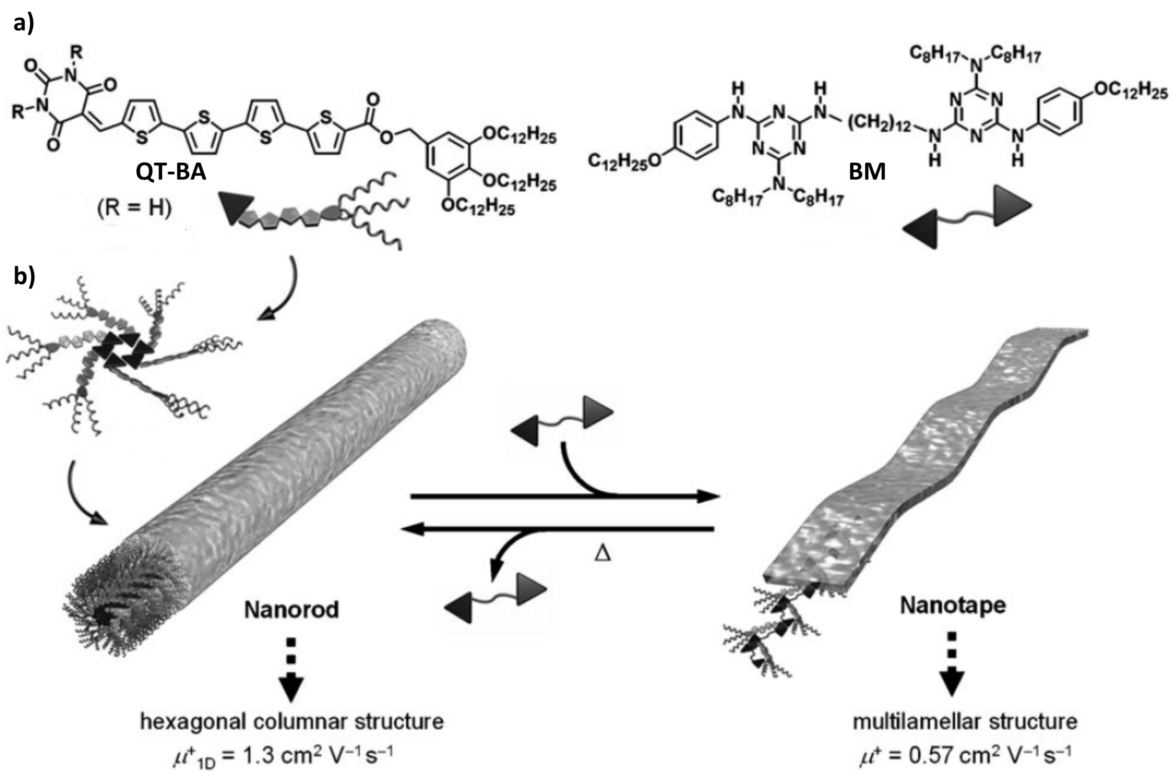

Figure 3.1. a) Molecular structures of **QT-BA and BM**. Schematic representation of b) lamellar and c) columnar structures. (Adapted with permission from ref. 4. Copyright 2008 Wiley-VCH.)

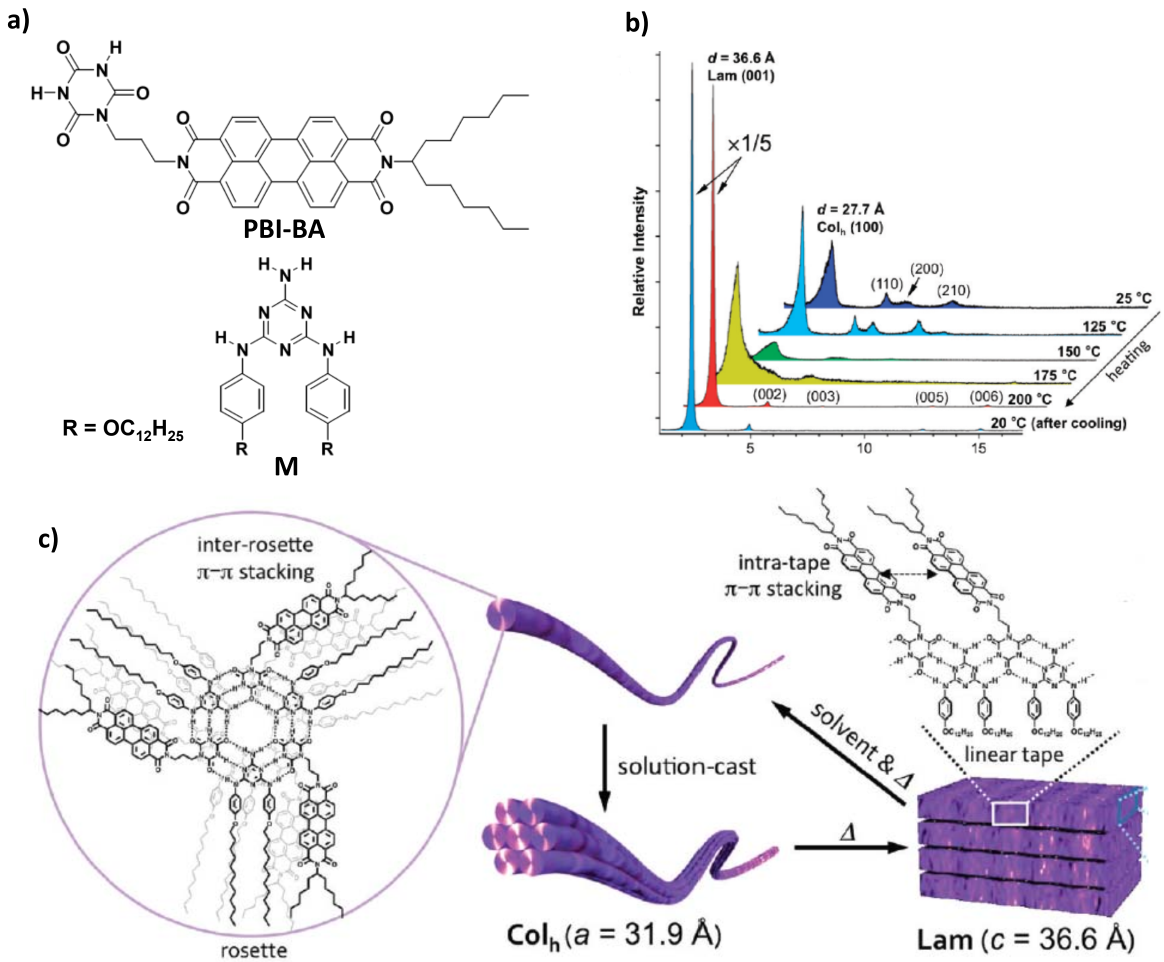

Figure 3.2. a) Molecular structures of **PBI-BA** and **M**. b) Variable temperature XRD experiments of a film of **PBI-BA** and **M**. c) Schematic representation of thermoresponsive supramolecular organization of **PBI-BA** and **M**. Adapted with permission from ref. 5. Copyright 2012 American Chemical Society.)

A well-defined columnar assembly has been reported from the film made of 1:1 mixture of perylene tetracarboxylic acid bisimide-barbituric acid (**PBI-BA**) and melamine **M** (Figure 3.2).[5] The authors have suggested that H-bonded rosettes possessing three PBI and three melamine units formed in the solution are hierarchically organized into cylindrical columnar assemblies in the film state (Figure

3.2c). X-ray diffraction studies have confirmed the formation of hexagonal columnar structure for the solution cast film. These columnar assemblies show fibrillar nanostructures that could also be visualized by TEM and AFM.

Temperature-dependent X-ray diffraction studies have revealed the transition from the columnar structure in the bulk state to a highly ordered lamellar structure (Figure 3.2b). FT-IR studies showed that the structural transition is due to the rearrangement of the H-bonding motifs. FP-TRMC measurements showed a remarkable increase in the transient photoconductivity upon converting the columnar structure to lamellar assembly. Furthermore, transient absorption spectroscopy revealed that the electron transfer takes place from the electron-donating alkoxyphenyl groups of melamine components to the electron-deficient PBI moieties in the lamellar structure, resulting in a higher charge carrier generation. The above result illustrates a new approach to thermo responsive functional materials.

Organic materials with ability to switch their photoluminescent properties in response to various external stimuli have attracted considerable attention because of their potential application for memory devices, sensors, security materials, and displays.[6–10] Furthermore, switching and tuning of fluorescence, by controlling the mode of molecular packing [11] and this variation of the luminescent colors by thermal stimuli have already been reported in single crystals,[12] liquid crystals,[13] as well as in polymers.[14]

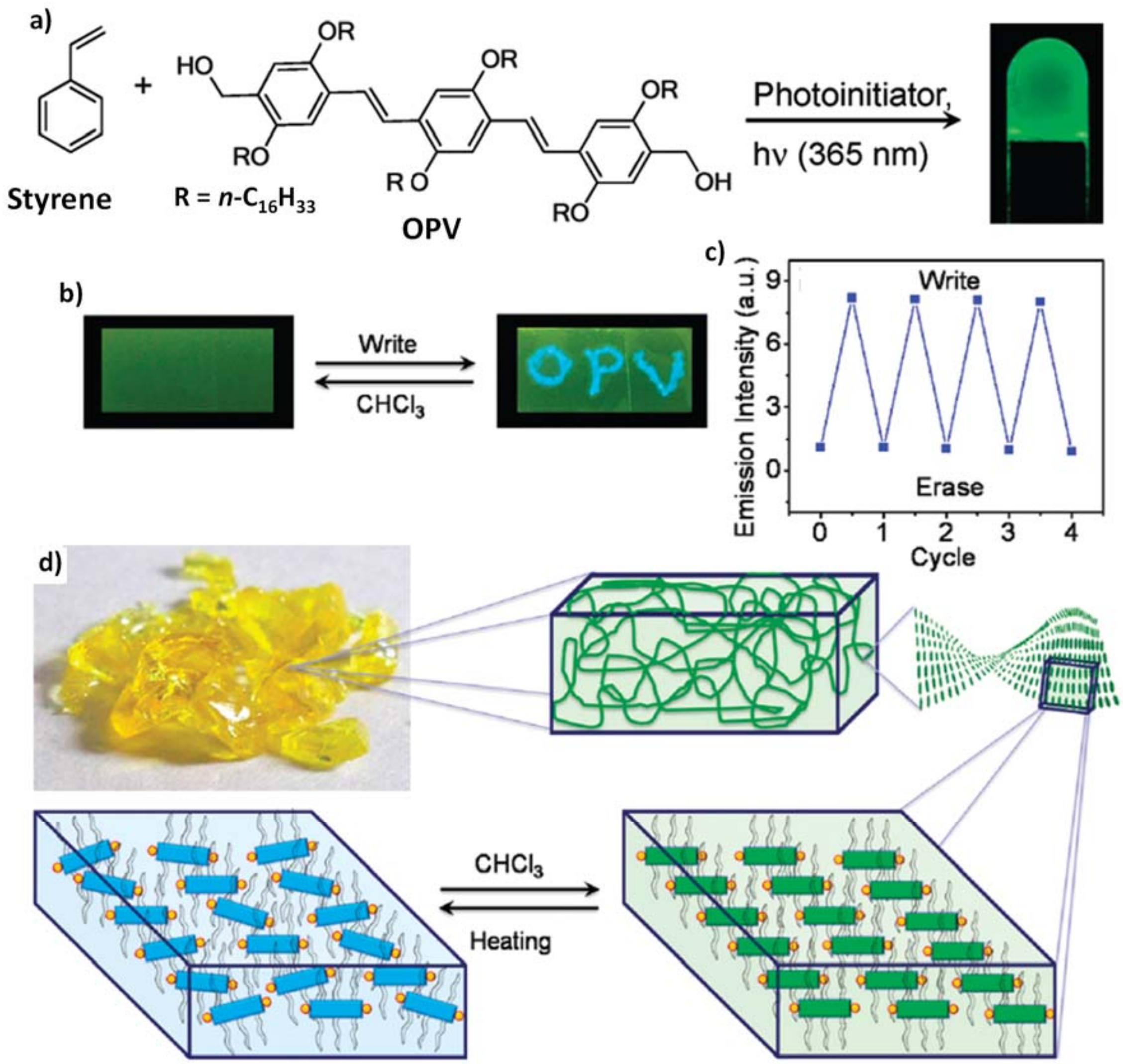

Figure 3.3. a) Photopolymerization of a fluorescent gel of **OPV** in styrene. b) Thermal writing and erasal on a film of **OPV** in polystyrene. c) Fluorescence response of the **OPV-Polystyrene** film over four continuous cycles of writing and erasing. d) Schematic representation of the solvent vapor assisted reversible self-assembly of **OPV** in polystyrene.

Fluorescence of π-gelators undergoes significant change upon gelation. These changes have been found very predominant in the case of gels when compared to the corresponding solution. Therefore, fluorescent organogels can be used for fluorescence imaging as well as sensing various analytes such as acids, explosives and volatile organic compounds. Since the excitonic interactions during gelation leads to significant changes in the optical and physical properties of the gelators, it is easier to follow the changes when used as a sensor. From our group, we have demonstrated gelation-assisted trapping of fluorescent supramolecular architectures in a polymer film and its application in erasable thermal imaging (Figure 3.3).[15] A film prepared from the composite containing fluorescent **OPV** gelator and styrene polymer showed a green fluorescence due to the self-assembled gelator which turned light blue upon heating due to the disassembly of the gelator. The green emission could be recovered upon exposure of the film to chloroform. This has been used to create stable images which were visible only under UV light and could be erased and rewritten any number of times.

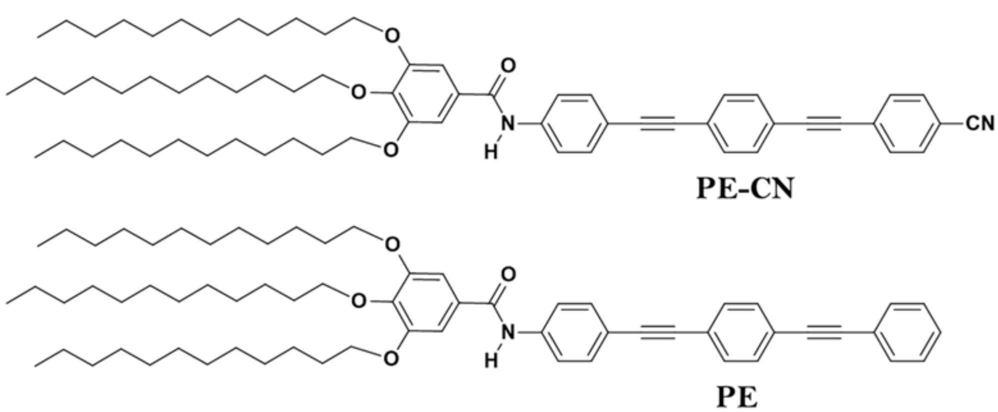

Figure 3.4. Structure of **PE-CN** and **PE** under investigations.

External stimuli such as temperature (heating or cooling) can be further exploited for switching the luminescent properties of molecular assemblies by controlling the different molecular packing in the gel state. In the present study, we have investigated the cyano substituted phenyleneethynylene derivative **PE-CN** and a control compound **PE** for their self-assembly, gelation, optical and morphological properties. For this purpose, **PE-CN** and **PE** with and without cyano group having H-bonding motif (Figure 3.4) were synthesized and characterized.

3.2. Results and Discussion

3.2.1. Synthesis of PE-CN and PE

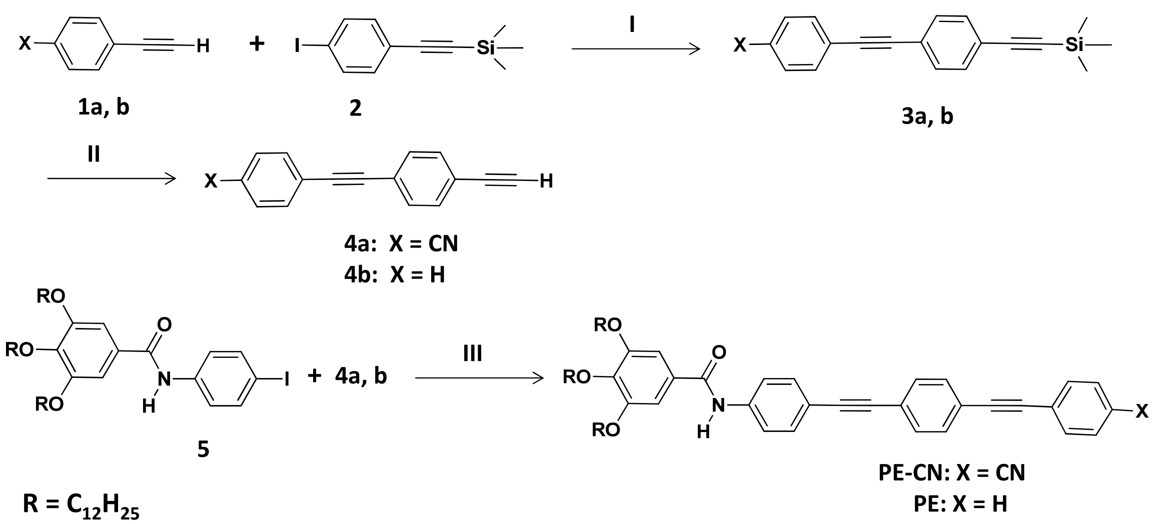

Scheme 3.1. Synthesis of **PE-CN**. Reagents and conditions: I) $PdCl_2(PPh_3)_2$, CuI, THF, Et_3N, rt., 12 h; II) KF, CH_2Cl_2, CH_3OH, rt., 6 h; III) $PdCl_2(PPh_3)_2$, CuI, THF, Et_3N, rt., 24 h.

The precursor 4-((4-Ethynylphenyl)ethynyl)benzonitrile **4a** was prepared from 4-ethynylbenzonitrile **1a** which on Sonogashira-Hagihara cross coupling with ((4-iodophenyl)ethynyl)trimethylsilane **2** in the presence of $PdCl_2(PPh_3)_2$ and CuI gave 4-((4-((trimethylsilyl)ethynyl)phenyl)ethynyl)benzonitrile **3a**. Desilylation of **3a** in the presence of potassium fluoride gave **4a** (Scheme 3.1). The precursor 3,4,5-tris(dodecyloxy)-*N*-(4-iodophenyl)benzamide **5** was synthesized according to the procedure given in Chapter 2. The Sonogashira-Hagihara coupling between **5** and 4-

((4-ethynylphenyl)ethynyl) benzonitrile **4a** using $Pd(PPh_3)_2(Cl_2)_2$ and CuI afforded **PE-CN** in 52% yield. Similarly, **PE** was also synthesized in 48% yield.

3.2.2. Aggregation and Optical Properties

To understand the aggregation behavior of **PE-CN** and **PE**, UV-Vis absorption studies in chloroform and *n*-decane have been carried out. In chloroform at 25 °C, **PE-CN** ($c = 1 \times 10^{-4}$ M) showed a strong π-π* absorption band at 342 nm (Figure 3.5a). However, in *n*-decane ($c = 1 \times 10^{-4}$ M) at 25 °C, a decrease in the intensity of absorption maximum at 342 nm was observed along with the formation of a new shoulder band at 392 nm (Figure 3.5a). Similarly, the absorption spectra of **PE** in chloroform ($c = 1 \times 10^{-4}$ M) at 25 °C, exhibited a strong π-π* absorption band at 333 nm, while in *n*-decane, at same condition the absorption maximum was found blue shifted to 306 nm with the formation of a new band at 372 nm (Figure 3.5b).

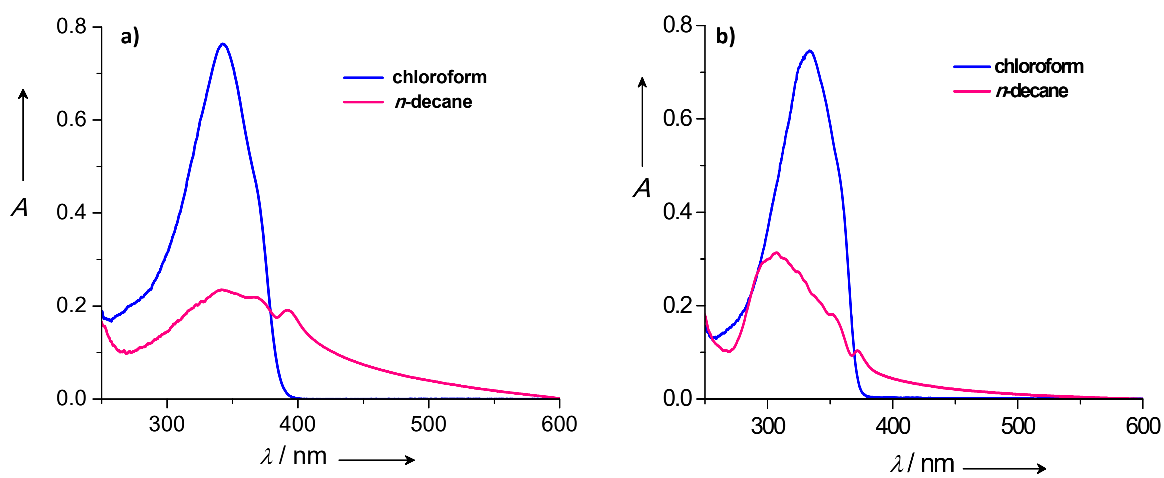

Figure 3.5. Absorption spectra of a) **PE-CN** and b) **PE** in chloroform (——) and *n*-decane (——) at 25 °C ($c = 1 \times 10^{-4}$ M).

The distinct absorption features observed in *n*-decane in comparison to that in chloroform indicate that both **PE-CN** and **PE** exist as aggregates and monomers in these solvents, respectively. In order to understand the molecule aggregation, we have carried detailed variable temperature absorption studies of both **PE-CN** and **PE** in *n*-decane. **PE-CN** in *n*-decane showed a transition from the self-assembled species to the molecularly dissolved species as the temperature increased from 20 to 70 °C (Figure 3.6a). Upon heating, an increase in the intensity of the monomeric absorption band at 342 nm was observed. This has been further accompanied by a concomitant decrease in the intensity of the shoulder band at 392 nm through an isosbestic point at 374 nm (Figure 3.6a). Similarly, absorption spectrum of **PE** also showed a temperature-dependent increase in the intensity of the absorption maximum at 306 nm with concomitant decrease in the intensity of the shoulder band at 372 nm along with an isosbestic point at 365 nm (Figure 3.6b). The melting point transition temperature (T_m, temperature at which $\alpha_{agg} = 0.50$) of both the aggregates was calculated from the plot of fraction of aggregates (α_{agg}) versus temperature. The T_m was found to be 52 °C for **PE-CN** (Figure 3.6c), but in the case of **PE**, the T_m was observed at 34 °C (Figure 3.6d). The difference in T_m implies that **PE-CN** aggregates are comparatively stronger than that of the **PE** aggregates.

Emission studies of **PE-CN** and **PE** have been carried out in chloroform and *n*-decane at a concentration of 1×10^{-4} M. In chloroform, **PE-CN** showed a broad emission with maximum centered at 402 nm. In *n*-decane, **PE-CN** aggregates displayed a structured emission (λ_{max} = 420 nm) with increase in emission intensity (Figure 3.7a and b). The quantum yield Φ_F in chloroform is 0.35 which increased to 0.43 in *n*-decane. However, in the case of **PE**, the intensity of emission spectrum in chloroform was relatively weak (Φ_F = 0.02) when compared to that (Φ_F = 0.34) of *n*-decane aggregates (Figure 3.7c and d).

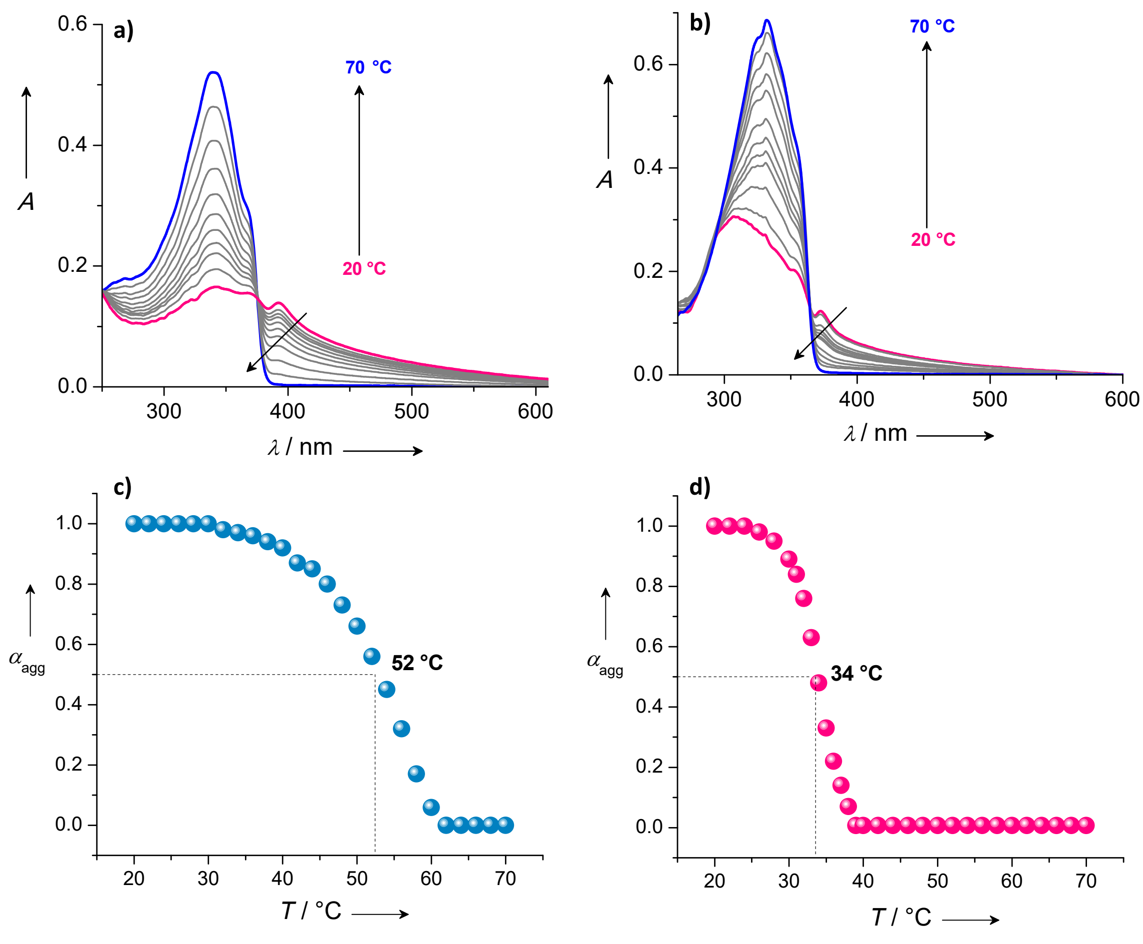

Figure 3.6. Temperature dependent absorption spectra of a) **PE-CN** and b) **PE** in *n*-decane at (c = 1 x 10 $^{-4}$ M). Plots of fraction of aggregates (α_{agg}) versus temperature c) **PE-CN** and d) **PE** (data points are collected from the temperature dependent absorption measurements).

The aggregation of **PE** in *n*-decane resulted in 5.7 times enhancement in fluorescence intensity, indicating aggregation induced enhanced emission (AIEE) behavior, whereas AIEE[16] phenomena is not much obvious in the case of **PE-CN** aggregates.

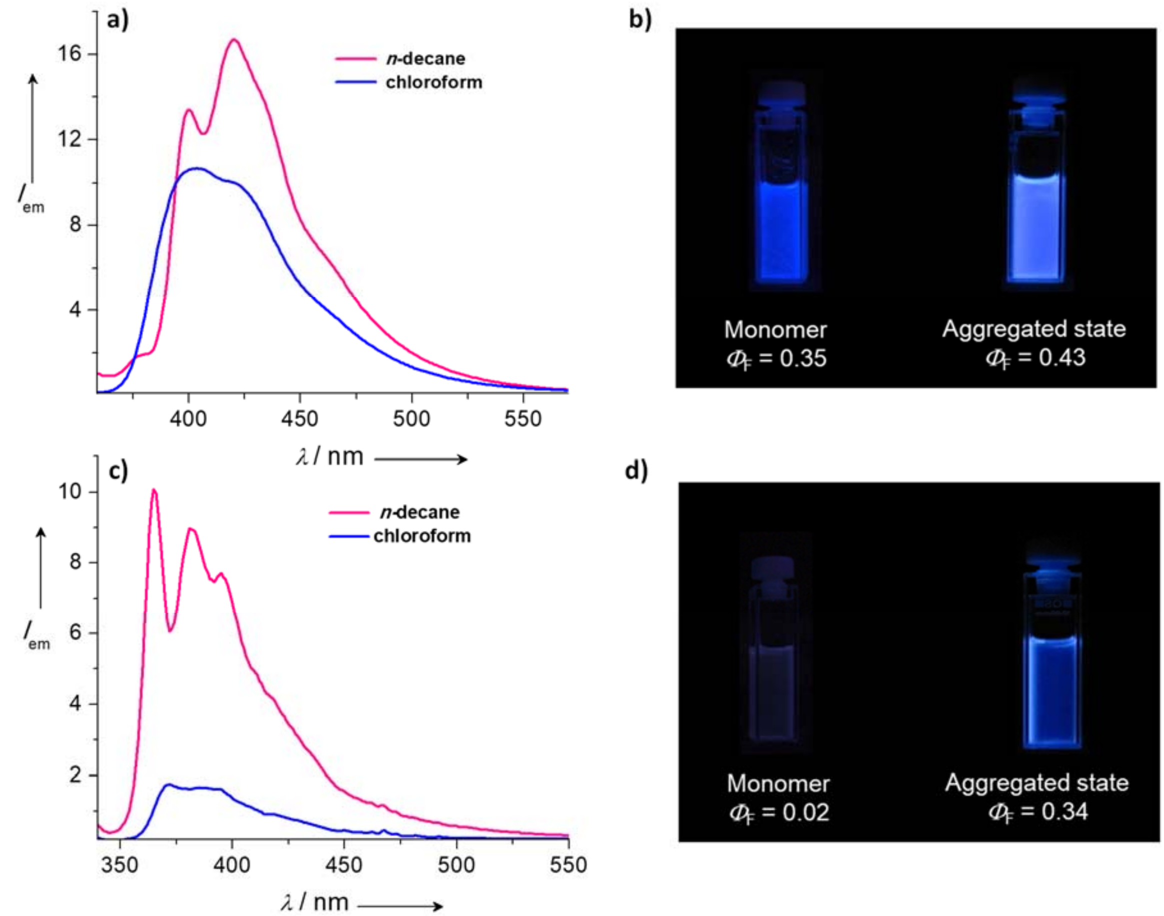

Figure 3.7 Emission spectra of a) **PE-CN** and c) **PE** in chloroform (——) and decane (——) at (c = 1 × 10^{-4} M), λ_{ex} = 330 nm. Photographs taken under 365 nm UV light illumination: left (monomers) and right (aggregates) for b) **PE-CN** and d) **PE**.

Variable temperature emission spectra of **PE-CN** in *n*-decane (c = 1 × 10^{-4} M) showed enhancement in emission intensity upon heating from 20 to 70 °C when excited at 330 nm (Figure 3.8a). The transition from aggregates into monomers on heating resulted in the enhancement of emission indicating the absence of AIEE behavior (Figure 3.8c).

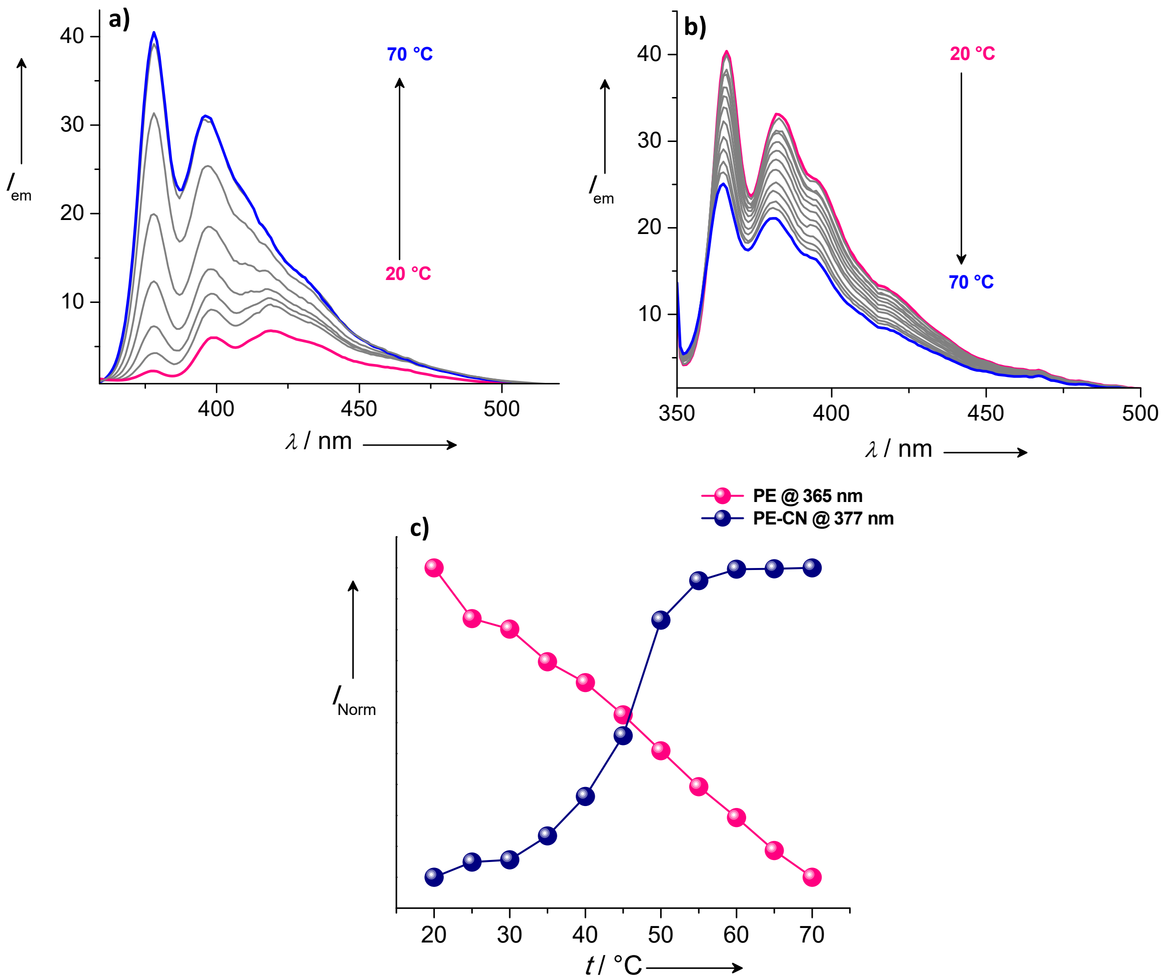

Figure 3.8. Temperature-dependent emission spectra of a) **PE-CN** and b) **PE** in *n*-decane (c = 1 × 10^{-4} M). c) Plot of changes in emission intensity versus temperature for **PE-CN** ( ) and **PE** ( ).

On the contrary, the emission intensity of **PE** aggregates in *n*-decane (c = 1 × 10^{-4} M) showed a decrease upon heating (Figure 3.8b and c). In monomer state, intramolecular phenyl ring rotation for **PE** molecules makes energy dissipation in a non-radiative way resulting in the decrease in the emission intensity.[17]

3.2.3. Gelation Studies

Gelation ability of both **PE-CN** and **PE** were examined in different hydrocarbon solvents by dissolving different amounts of both the compounds in a definite volume (1 mL) of the solvent by heating followed by cooling at room temperature. Gel formation was detected readily by the failure of the resultant mass to flow when the vial was tilted upside down. The results of the gelation experiments are summarized in Table 3.1. The critical gelator concentrations (CGC) of **PE-CN** and **PE** in *n*-decane are 6.0 and 8.8 mM, respectively. Similar trend was also observed for methyl cyclohexane gels where CGC of **PE-CN** (12.5 mM) was found to be less than that of **PE** (13.8 mM). Both compounds failed to form gel in toluene as well as in chloroform due to their high solubility in these solvents. Both **PE-CN** and **PE** gels in nonpolar aliphatic solvents like *n*-decane exhibited blue emission (Figure 3.9). The emission spectra of **PE-CN** and **PE** *n*-decane gel are shown in Figure 3.9a and 3.9c, respectively. The morphology of both the molecules in the gel state was characterized by SEM. The image obtained from SEM of the **PE-CN** gel in *n*-decane showed inter-connected micro rods (Figure 3.9b). However, the SEM image of **PE** gel at similar condition revealed the formation of entangled fibers having length of several micrometers (Figure 3.9d). From these observations, it can be concluded, that the microrod and nanofiber like morphology obtained in the gel state at relatively higher concentration is similar to that of the morphologies of the aggregates obtained at lower concentration of **PE-CN** and **PE**, respectively.

Table 3.1. Critical gelator concentrations (mM)[a] of **PE-CN** and **PE** in different solvents.

Gelator	*n*-Decane	Methyl cyclohexane	Toluene	Chloroform
PE-CN	6.0 (G)	12.5 (G)	(S)	(S)
PE	8.8 (G)	13.8 (G)	(S)	(S)

[a]CGC = Critical gelator concentration, which is the minimum concentration required for the formation of a stable gel at room temperature. In parenthesis, G = gel, P = precipitate and S = soluble at room temperature.

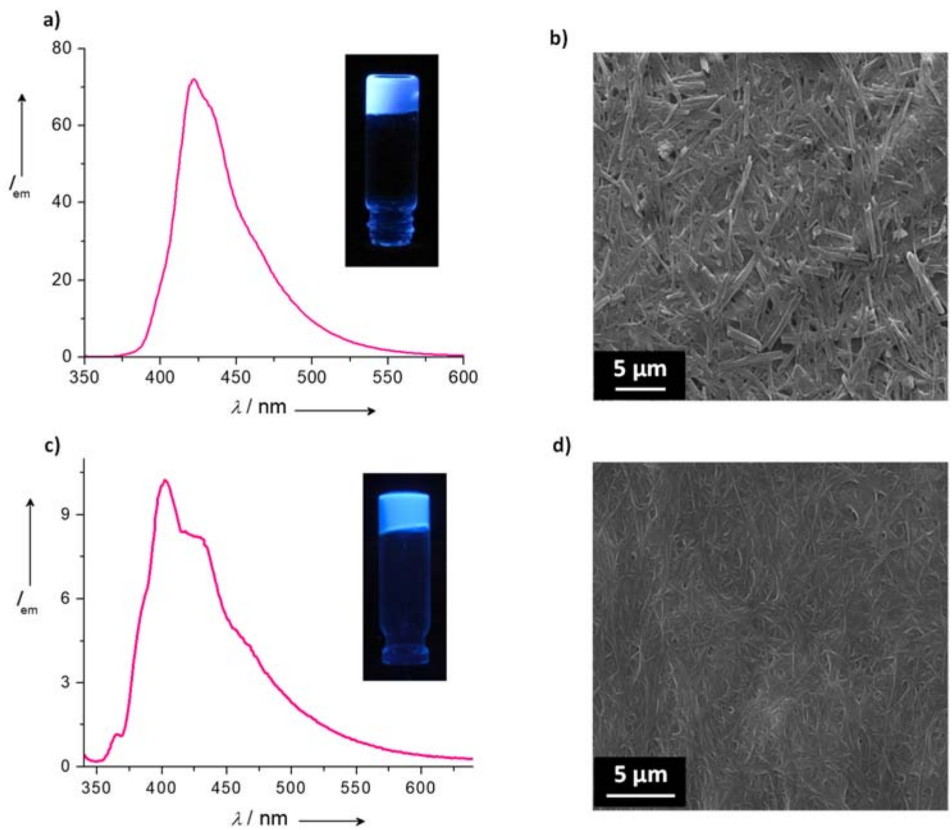

Figure 3.9 Emission spectra of the *n*-decane gels (λ_{ex} = 340 nm): a) **PE-CN** and c) **PE**. Insets show the photographs of the gels under 365 nm UV light illumination. SEM images of the b) **PE-CN** and d) **PE** *n*-decane gels.

Furthermore, the viscoelastic nature of both gels formed in *n*-decane was confirmed from the rheological studies using dynamic frequency sweep experiments. Results obtained from the rheological studies indicate that the storage modulus (*G′*) and the loss modulus (*G″*) values are independent of the oscillation frequency within the range of 1-100 rads^{-1} with strain amplitude (γ) at 0.01 (Figure 3.10). In addition, considerably higher storage modulus (*G′*) value was obtained in comparison to that of the loss modulus (*G″*) for both **PE-CN** and **PE** gels, which confirms their viscoelastic nature.[18] In addition, gel strength of **PE-CN** is relatively higher than that of the **PE** gel because of the higher storage modulus (G′) amplitude as well as significant difference between the storage and loss modulus (G″) value.

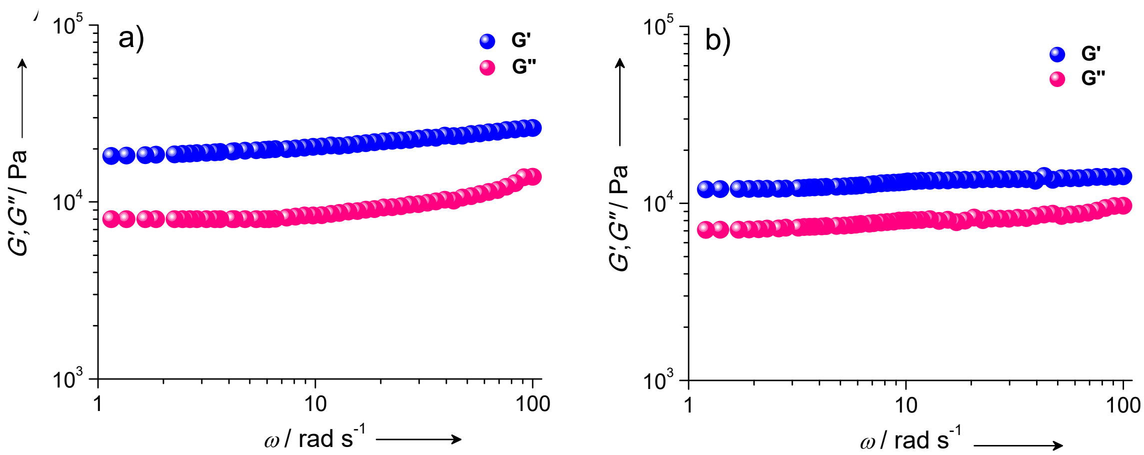

Figure 3.10. Plot of dynamic storage modulus (*G′* - ●) and loss modulus (*G″*- ●) versus angular frequency (*ω*) for a) **PE-CN** and b) **PE** in *n*-decane at 20 °C with the strain amplitude (γ) at 0.01.

3.2.4. Effect of Cooling Rate on Molecular Self-Assembly

The strategy adopted for the molecular design of π-gelators, especially that of **PE-CN** seems to be important for evaluating its gelation properties under different conditions. The gelator contains a linear triple-bonded aromatic π-backbone of phenyleneethynylene as the fluorescent core interconnected to a bulky end group composed of flexible dodecyl chains through an amide linkage leading to have an overall control over the molecular assembly process through H-bonding. Presence of the cyano group at the extreme end of the phenyleneethynylene core in **PE-CN** can give rise to an effective dipolar interaction for the supramolecular assembly formation. Hence, while dealing with the molecular self-assembly of **PE-CN**, it is necessary to consider the fact that both these noncovalent interactions may be operating orthogonally to each other.

As described in the previous section, a blue emitting opaque gel was obtained at a critical gelator concentration (CGC) of 6 mM when the homogeneous **PE-CN** solution in *n*-decane was spontaneously cooled down to room temperature from a relatively higher temperature (80 °C). Interestingly, rapid cooling of an identical solution by inserting the sample in an ice bath at 0 °C led to form a semi-transparent green emitting gel. These two distinct observations obtained from the gelation studies prompted us in gaining deeper insight into the molecular self-assembly process in the gel state in detail. In the light of the above results, we have extended our investigation on finding the optimum concentration at which the different modes of self-assembly pathways are occurring.

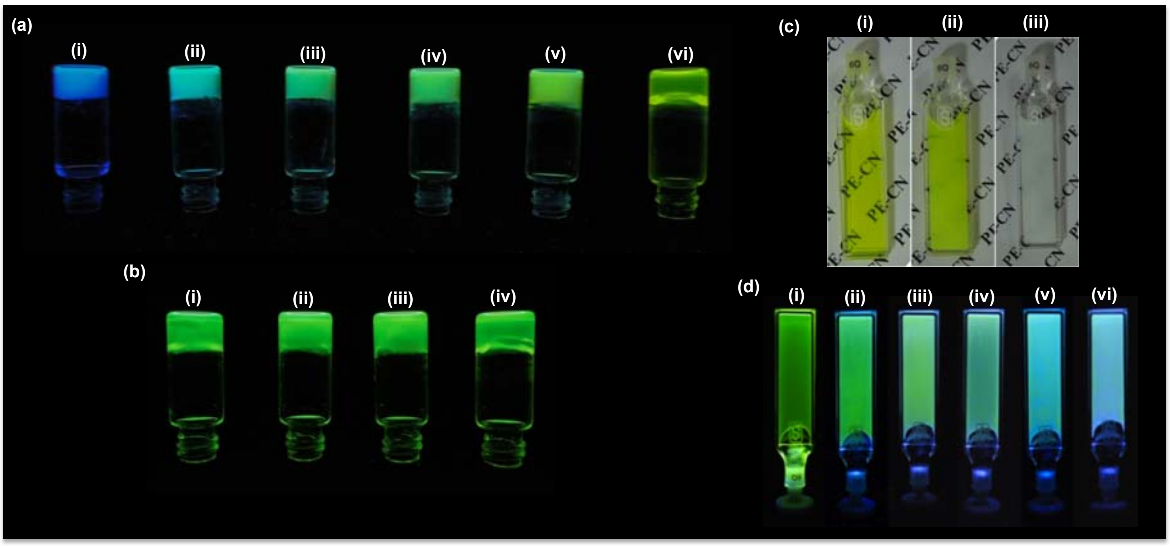

Figure 3.11. Photographs of a) **PE-CN** *n*-decane gels obtained while cooling hot homogenous solutions to room temperature spontaneously: i) 6, ii) 10, iii) 15, iv) 20, v) 25, and vi) 26.3 mM. b) Gels obtained by rapid cooling to 0 °C: i) 6, ii) 10, iii) 15 and iv) 20 mM. c) Photographs of **PE-CN** green emissive *n*-decane gel under normal light i) initial and ii) after 48 h, showing time-dependent change in transparency and iii) **PE-CN** blue emissive *n*-decane gel. d) Change in emission of **PE-CN** green *n*-decane gel with time i) initial, after ii) 5, iii) 10, iv) 15, v) 18, and vi) 30 days. Photographs were taken under 365 nm UV light illumination.

Initially, the homogeneous *n*-decane solutions of **PE-CN** at various concentrations were prepared by heating at 80 °C and kept at room temperature to spontaneously cool down. Interestingly, an increase in concentration from 6 to 25 mM resulted in gradual change in emission color of opaque gel from blue to green (Figure 3.11a). A further increase in concentration to 26.3 mM, led to the formation of a transparent green emitting gel (Figure 3.11a). The change in emission color as well as transparency of the gels encouraged us to verify the role of rapid cooling on concentration-dependent gelation studies. For this purpose, the homogeneous solution prepared by heating at high temperature was immediately brought down to 0 °C by keeping the samples in an ice bath. A systematic increase in concentration enhanced the transparency of the green emitting gel and finally at a concentration of 20 mM, a transparent green emitting gel was obtained (Figure 3.11b).

The green emitting gels (26 mM) prepared by rapid cooling undergo time-dependent changes of both transparency and emission color. For example, the transparency of the green emitting gel started decreasing within 16 h and became opaque after 2 days, whereas the nature of the opaque blue emitting gel remained unaltered (Figure 3.11c). In addition, the emission of the green emitting gel slowly converted to an intermediate (mixture of green and blue) state after 12 days and a complete conversion to a blue emitting gel was observed after one month of time (Figure 3.11d). However, no such alteration in emission took place in case of the blue emitting gel. This gel state interconversion confirmed that the green emitting gel is a metastable state having the tendency to convert back to a thermodynamically stable blue opaque gel with time. It is worthy to note that gelation allows trapping of metastable state for a sufficient duration of time, which is considered to be a challenging aspect.[19]

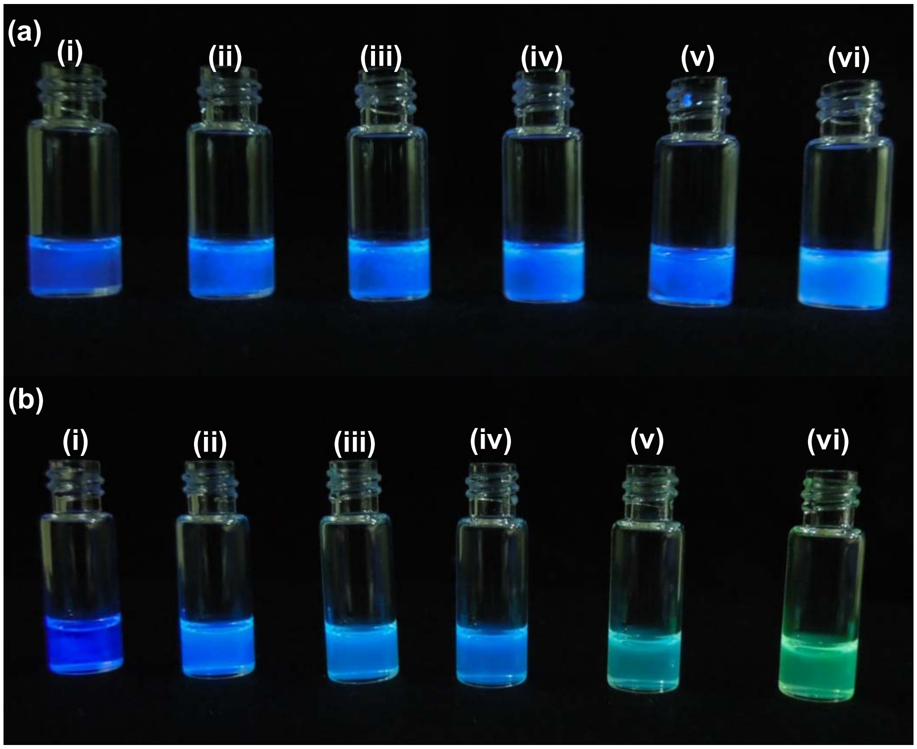

Figure 3.12. Photographs of **PE-CN** aggregates formed by a) slow and b) rapid cooling of pre-heated *n*-decane solution of concentration i) 0.1, ii) 0.2, iii) 0.3, iv) 0.5, v) 0.75 and vi) 1 mM. All photographs are taken under 365 nm UV light illumination.

It has been found that at high concentrations, the conversion of the metastable gel to a thermodynamically stable gel is a slow process. To find out the effect of concentration on the conversion of the metastable state, a detailed investigation has been carried out in *n*-decane at lower concentrations. Slow cooling of **PE-CN** in *n*-decane from 80 °C to room temperature resulted in the formation of blue emitting aggregates throughout the concentration range 0.1 to 1 mM (Figure 3.12a). Rapid cooling of 0.1 to 0.5 mM solution was identical to that of the slow cooling experiment (Figure 3.12b, i-iv), whereas green emitting aggregates were obtained at concentrations of 0.75 and 1 mM (Figure 3.12b, v and vi).

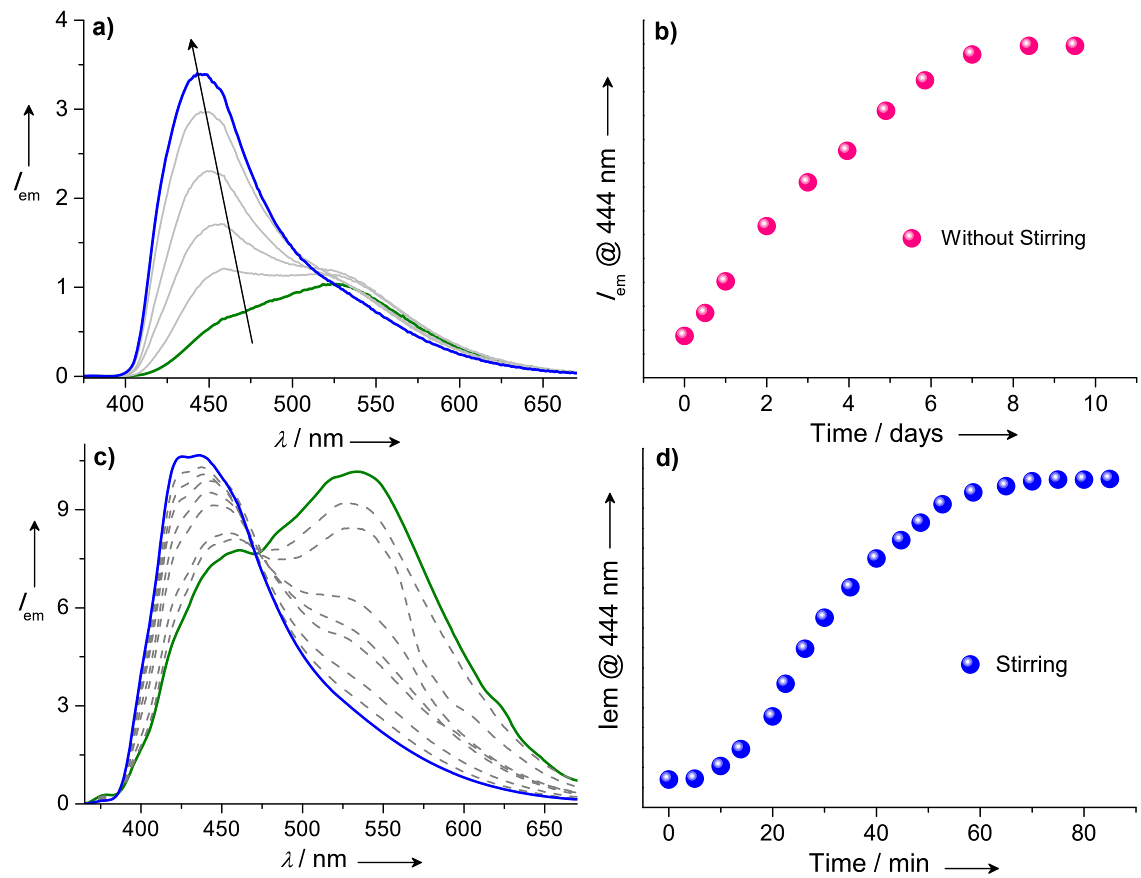

Figure 3.13. Time-dependent changes in emission spectra (λ_{ex} = 340 nm) of **PE-CN** green emitting aggregates in *n*-decane (1 mM) upon keeping the sample a) undisturbed and c) upon stirring at 200 r.p.m. Plots showing the time-dependent changes occurring in the emission of the aggregates while keeping the sample b) undisturbed and d) upon stirring.

The undisturbed *n*-decane solution of the green emitting aggregates (1 mM) showed a gradual transition from the metastable state (λ_{max} = 534 nm) to the thermodynamically stable blue emitting aggregates (λ_{max} = 444 nm) within seven days of time (Figure 3.13a and b). It is noteworthy that the transformation of the green emitting aggregates (1mM) to the blue emitting aggregates can be accelerated by stirring (at 200 r.p.m), which is clear from the Figure 3.13c. Upon stirring, the initial green emission intensity at ($\lambda_{\max}$ = 534 nm) gradually reduced with time and after 85 min the emission spectrum was completely converted to that of blue emitting aggregates ($\lambda_{\max}$ = 444 nm). The corresponding secondary plots while monitoring the emission intensity at 444 nm with time is shown in Figure 3.13d. A non-linear sigmoidal transition profile, which is the characteristic of an autocatalytic or self-replicating process was observed where stirring mediated initial conversion to blue aggregates accelerated its own propagation.[20]

Interestingly, the time dependent fluorescence change as observed in the case of **PE-CN** was not found for the **PE** gel. This observation indicates that the origin of the green emission in **PE-CN** aggregates is dependent of the presence of the CN moiety, which can direct the self-assembly to an excimer-like emission.[17] This is verified by measuring the fluorescence lifetime values of the blue and the green aggregates, which are found to be τ_{av} = 2.61 and 26.5 ns, respectively. Hence, it is assumed that the presence of CN group in **PE-CN** helps in the formation of different supramolecular assemblies based on the rates of cooling, whereas the supramolecular assemblies formed out of **PE** remained unaltered.

3.2.5. Morphological Studies

In order to get insight about the morphological features of **PE-CN** and **PE** aggregates in *n*-decane, we have carried out detailed transmission electron microscopy (TEM) and scanning electron microscopy (SEM) studies. Samples for TEM analysis were prepared by dropcasting the *n*-decane aggregates (c = 5 × 10^{-5} M) of both the molecules on a carbon coated copper grid followed by the removal of the solvent under vacuum. TEM images of **PE-CN** aggregates obtained from *n*-decane showed micrometer sized rod-like structures having diameter within the range of 200-300 nm (Figure 3.14a). However, in the case of **PE**, formation of micrometer long entangled fibres with diameter less than 100 nm was observed (Figure 3.14b). SEM images of samples prepared by drop casting the *n*-decane aggregates ($c = 5 \times 10^{-5}$ M) of both the molecules on an aluminium substrate revealed the formation of rods and entangled fibers (Figure 3.14c and d) as observed in TEM images.

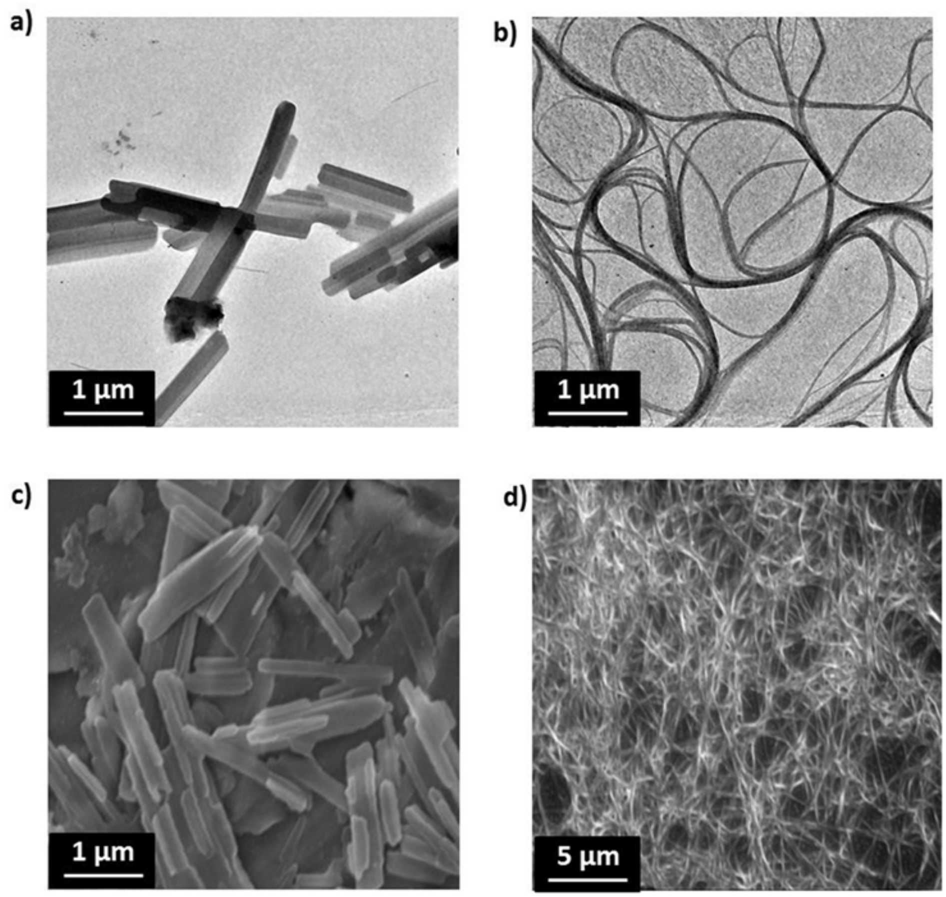

Figure 3.14. TEM images of a) **PE-CN** and b) **PE** in *n*-decane. SEM images of c) **PE-CN** and d) **PE**. In all the studies concentration of solution is 5×10^{-5} M.

In order to gain on about the morphological features of the metastable and thermodynamic aggregates of **PE-CN** we have carried out extensive microscopic studies. TEM images of the blue emitting aggregates (obtained by slow cooling of the solution) revealed the formation of crystalline rod-like structures (Figure 3.15a), whereas the green emitting aggregates showed entangled fibrous networks having length several micrometers (Figure 3.15b).

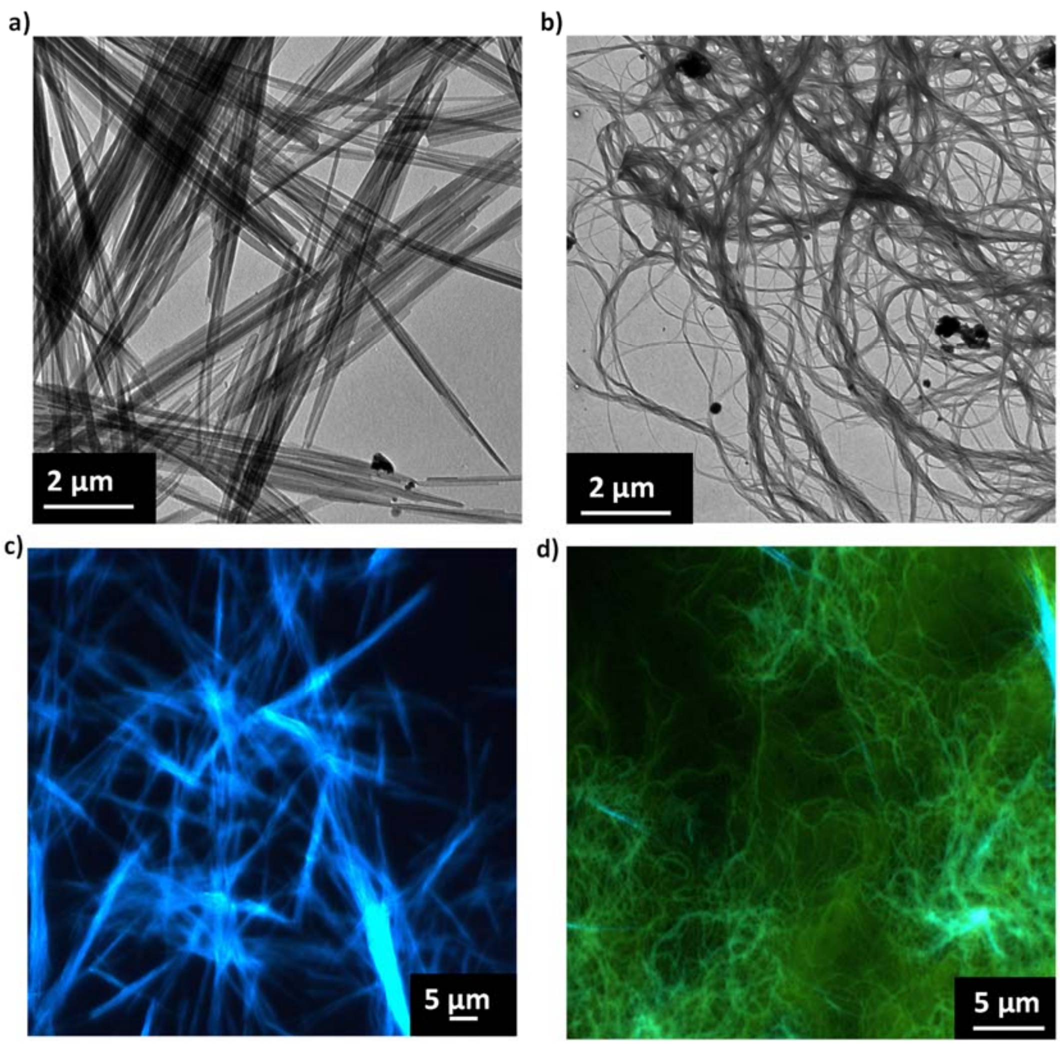

Figure 3.15. TEM and fluorescence microscopy images of **PE-CN** a) and c) blue emitting aggregates and b) and d) green emitting aggregates, respectively prepared by slow and rapid cooling of *n*-decane solution (1 mM).

It is known that rate of cooling is an important factor in determining crystallinity as well as branching of fiber.[21] The nucleation and fiber growth phenomena is mainly driven by the chemical potential operating between the growing crystalline phase and the solution phase. An increase in the rate of cooling can lead to crystallographic mismatch resulting in branching of the fiber and network formation. The presence of these tiny fiber networks reduces the scattering of light leading to the formation of transparent gel at higher concentration. On the other hand, mass transfer of the solute from the bulk of the solvent to the growing crystalline nucleus becomes dominant while the cooling rate is low.[21] Hence, crystallographic mismatch is not observed when the system gets enough time to orient in an organized manner. This leads to the formation of unbranched crystalline rod-like structure of **PE-CN**. These micrometer sized crystalline rod-like structures can easily scatter light resulting in opaque nature of the gel.

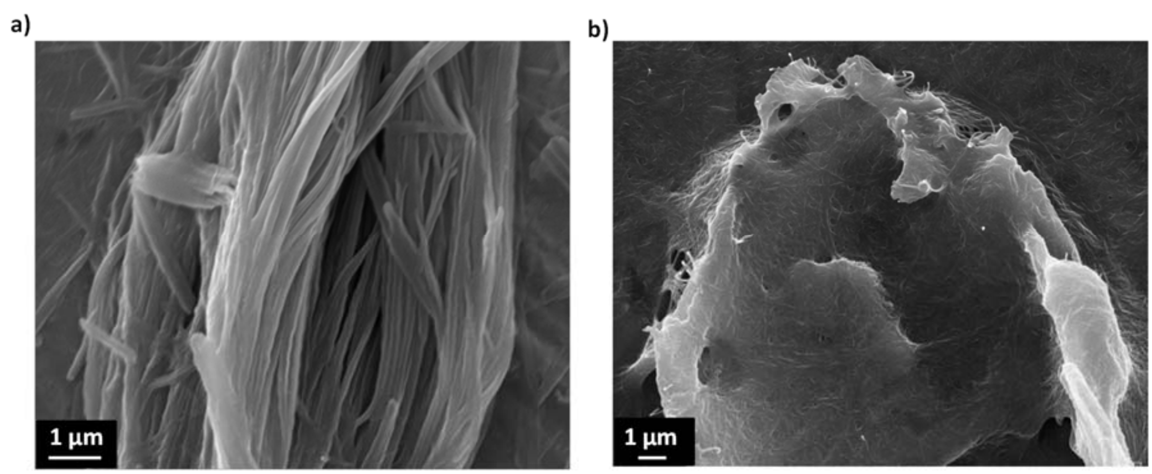

Figure 3.16. SEM images of **PE-CN** a) blue xerogel and b) green xerogel.

Fluorescence microscopy images have also revealed the formation of crystalline blue emitting rod type structures (Figure 3.15c) as well as green emitting entangled fiber networks (Figure 3.15d). In addition, SEM analysis of blue xerogel exhibited long fiber like structures whereas entangled fibers were obtained for the green xerogel (Figure 3.16).

3.2.6. Molecular Packing of PE-CN and PE Aggregates

For a better understanding of the molecular packing in **PE-CN** and **PE** self-assemblies, we have carried out small angle X-ray scattering (SAXS) analysis. Figure 3.17a shows the SAXS pattern of the blue-emitting **PE-CN** xerogel exhibiting two well-resolved peaks with a reciprocal *d*-spacing ratio of 1:2. The two intense sharp diffraction bands observed at 53.6 Å (001) and 26.6 Å (002) indicate a long-range crystalline lamellar type arrangement of the molecules (Figure 3.17d). The intense sharp peak at 53.6 Å corresponds to the width of a single one-dimensional (1-D) layer of the molecules where dipole-dipole interaction is nullified upon minute interdigitation of the two oppositely oriented cyano groups present in the extreme ends of **PE-CN** molecules. The other peak at 26.6 Å corresponds to the rigid rod **PE-CN** moiety. On the other hand, the SAXS pattern of the green **PE-CN** xerogel suggests hexagonal columnar packing (Figure 3.17b). In the case of the green-emitting xerogel, the extended lamellar structure is completely broken up into micro-segregates between the rigid rod segment and the liquid like aliphatic chain, which can afford columns consisting of finite stacks of supramolecular polymers arranged in a hexagonally ordered manner.[22] This assumption about the structural transition was supported by the movement of most intense small angle reflection to 47.6 Å. Additional sharp reflections obtained at 27.9 Å and 23.3 Å indicates the hexagonal columnar packing with *d*-spacing ratio of 1:1/√3:1/2 with an intercolumnar distance of 47.6 Å. Assuming the density to be 1 g cm^{-3}, number of molecules filling a slice of each of the column is calculated to be 7.[22] Thus, randomly hydrogen-bonded supramolecular polymer containing 7 molecules stack together to form a column (Figure 3.17e).

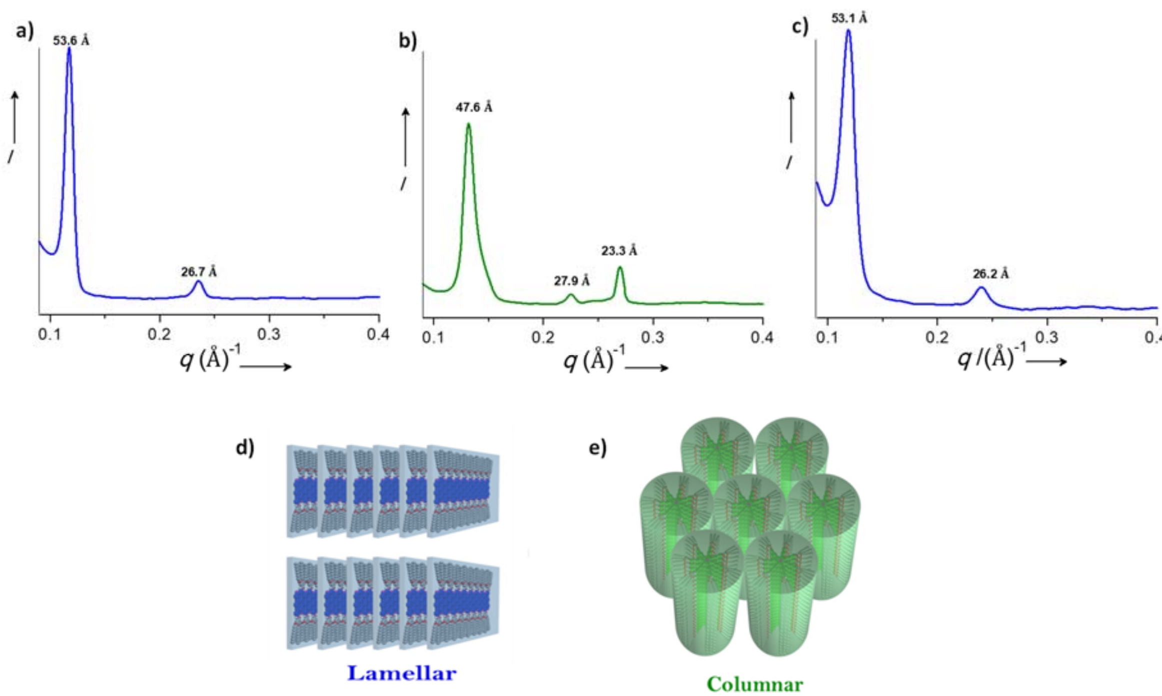

Figure 3.17. SAXS pattern of **PE-CN** a) blue xerogel and b) green xerogel and c) **PE** xerogel. Schematic illustration of molecular packing of d) blue and e) green emitting **PE-CN** aggregates.

The SAXS pattern of the PE xerogel exhibited a lamellar type arrangement consisting of well-resolved peaks with a reciprocal *d*-spacing ratio of 1:2 (Figure

3.17c). The two intense sharp diffraction bands observed at 53.1 and 26.2 Å suggest a long-range crystalline lamellar type arrangement of the molecules similar to that of **PE-CN**.

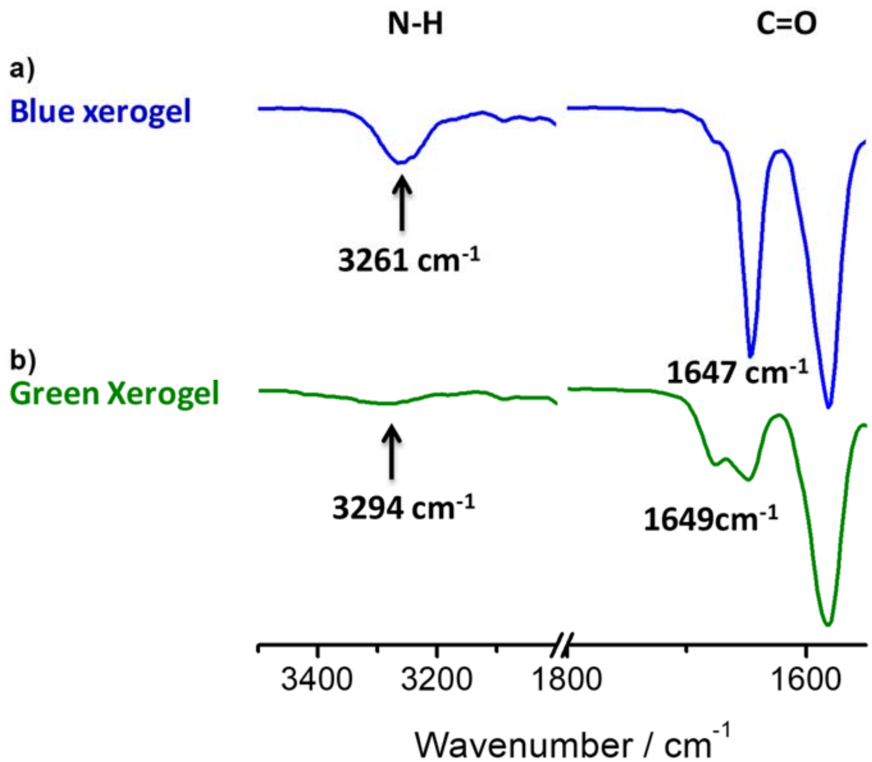

Figure 3.18. FT-IR spectra of **PE-CN** a) blue and b) green emitting xerogel.

The proposed molecular packing of **PE-CN** aggregates was further confirmed by FT-IR studies. In general, a secondary amide group is characterized by three distinct IR stretching frequencies rationalized to be symmetric N-H stretch (amide A band) and C=O stretch (amide I band).[23] The FT-IR spectrum of the blue emitting xerogel revealed H-bonded N-H stretching frequency at 3261 cm^{-1} and the amide I band at 1647 cm^{-1} clearly confirms the formation of lamellar structure through intermolecular H-bonding (Figure 3.17). The decrease in the intensity of the N-H stretching frequency and splitting of the carbonyl stretching band suggests partial breaking as well as weakening of the amide H-bonding in case of the green emitting xerogel (Figure 3.18).

3.2.7. Sensing Organic Vapors in Film State

PE-CN green gel was transferred to a glass substrate and the solvent was evaporated by applying vacuum. After evaporation of the solvent, the green xerogel film was exposed to saturated organic vapors (chloroform, dichloromethane etc.) for 30 s. As a result, the initial green emission was changed to blue and the process can be reversed by heating the blue emitting film at 110 °C for 60 s (Figure 3.19).

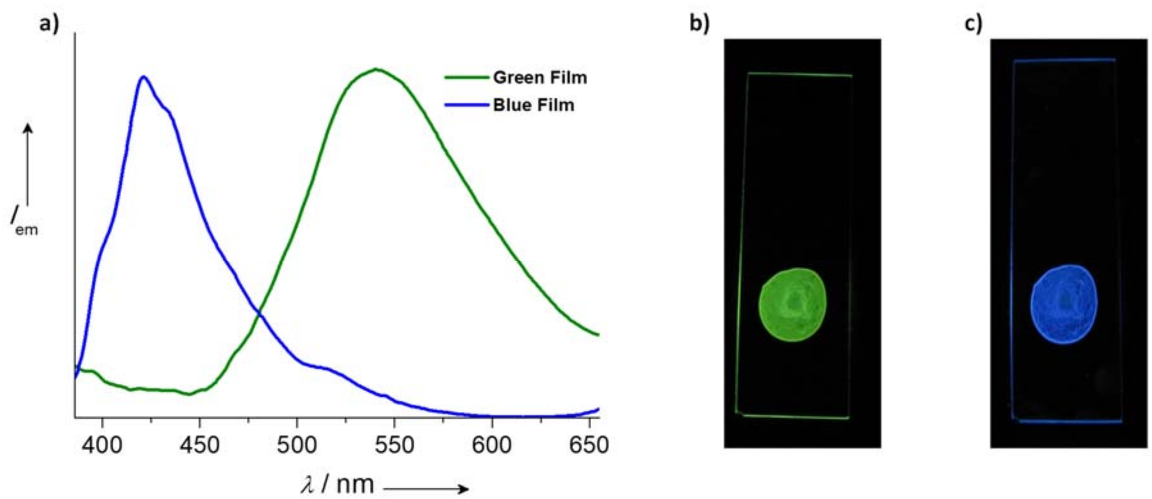

Figure 3.19. a) Emission spectra of **PE-CN** xerogel films. Photographs of **PE-CN** b) Green xerogel film and c) Blue xerogel film taken under 365 nm UV light illumination.

3.2.8. Flash-Photolysis Time-Resolved Microwave Conductivity Studies

The photoconductivity of **PE-CN** in both blue and green emitting xerogel states was evaluated by flash-photolysis time-resolved microwave conductivity (FP-TRMC) experiments. In this technique, changes in conductivity are monitored during the pulsed laser excitation without electrodes. A change in the conductivity of the medium resulting from mobile charge carriers is measured as a change in the power level of microwaves. For this purpose, the xerogel samples were loaded in between two quartz plates and then excited using 355 nm laser pulse.

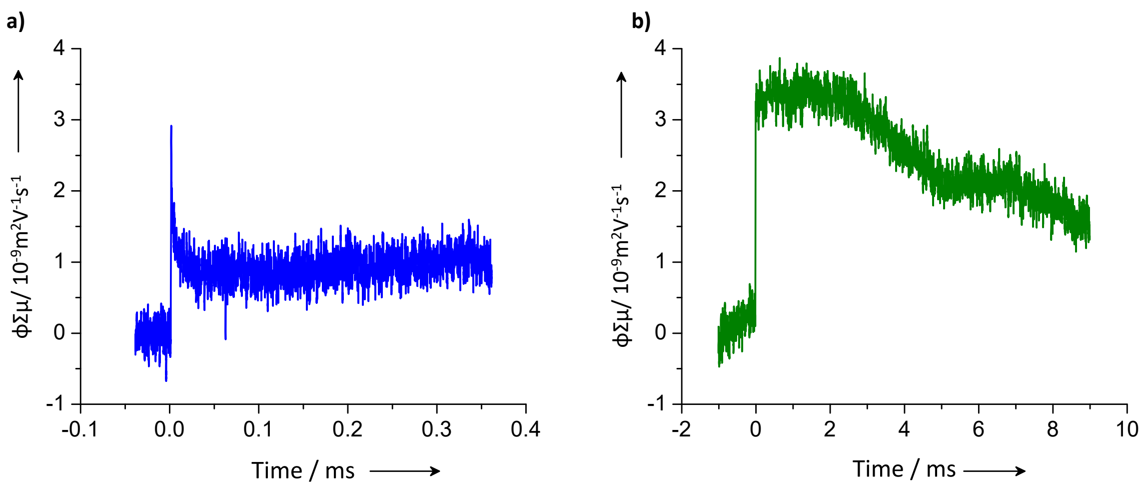

Figure 3.20. FP-TRMC transient conductivity profiles (λ_{ex} = 355 nm) of **PE-CN**: a) blue and b) green emitting xerogel.

Figure 3.20 shows the transient profiles of the photoconductivity ($\phi\Sigma\mu$) of **PE-CN** aggregates. The maximum photoconductivity obtained ($\phi\Sigma\mu$) for the blue emitting xerogel is 1.56 x 10^{-9} $m^2V^{-1}s^{-1}$ and for the green emitting xerogel the maximum photoconductivity increased to double in magnitude to 3.46 x 10^{-9} $m^2V^{-1}s^{-1}$. The green emitting xerogel showed long charge carrier half-lifetime of 8.0 milliseconds, whereas the charge carrier half-lifetime of blue phase is only 110 microseconds. The better photoconductivity of the green emitting xerogel might be due to the closer molecular packing of the cyano substituted phenyleneethynylene rigid core and the long charge carrier half-lifetime value may arise from the presence of small thin fibers in the green phase.

3.3. Conclusions

The molecular assembly derived from cyano-substituted phenyleneethynylene **PE-CN** possesses a unique luminescence switching property in the gel state. Slow heating and cooling of the **PE-CN** (*n*-decane, 6 mM) yielded an opaque blue gel with highly ordered lamellar structure. On the other hand, fast cooling of the same solution resulted into a green gel with columnar structure which slowly transformed into thermodynamically more stable blue gel and thus showing metastable nature of the green gel. In addition to different fluorescence properties, for both gels, two distinct morphological features were observed by SEM, TEM and fluorescence microscopic studies. The FP-TRMC studies revealed that the green emitting xerogel exhibited nearly 1000 times larger charger carrier mobility half-life time than blue emitting xerogel. The strategy adopted for the molecular design of **PE-CN** is crucial for the observed two stage gelation and fluorescence behavior. The presence of the amide hydrogen bonding unit and a cyano group are essential for the emission switching behavior, as the phenyleneethynylene molecule without a cyano group does not show any structural transition and emission switching properties under similar conditions. To the best of our knowledge this is the first report of its kind showing emission switching in organogel with two different states displayed by the same molecule and the present design strategy may lead to the design of new molecules having switchable emission properties.

3.4. Experimental Section

General procedure for the purification, drying of solvents and other common experimental techniques used are described in the experimental section (section 2.4.1) of Chapter 2.

3.4.1. Synthesis and Characterization

Synthesis of 4-((4-((trimethylsilyl)ethynyl)phenyl)ethynyl)benzonitrile (3a): In a two neck round bottom flask purged with argon, ((4-iodophenyl)ethynyl)trimethylsilane **2** (0.82 g, 2.72 mmol), $PdCl_2(PPh_3)_2$ (0.14 g, 0..27 mmol) and CuI (0.03 g, 0.27 mmol) were dissolved in a degassed 30 mL (1:1) mixture of triethylamine and THF. Compound **1a** (0.35 g, 2.72 mmol) was added to the reaction mixture and stirred at room temperature under argon atmosphere for 12 h. After completion of reaction, chloroform (50 mL) was added to the reaction mixture and then stirred well with 10% HCl to neutralize triethylamine. The organic layer was washed with water, brine and then dried over anhydrous sodium sulphate. After the removal of the solvent, residue was purified by silica gel column chromatography using 2% ethylacetate/*n*-hexane as an eluent.

Yield: 80%; ^{1}H NMR (500 MHz, $CDCl_3$): δ = 7.65 (d, J = 8.5 Hz, 2H), 7.60 (d, J = 8.5 Hz, 2H), 7.47 (s, 4H), 0.26 (s, 9H) ppm; HRMS (FAB): (m/z) calculated for $C_{20}H_{17}NSi$ $[M]^+$: 299.11; found: 299.78.

Synthesis of 4-((4-ethynylphenyl)ethynyl)benzonitrile (4a): To a solution of **3a** (0.65 g, 2.20 mmol) in 5 mL dichloromethane, KF (1.2 g, 22.0 mmol) in 15 mL methanol was added and stirred at room temperature for 6 h. After completion of the reaction, the reaction mixture was extracted using chloroform, washed with water, brine and then dried over anhydrous sodium sulphate. Solvent was evaporated under reduced pressure and the residue was used for the next step without further purification.

Yield: 90%; ^{1}H NMR (500 MHz, $CDCl_3$): δ = 7.66 (d, J = 8.0 Hz, 2H), 7.61 (d, J = 8.5 Hz, 2H), 7.49 (s, 4H), 3.21 (s, 1H) ppm; HRMS (FAB): (m/z) calculated for $C_{17}H_9N$ $[M]^+$: 227.07; found: 227.78.

Synthesis and characterization of PE-CN and PE. In a general synthetic procedure, the aryl halide (0.70 mmol), $PdCl_2(PPh_3)_2$ (10 mol%), and CuI (10 mol%) were added to an oven-dried two neck round bottom flask equipped with a magnetic stirring bar. The round bottom flask was then sealed with a rubber septum, evacuated and backfilled with argon three times. Degassed triethylamine (10 mL) was added followed by degassed THF (10 mL) to serve as the co-solvent. After stirring for 5 minutes at room temperature, the terminal alkyne (0.80 mmol) dissolved in 10 mL (1:1) mixture of degassed triethylamine and THF was added and the reaction mixture was stirred at room temperature until completion of the reaction was noted by the TLC. The reaction mixture was extracted using chloroform and washed with dilute HCl. The organic layer was washed with brine and dried over anhydrous sodium sulphate and then evaporated under reduced pressure. The crude product was then purified by column chromatography using silica gel as the adsorbent.

PE-CN: Yield, 52%; R_f = 0.52 ($CHCl_3$:MeOH, 97:3 v/v); m.p.: 143-145 °C; FT-IR (KBr): ν_{max} = 3255, 2920, 2852, 2214, 1647, 1583 cm^{-1}; ^{1}H NMR (500 MHz, $CDCl_3$): δ = 7.75 (s, 1H), 7.67-7.65 (m, 4H), 7.62-7.60 (m, 2H), 7.56-7.53 (m, 6H), 7.04 (s, 2H), 4.05-4.01 (m, 6H), 1.84-1.74 (m, 6H), 1.50-1.45 (m, 6H), 1.36-1.27 (m, 48H), 0.89-0.87 (t, 9H) ppm; ^{13}C NMR (125 MHz, $CDCl_3$): δ = 165.6, 153.3, 141.7, 138.4, 132.6, 132.1, 131.7, 131.6, 129.6, 128.1, 121.8, 119.8, 118.6, 111.6, 105.8, 93.5, 91.7, 89.4, 88.7, 73.6, 69.5, 31.9, 30.3, 29.7, 29.6, 29.5, 29.3, 26.1, 22.7, 14.1 ppm; HRMS (ESI): (m/z) calculated for $C_{66}H_{90}N_2O_4$ $[M+1]^+$: 974.69; found: 976.23.

PE: Yield, 48%; R_f = 0.55 (*n*-hexane:$CHCl_3$, 1:1 v/v); m.p.: 114-116 °C; FT-IR (KBr): ν_{max} = 3255, 2920, 2852, 2214, 1647, 1583 cm^{-1}; ^{1}H NMR (500 MHz, $CDCl_3$): δ = 7.77 (s, 1H), 7.66 (d, J = 9.0 Hz, 2H), 7.55-7.51 (m, 8H), 7.37-7.35 (m, 3H), 7.04 (s, 2H), 4.05-4.01 (m, 6H), 1.83-1.70 (m, 6H), 1.52-1.47 (m, 6H), 1.35-1.27 (m, 48H), 0.90-0.88 (t, 9H) ppm; ^{13}C NMR (125 MHz, $CDCl_3$): δ = 165.2, 154.5, 142.3, 137.5, 135.2, 132.4, 129.7, 128.5, 127.6, 126.7, 125.2, 118.7, 105.6, 90.2, 71.2, 69.5, 32.2, 28.9, 27.2, 25.3, 22.1, 15.7 ppm; HRMS (ESI): (m/z) calculated for $C_{65}H_{91}NO_4$ $[M+1]^+$: 949.69; found: 950.70.

3.4.2. Description on Experimental Techniques

Flash–Photolysis Time Resolved Microwave Conductivity (FP–TRMC): A resonant cavity was used to obtain a high degree of sensitivity in the conductivity measurement. The resonant frequency and microwave power were set at ca. 9.1 GHZ and mW, respectively, so that the electric field of the microwave was sufficiently small to not disturb the motion of charge carriers. The third harmonic generation (THG; 355nm) of a Nd:YAG laser (Continuum Inc., Surelite II, 5-8 ns pulse duration,10 Hz) were used as an excitation source. The laser power was fixed at 2.5 mJ cm^{-2} $pulse^{-1}$ for all excitation wavelengths (incident photon density, $I_0 = 4.6 \times 10^{15}$ photons cm^{-2} $pulse^{-1}$). An in-house-built Xe-flash lamp (10 µs pulse duration, 10 Hz) with a power of 0.3 mJ cm^{-2} $pulse^{-1}$ was used for the Xe-flash TRMC experiments. For the attenuation of excitation light energy, neutral density filters were used for both Xe-flash and laser-flash TRMC. In the case of laser-flash TRMC, the photoconductivity transient $\Delta\sigma$ is converted to the product of the quantum efficiency: ϕ and the sum of charge carrier mobilities, $\Sigma\mu$, by $\phi\Sigma\mu = \Delta\sigma$ (eI_0Flight$)^{-1}$, where e and F_{Light} are the unit charge of a single electron and a correction (or filling) factor. The above experiment was performed in Department of Applied Chemistry, Graduate School of Engineering, Osaka University, Japan.

General Procedure for Gelation Studies: A weighed amount of the compound in an appropriate solvent was placed in a glass vial, which was sealed and heated until the compound was dissolved. The solution was allowed to cool to room temperature. The gel formation was confirmed by the failure of the gel mixture to flow by inverting the glass vial. The thermo reversibility of the gelation was confirmed by repeated heating and cooling process.

Rheological Studies: Rheological measurements were conducted on an Anton Paar modular compact (MCR 150) stress controlled rheometer (Physica) equipped with a parallel plate geometry (20 mm diameter), striated cone and a rough plate to minimize the errors due to sliding of the gel layers. A hot solution of compound (3×10^{-3} M) in *n*-decane was poured on to the Peltier kept at 20 °C and was allowed to form a uniform layer. In order to avoid the solvent evaporation the plate was properly covered. The gap between the cone and the plate was fixed between 0.25 mm.

The experimental techniques for SAXS, SEM, TEM, Fluorescence microscopy and Optical measurements are described in section 2.4.5 of Chapter 2.

3.5. References

[1] (*a*) F. J. M. Hoeben, P. Jonkheijm, E.W. Meijer, A. P. H. J. Schenning, *Chem. Rev.* **2005**, *105*, 1491–1546; (*b*) A. Ajayaghosh, V. K. Praveen, *Acc. Chem. Res.* **2007**, *40*, 644–656.

[2] (*a*) L. Zang, Y. Che, J. S. Moore, *Acc. Chem. Res.* **2008**, *41*, 1596–1608; (*b*) A. Saeki, Y. Koizumi, T. Aida, S. Seki, *Acc. Chem. Res.* **2012**, *45*, 1193–1202.

[3] (*a*) J.-M. Lehn, *Science* **2002**, *295*, 2400–2403; (*b*) P. Terech, R. G. Weiss, *Chem. Rev.* **1997**, *97*, 3133–3159.

[4] S. Yagai, T. Kinoshita, Y. Kikkawa, T. Karatsu, A. Kitamura, Y. Honsho, S. Seki, *Chem. Eur. J.* **2009**, *15*, 9320–9324.

[5] S. Yagai, M. Usui, T. Seki, H. Murayama, Y. Kikkawa, S. Uemura, T. Karatsu, A. Kitamura, A. Asano, S. Seki, *J. Am. Chem. Soc.* **2012**, *134*, 7983–7994.

[6] C. Weder, C. Sarwa, A. Montali, C. Bastiaansen, P. Smith, *Science* **1998**, *279*, 835–837.

[7] M. Irie, T. Fukaminato, T. Sasaki, N. Tamai, T. Kawai, *Nature* **2002**, *420*, 759–760.

[8] X. Zhang, S. Rehm, M. M. Safont-Sempere, F. Würthner, *Nat.Chem.* **2009**, *1*, 623 –629.

[9] T. Mutai, H. Satou, K. Araki, *Nat. Mater.* **2005**, *4*, 685–687.

[10] Y. Sagara, T. Kato, *Nat. Chem.* **2009**, *1*, 605–610.

[11] (*a*) A. Ajayaghosh, V. K. Praveen, C. Vijayakumar, *Chem. Soc. Rev.* **2008**, *37*, 109–122; (*b*) S. Varghese, S. Das, *J. Phys. Chem. Lett.* **2011**, *2*, 863–873.

[12] (*a*) Y. Sagara, T. Mutai, I. Yoshikawa, K. Araki, *J. Am. Chem. Soc.* **2007**, *129*, 1520–1521; (*b*) H. Ito, T. Saito, N. Oshima, N. Kitamura, S. Ishizaka, Y. Hinatsu, M.Wakeshima, M. Kato, K. Tsuge, M. Sawamura, *J. Am. Chem. Soc.* **2008**, *130*, 10044 –10045. (*c*) S.-J. Yoon, J.W. Chung, J. Gierschner, K. S. Kim, M.-G. Choi, D. Kim, S. Y. Park, *J. Am. Chem. Soc.* **2010**, *132*, 13675–13683.

[13] (*a*) Y. Sagara, T. Kato, *Angew. Chem. Int. Ed.* **2008**, *47*, 5175–5178; (*b*) Y. Sagara, S. Yamane, T. Mutai, K. Araki, T. Kato, *Adv. Funct. Mater.* **2009**, *19*, 1869–1875; (*c*) S. Yamane, Y. Sagara, T. Kato, *Chem. Commun.* **2009**, 3597–3599.

[14] (*a*) C. L. We, C. Weder, *Adv. Mater.* **2002**, *14*, 1625–1629; (*b*) B. R. Crenshaw, C. Weder, *Chem. Mater.* **2003**, *15*, 4717–4724; (*c*) A. Pucci, F. D. Cuia, F. Signori,G. Ruggeri, *J. Mater. Chem.* **2007**, *17*, 783–790.

[15] S. Srinivasan, P. A. Babu, S. Mahesh, A. Ajayaghosh, *J. Am. Chem. Soc.* **2009**, *131*, 15122–15123.

[16] B-K. An, J. Gierschiner, S. Y. Park, *Acc. Chem. Res.* **2012**, 45, 544–554.

[17] M. Levitus, K. Schmieder, H. Ricks, K. D. Shimizu, U. H. F. Bunz, M. A. Garcia-Garibay, *J. Am. Chem. Soc.* **2001**, *123*, 4259–4265.

[18] S. Srinivasan, S. S. Babu, V. K. Praveen, A. Ajayaghosh, *Angew. Chem. Int. Ed.* **2008**, *47*, 5746–5749.

[19] A. Sorrenti, J. Leira-Iglesias, A. J. Markvoort, T. F. A. De Greef, T. M. Hermans, *Chem. Soc. Rev.* **2017**, DOI: 10.1039/C7CS00121E.

[20] S. Ogi, K. Sugiyasu, S. Manna, S. Samitsu, M. Takeuchi, *Nat. Chem.* **2014**, *6*, 188–195.

[21] J.-L. Li, X.-Y. Liu, *Adv. Funct. Mater.* **2010**, *20*, 3196–3216.

[22] S. Yagai, S. Kubota, T. Iwashima, K. Kishikawa, T. Nakanishi, T. Karatsu, A. Kitamura *Chem. Eur. J.* **2008**, *14*, 5246–5257.

[23] J. M. Malicka, A. Sandeep, F. Monti, E. Bandini, M. Gazzano, C. Ranjith, V. K. Praveen, A. Ajayaghosh, N. Armaroli, *Chem. Eur. J.* **2013**, *19*, 12991–13001.

Chapter 4

Acid Induced Modulation of Supramolecular Helicity in Fluorescent Molecular Assemblies

Abstract

Supramolecular helicity in molecular assemblies is a manifestation of the chiral centre present in the molecule. However, in many cases external stimuli such as metal ions, protons, light and other chemical species may have strong influence on the overall helicity. Herein we describe the effect of an organic acid on the supramolecular helicity of two p-phenyleneethylene based chiral molecular building blocks ***PE-CN-Chiral*** *and* ***PE-Chiral****.* ***PE-CN-Chiral*** *forms blue emitting aggregates in n-decane showing a bisignate CD with a negative response followed by a positive signal. When trifluoroacetic acid (TFA) was added to the blue aggregates, with time, the emission of the aggregates changed from blue to green along with the reversal of the CD. Addition of TFA results in the breaking of the H-bonds within the molecular self-assembly, which eventually allows the molecules to re-organize in a manner different from the initial assembly.*

4.1. Introduction

Chirality is one of the most fascinating phenomena Nature encompasses and it has the ability to create functional architectures with a preferred handedness at various hierarchical levels. Inspired by the unique features of biological superstructures, researchers have been trying to create variety of helical supramolecular assemblies by utilizing various noncovalent forces such as H-bonding, π-π stacking and van der Waals interaction.[1] In this regard, the supramolecular organization of π-conjugated systems into helices of definite dimensions has become a desirable goal.[2-4] Helical organization of supramolecular π-systems is important not only for understanding the role of chirality in biological functions, but also due to its increasing importance in the fields of sensing, optics and catalysis.[5]

In recent years, stimuli induced modulation of supramolecular helicity in a controllable manner has become a fascinating research area of supramolecular chemistry. The helicity of the self-assembled structures can be inverted by varying the preferences toward the available intermolecular interactions. The modulation of helicity in optically active helical systems has been successfully achieved via various external stimuli, such as temperature,[6] solvent,[7] light,[8] pH,[9] sonication,[10] pressure,[11] and chiral[12] or achiral additives.[13] Lee *et al*., have designed unique supramolecular nanotubules using a bent-shaped aromatic amphiphile **1**, which self-assemble into hexameric macrocycles in aqueous solution and forming chiral tubules by spontaneous one-dimensional (1D) stacking with specific handedness (Figure

4.1).[14] The adjacent aromatic segments within the hexameric macrocycles reversibly slide along one another in response to thermal stimulus, resulting in pulsating motions of the tubules accompanied by a chiral inversion. The bent-shaped rod amphiphile **1** (0.02 wt% aqueous solution) formed elongated tubules with a uniform external diameter of 11 nm and internal diameter of 4 nm at room temperature which was contracted to 7 nm upon heating (Figure 4.1c).

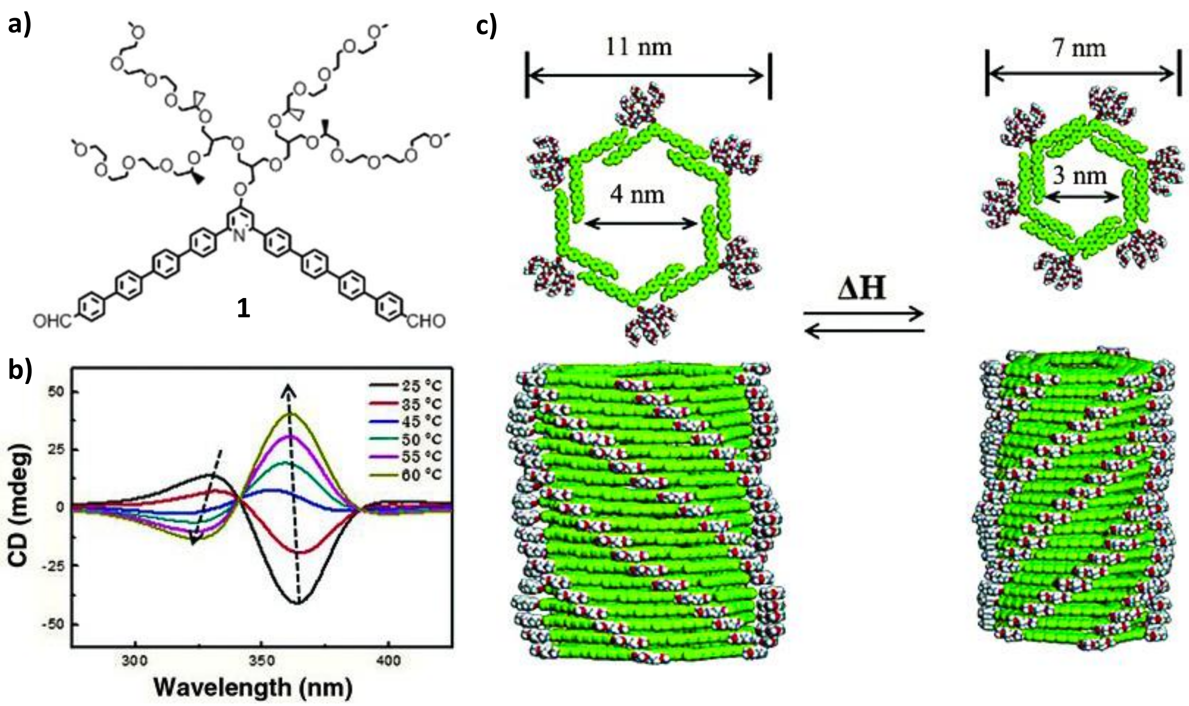

Figure 4.1. a) Molecular structure of **1**. b) Temperature-dependent CD spectra of **1** (0.01 wt%) in aqueous solution. c) Schematic representation of reversible switching of the tubules between expanded and contracted states with chirality inversion (Adapted with permission from ref. 14. Copyright 2012 AAAS.)

The formation of hollow tubules with oligoether dendritic exterior and pyridine interior suggested that aqueous solutions of **1** would exhibit thermo-responsive behavior. Since pyridine is well known to form water clusters through H-bonding,[15] it may undergo thermally regulated dehydration upon heating and allow sliding motion of the aromatic segments, causing the nanotube to shrink. The chirality inversion with respect to temperature was further supported with molecular dynamics simulations. According to this, the expanded macrocycles stack on top of each other with mutual rotations at an angle of –10° in the same direction to give rise to left-handed helical tubules, whereas the contracted macrocycles twist +6° to give right-handedness. The observed inversion of helical handedness seems to result from two independent orientations of the dendritic moieties with respect to both the helical axis and macrocycle plane.

Modulating the helicity of self-assembled molecule through simple solvent interactions has been demonstrated by Wei and co-workers (Figure 4.2).[16] The sugar-based amphiphilic perylene diimide derivative **2** forms aggregates at various volume ratios of chloroform/*n*-octane and THF/H_2O solvent mixtures. A well-resolved bisignate circular dichroism (CD) signal with positive Cotton effect at 450 nm and negative at 503 and 543 nm was observed for chloroform/*n*-octane mixture (Figure 4.2c). However, in THF/H_2O mixture, the aggregates exhibited exactly opposite behavior in terms of chirality and produced mirror image Cotton effect with negative signal at 470 nm and positive at 520 and 560 nm as shown in Figure 4.2d. The difference in handedness indicates that the solvent plays a critical role in determining the packing and thus chirality of the amphiphilic molecule

In chloroform/*n*-octane, the galactosyl group of **2** is buried inside the aggregates to form a hydrophilic core that is sheltered from *n*-octane (Figure 4.2b). The 1-hexylheptyl chains tend to gather on the outside to stabilize the aggregates in *n*-octane. In contrast, **2** has an opposite arrangement in polar THF/H_2O, in which galactosyl groups are present at the exterior of the amphiphilic aggregates.

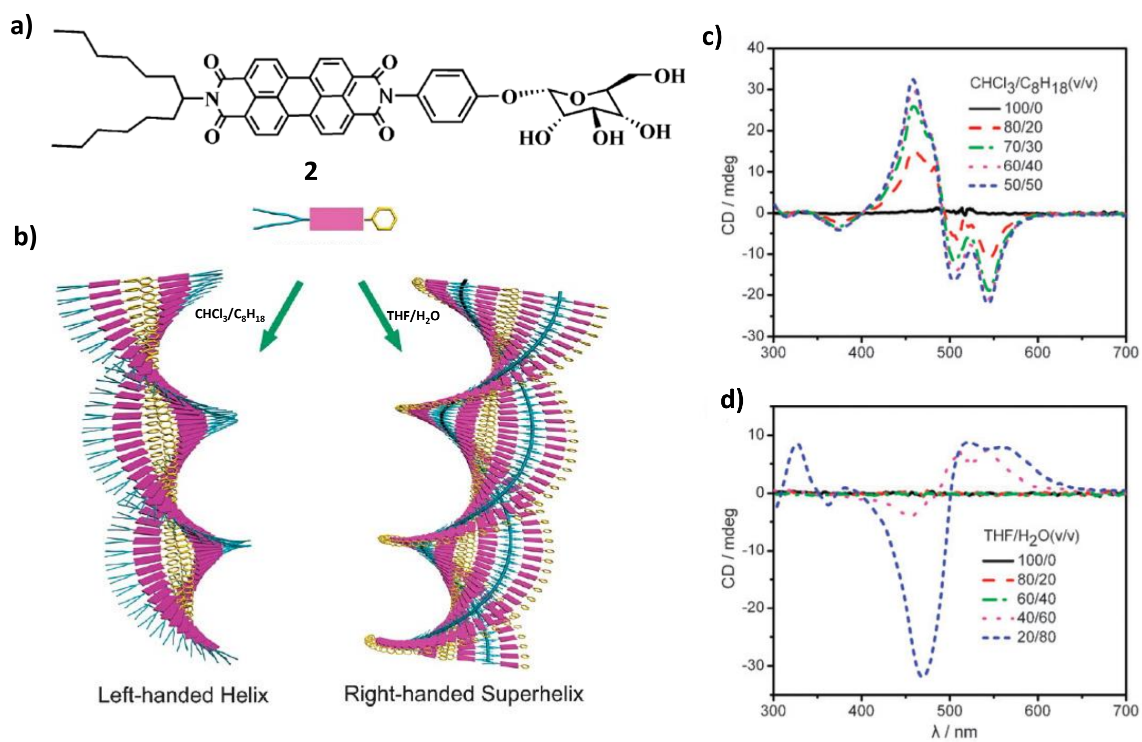

Figure 4.2. a) Molecular structure of **2**. b) Schematic representation of helical structures formed from two different solvent mixtures. CD spectra of **2** in different volume ratios of solvents c) $CHCl_3/C_8H_{18}$ and d) THF/H_2O (Adapted with permission from ref. 16. Copyright 2011 The Royal Society of Chemistry.)

Riguera *et al.*, have constructed helical supramolecular assemblies from poly(phenylacetylene) bearing chiral pendant phenylglycine methyl ester groups (Figure 4.3). The induction and inversion of helical sense of this polymer could be achieved by choosing appropriate metal cations as external stimuli.[17] The highly dynamic helical polymer with a chiral pendant shows no CD effect, but the discriminating interaction of the polymer with mono and divalent metal ions induces either left- or right-handed helical sense. AFM images of polymer/Ba^{2+} and polymer/Ag^{+} on highly oriented pyrolytic graphite provided important insights into the helicity and morphology.

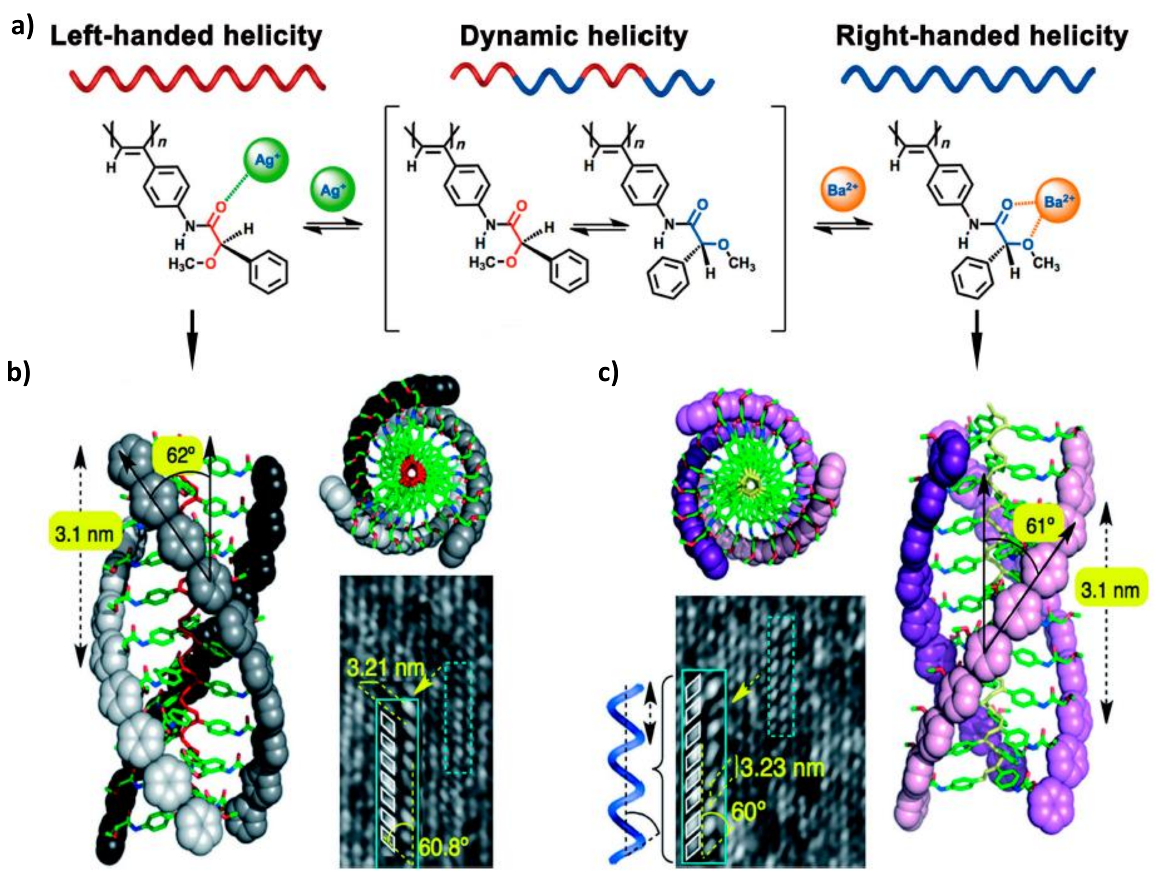

Figure 4.3. a) Schematic illustration of selective regulation of the helix sense by control of the conformation of the pendants upon Ag^{+} (left) Ba^{2+} (right). Atomic force microscopy (AFM) images and theoretical models (form the top and side views) of b) left-handed helix of polymer/Ag^{+} and c) right-handed helix of polymer/Ba^{2+} (Adapted with permission from ref. 17. Copyright 2011 Wiley-VCH.)

Upon addition of Ba^{2+}, the polymer forms a right-handed (clockwise) pendant disposition with the periodic oblique stripes forming 60.08º and a helical pitch of 3.23 nm (Figure 4.3c). In the case of Ag^{+}, the polymer shows a left-handed (counterclockwise) pendant disposition with the periodic oblique stripes forming 60.88º and a helical pitch of 3.21 nm (Figure 4.3b). The difference in behavior of the dynamic polymer in the presence of mono and divalent cations can be attributed to the different conformations of the pendants favored by respective cations. Molecular mechanics calculations show that a right-handed helix is formed when the pendants adopted synperiplanar conformations. On the other hand, a left-handed helix of similar energy arose when the pendants adopted antiperiplanar conformations.

Although the modulation of helicity was observed in several cases under specific conditions as discussed above, helicity modulation using acid-induced reorganization of chromophore packing of a π-system remains interesting. Furthermore, it is highly challenging to achieve helicity modulation with simultaneous switching of the emission properties of a π-assembly. These facts prompted us to design a linear π-conjugated oligomer having chiral side chains with emission switchable π-core, **PE-CN-Chiral** and **PE-Chiral** (Figure 4.4). In these molecules, the triple bonded linear aromatic π-backbone (phenyleneethynylene, **PE**) is the fluorescent core, which is connected to a bulky end group through an amide bond. The bulky terminal group is composed of flexible chiral side chains. The amide linkage provides H-bonds that control the molecular assembly and the terminal cyano group provides additional dipolar interaction. These molecules were synthesized through multistep synthetic procedures using palladium-catalyzed Sonogashira–Hagihara cross coupling reactions. Detailed self-assembly, morphological, photophysical and chiroptical studies were carried out and the results are summarized in this chapter.

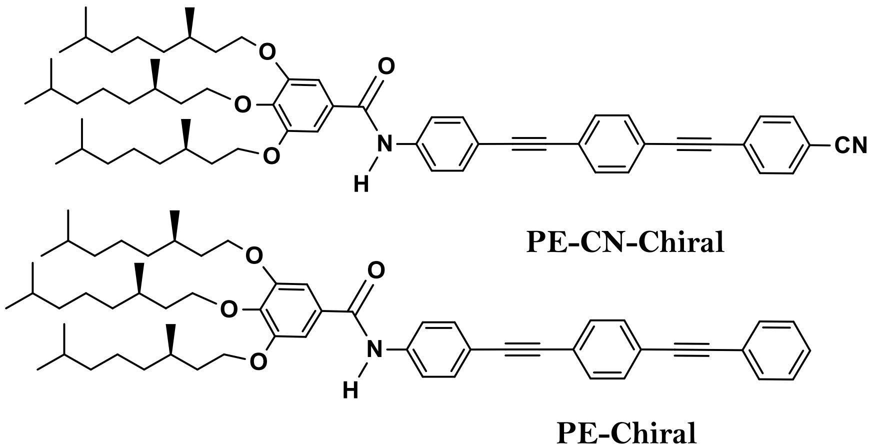

Figure 4.4. Molecular structures of **PE-CN-Chiral** and **PE-Chiral**.

4.2. Results and Discussion

4.2.1. Synthesis of PE-CN-Chiral and PE-Chiral

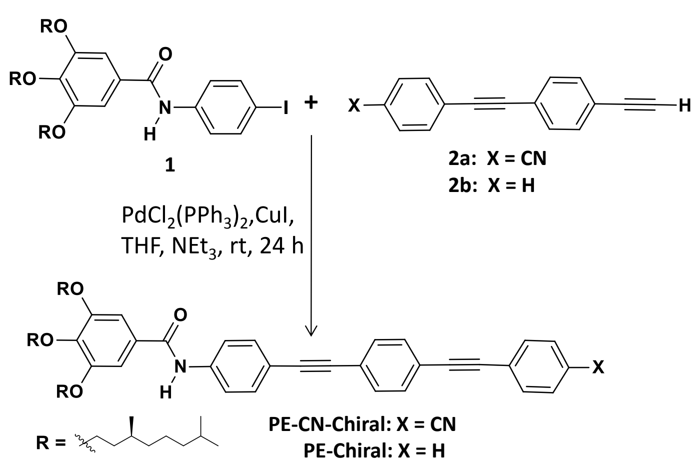

Scheme 4.1

The precursors 3,4,5-tris(((*S*)-3,7-dimethyloctyl)oxy)-N-(4-iodophenyl)benzamide **1**, 4-((4-ethynylphenyl)ethynyl)benzonitrile **2a** and 1-ethynyl-4-(phenylethynyl)benzene

2b were synthesized according to the procedures reported in the previous chapters. The Sonogashira-Hagihara coupling between **1** and 4-((4-ethynylphenyl)ethynyl) benzonitrile **2a** using $Pd(PPh_3)_2(Cl_2)_2$ and CuI as the catalyst gave **PE-CN-Chiral** in 57% yield. The coupling of **1** with **2b** gave **PE-Chiral** in 60% yield (Scheme 4.1).

4.2.2. Aggregation Studies of PE-CN Chiral and PE-Chiral

4.2.2.1. Absorption and Emission Properties

In order to understand the aggregation properties, UV-Vis absorption studies of **PE-CN-Chiral** and **PE-Chiral** in chloroform and *n*-decane (c = 1 × 10^{-4} M) have been carried out. At 25 °C, **PE-CN-Chiral** in chloroform showed a strong π-π* absorption band with λ_{max} at 343 nm in *n*-decane. The intensity of π-π* band is significantly reduced and a shoulder band at 396 nm is formed (Figure 4.5a). The absorption spectra of **PE-Chiral** in chloroform and *n*-decane are shown in the Figure 4.5b. In chloroform (c = 1 × 10^{-4} M) at 25 °C, the molecule showed a strong π-π* absorption band with λ_{max} at 334 nm. In *n*-decane, a decrease in the intensity of absorption maximum (334 nm) was observed.

Variable temperature absorption studies of **PE-CN-Chiral** in *n*-decane (c = 1 × 10^{-4} M) showed a transition from the aggregated state to the monomers as the temperature is increased from 20 to 70 °C (Figure 4.6a). An increase in the intensity of the absorption maximum at 339 nm was observed upon increasing the temperature, which is accompanied by a concomitant decrease in the intensity of the shoulder band at 396 nm with an isosbestic point at 377 nm. Similarly, the temperature-dependent absorption spectra of **PE-Chiral** showed an increase in the intensity of the absorption maximum at 333 nm with concomitant decrease in the intensity of the shoulder band at 372 nm with an isosbestic point at 365 nm as shown in the Figure 4.6b. The stability of the aggregates was determined from the plot of the fraction of aggregate (α_{agg}) versus temperature (Fig- ure 4.6c and d). A melting transition temperature (T_m, temperature at which α_{agg} = 0.50) of 43 °C was obtained for **PE-CN-Chiral** in *n*-decane, whereas it was found to be 34 °C for **PE-Chiral**. This observation reveals that comparatively stronger aggregation of **PE-CN-Chiral** than the **PE-Chiral**, which emphasizes the importance of the terminal cyano group in facilitating the stability of aggregates.

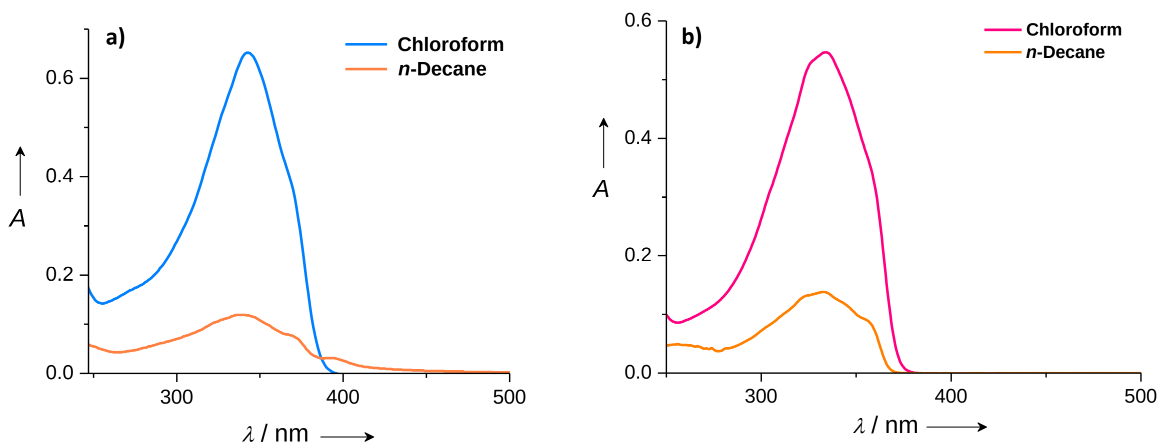

Figure 4.5. Absorption spectra of a) **PE-CN-Chiral** and b) **PE-Chiral** in chloroform and *n*-decane at (c = 1 × 10^{-4} M).

Similarly, the emission studies of **PE-CN-Chiral** and **PE-Chiral** have been carried out in chloroform and *n*-decane (c = 1 × 10^{-4} M). PE molecules are known to exhibit aggregation-induced enhanced emission (AIEE).[18] In general, AIEE active molecules will show weak emission in monomer state due to intramolecular rotation or twisted conformations of chromophores. In the case of **PE-CN-Chiral** in chloroform, a broad spectrum with the emission maximum centered at 403 nm (Φ_F = 0.48) was observed due to intramolecular charge-transfer interaction promoted by the presence of terminal cyano moiety (Figure 4.7a). However, in *n*-decane, aggregated **PE-CN-Chiral** showed a structured emission with maxima at 377 and 403 nm (Φ_F = 0.54).

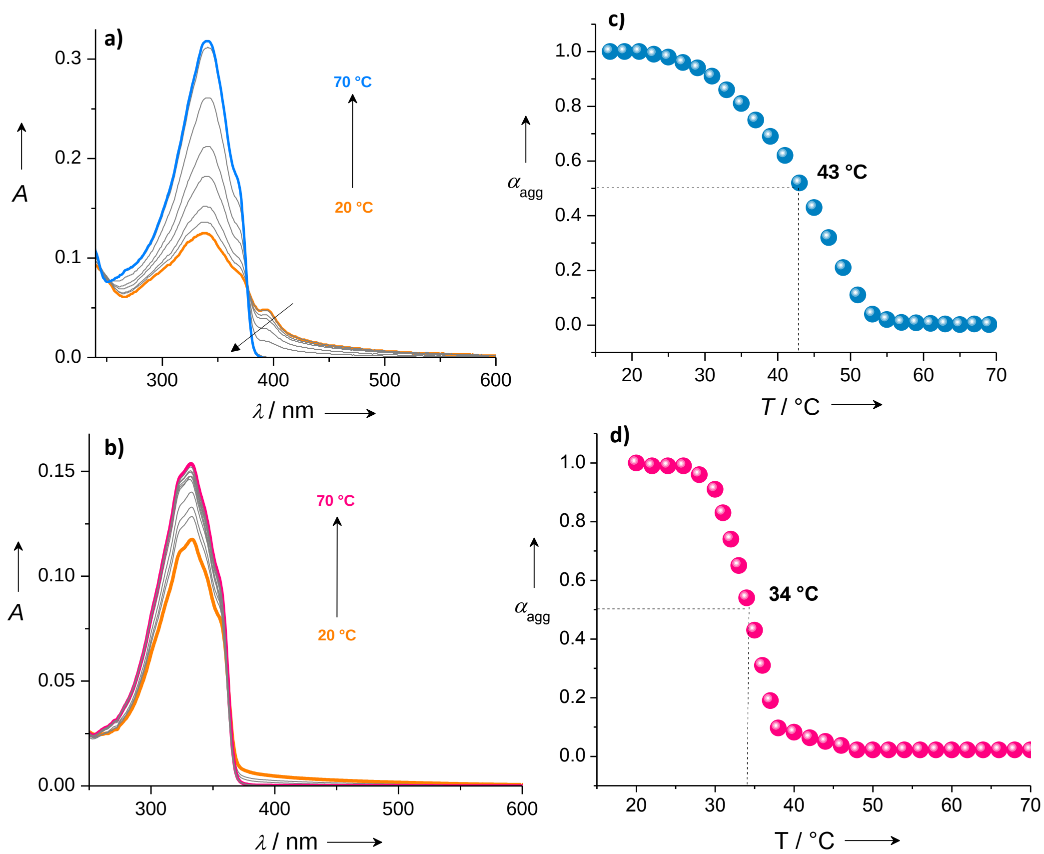

Figure 4.6. Temperature dependent absorption spectra of a) **PE-CN-Chiral** and b) **PE-Chiral** in *n*-decane ($c = 1 \times 10^{-4}$ M). Plots of aggregates fraction (α) versus temperature for c) **PE-CN-Chiral** and d) **PE-Chiral** (data points obtained from temperature dependent absorption measurements).

Furthermore, the emission spectrum of **PE-CN-Chiral** in *n*-decane showed a marginal enhancement in comparison to that in chloroform. On the other hand, **PE-Chiral** in monomeric state showed a weak emission in chloroform with maxima at 370 and 388 nm (Φ_F = 0.02), However, in *n*-decane the molecule exhibited 9.2 times enhancement in emission, Φ_F = 0.25 (Figure 4.7b). This observation indicates AIEE property of **PE-Chiral** whereas in the case of **PE-CN-Chiral**, AIEE is not conclusive.

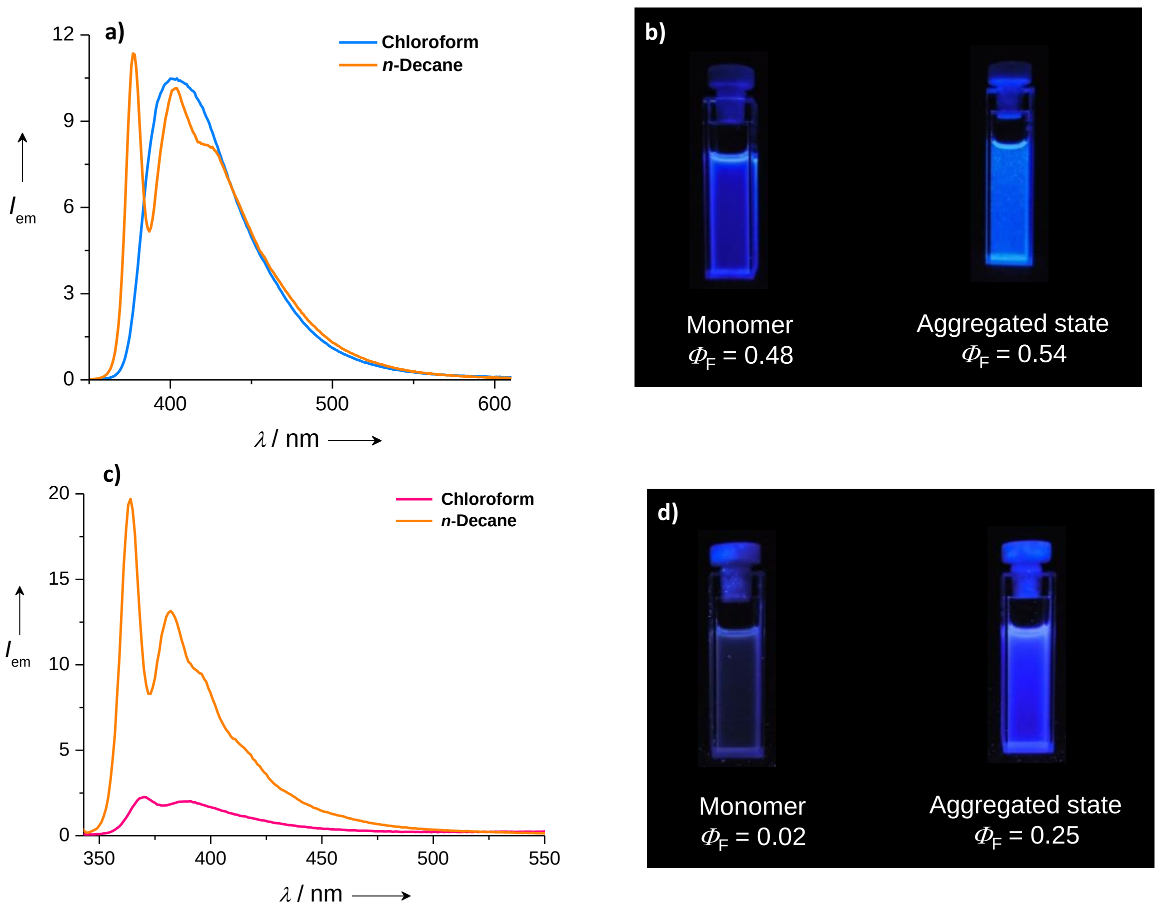

Figure 4.7. Emission spectra of a) **PE-CN-Chiral** and c) **PE-Chiral** in chloroform and *n*-decane at (c = 1 × 10^{-4} M), λ_{ex} = 340 nm. Photographs taken under 365 nm UV illumination: left (monomer) and right (aggregated state) for b**) PE-CN-Chiral** and d) **PE-Chiral**.

4.2.3. Gelation Studies

Gelation behavior of **PE-CN-Chiral** and **PE-Chiral** was examined in various hydrocarbon solvents by dissolving different amounts of compounds in a specific volume (1 mL) of the solvent by heating followed by cooling to the room temperature. It has been observed that gelation, precipitation or clear solution could be obtained depending upon the nature of the solvent and the gelator. Gel formation could be detected readily by the failure of the resultant mass to flow when the vial was tilted upside down and also from the soft appearance.

Table 4.1. Critical gelator concentration (CGC) (mM)[a] of **PE-CN-Chiral** and **PE-Chiral** in different solvents.

Gelator	*n*-Decane	MCH	Cyclohexane	*n*-Hexane	Toluene
PE-CN-Chiral	5.8 (G)	7.7 (G)	14.0 (G)	(P)	(S)
PE-Chiral	23.6 (G)	29.0 (G)	39.2 (G)	14.7 (G)	(S)

[a]CGC = is the minimum concentration required for the formation of a stable gel at room temperature. In parenthesis, G = gel, P = precipitates and S = solution at room temperature.

Results of the gelation experiments are presented in Table 4.1, which reveal that both **PE-CN-Chiral** and **PE-Chiral** could gelate nonpolar hydrocarbon solvents such as *n*-decane, methyl cyclohexane and cyclohexane. The CGC value of **PE-CN-Chiral** was found lower than that of **PE-Chiral**, for instance in *n*-decane CGC of **PE-CN-Chiral** was 5.8 mM and that of **PE-Chiral** was 23.6 mM. This observation implies that **PE-CN-Chiral** having a terminal cyano moiety is a better gelator in comparison to **PE-Chiral**. The gels formed by both the compounds are found to be opaque as well as emissive in the blue region.

4.2.3.1. Rheological Studies of Gel

The viscoelastic nature of the gels formed in *n*-decane was confirmed by rheological studies (Figure 4.8). Dynamic frequency sweep experiments revealed that the storage modulus (G') and the loss modulus (G'') values are independent of the oscillation frequency in the range of 1-100 rad s^{-1} with strain amplitude (γ) at 0.01. The G' value is nearly an order of magnitude higher than G'', indicating that the gel is elastically stronger for **PE-CN-Chiral** in comparison to that of **PE-Chiral**.[19]

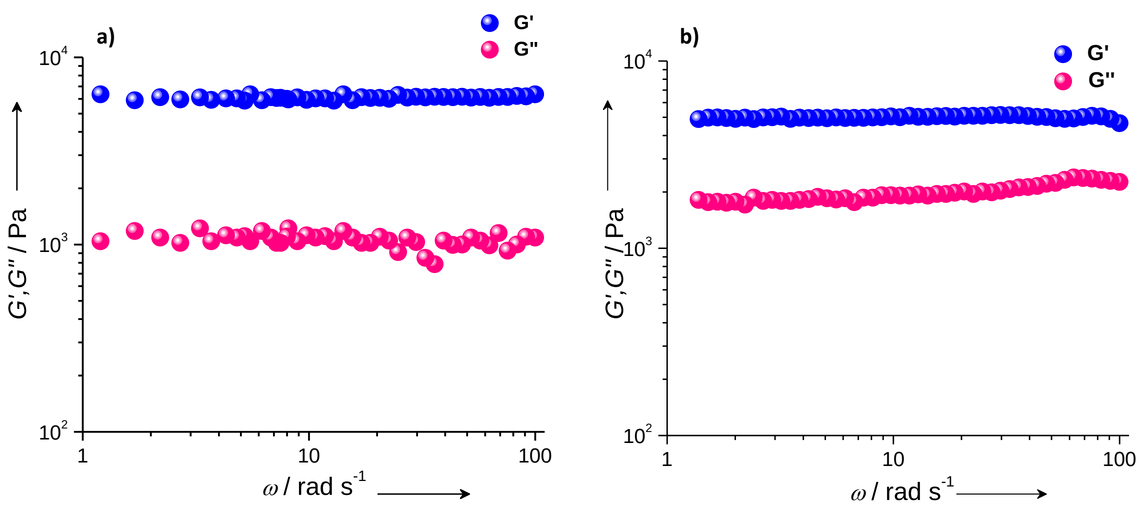

Figure 4.8. Plot of dynamic storage (G' -) and loss modulus (G'' -) vs angular frequency (ω) for a) **PE-CN-Chiral** and c) **PE-Chiral** in *n*-decane at 20 °C with strain amplitude (γ) at 0.01.

4.2.4. FT-IR Spectral Studies

It is known that H-bonding and van der Waals interactions play crucial roles in the self-assembly of molecules leading to gelation of solvents. FT-IR spectroscopy is an efficient technique to probe self-assembly and gelation. The IR spectra for **PE-CN-Chiral** and **PE-Chiral** indicate that the amide groups are involved in the H-bonding and no free C=O or N–H groups are present (Figure 4.9). The C=O stretching band for **PE-Chiral** is observed at 1651 cm^{-1} while in the case of **PE-CN-Chiral** it is observed at 1641 cm^{-1}. In addition, the N–H stretching bands of **PE-CN-Chiral** appeared at 3267 cm^{-1} at lower region when compared to N–H stretching band at 3285 cm^{-1} for **PE-Chiral**. The lowering of wavenumber values indicates the weakening of C=O and N–H stretching bands, which leads to the formation of intermolecular hydrogen bonding. From the above data it is clear that the hydrogen bonding ability is greater for **PE-CN-Chiral**.

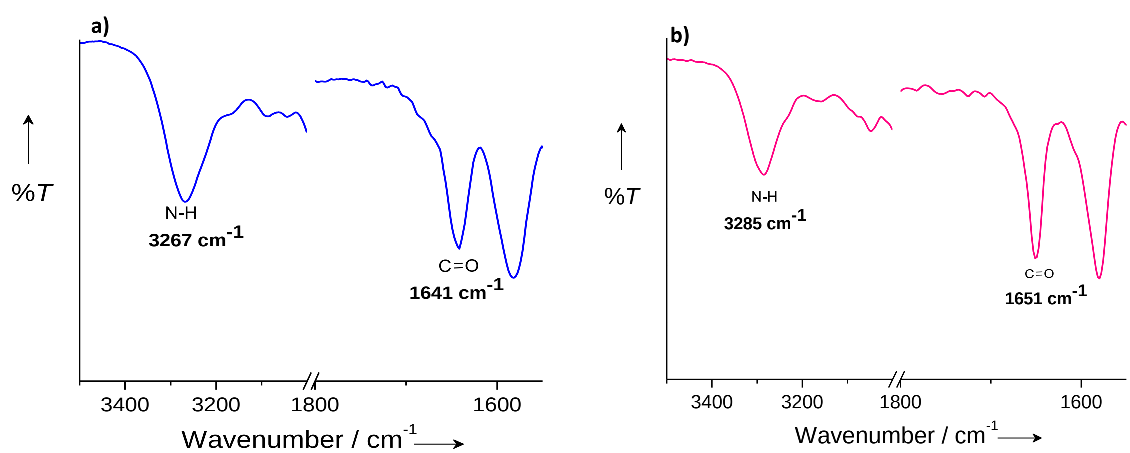

Figure 4.9. FT-IR **s**pectra of a) **PE-CN-Chiral** and b) **PE-Chiral**.

4.2.5. Emission Studies of Gels

The gels formed by **PE-CN-Chiral** and **PE-Chiral** in *n*-decane are found to be opaque as well as emissive in the blue region. Figure 4.10 shows the emission spectra of *n*-decane gels. Compared to **PE-Chiral** (λ_{max} = 395 nm), the emission maximum of **PE-CN-Chiral** (λ_{max} = 426 nm) was found to be red-shifted due to the presence of electron withdrawing cyano group and strong exciton coupling in the gel state.[20]

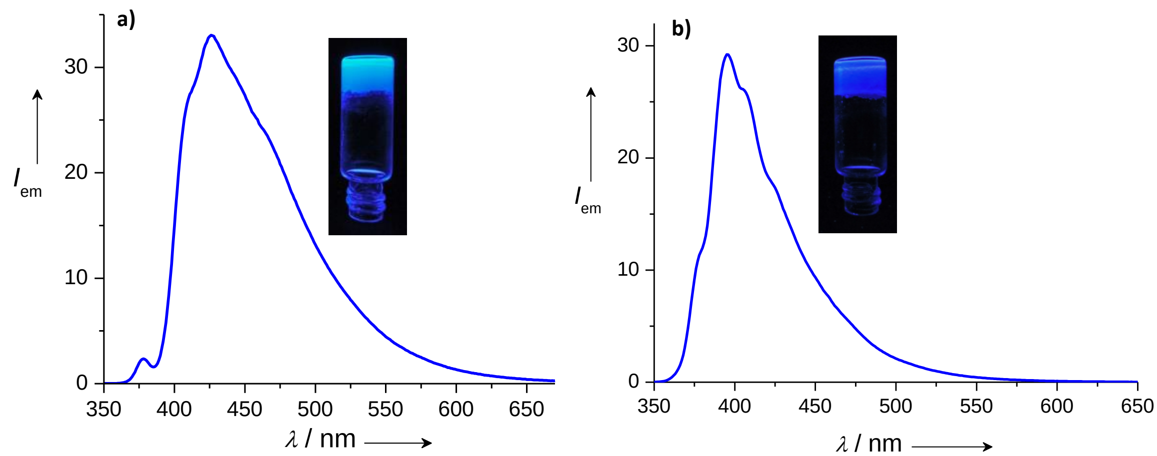

Figure 4.10. Emission spectra of gels: a) **PE-CN-Chiral** and b) **PE-Chiral, λ_{ex} = 340 nm**. Inset**s** show the photographs of gels under illumination of 365 nm UV light.

4.2.6. Electron and Fluorescence Microscopic Studies

In order to get insight about morphological features of **PE-CN-Chiral** and **PE-Chiral** assembly in *n*-decane, transmission electron microscopy (TEM) studies were carried out. For this purpose, *n*-decane aggregates of both the compounds were drop cast on carbon coated copper grid and dried under vacuum. TEM images of both compounds show the formation of micrometer long helical fibers having widths ranging 50-200 nm (Figure 4.11a and b). Further confirmation is obtained from fluorescence microscopy, which clearly showed the presence of blue emissive helical fibers (Figure 4.11c and d). In both the microscopic analyses formation of super-helical structures by coiling of small fibers is observed.[22] Furthermore, most of the helical fibers are found as right handed.

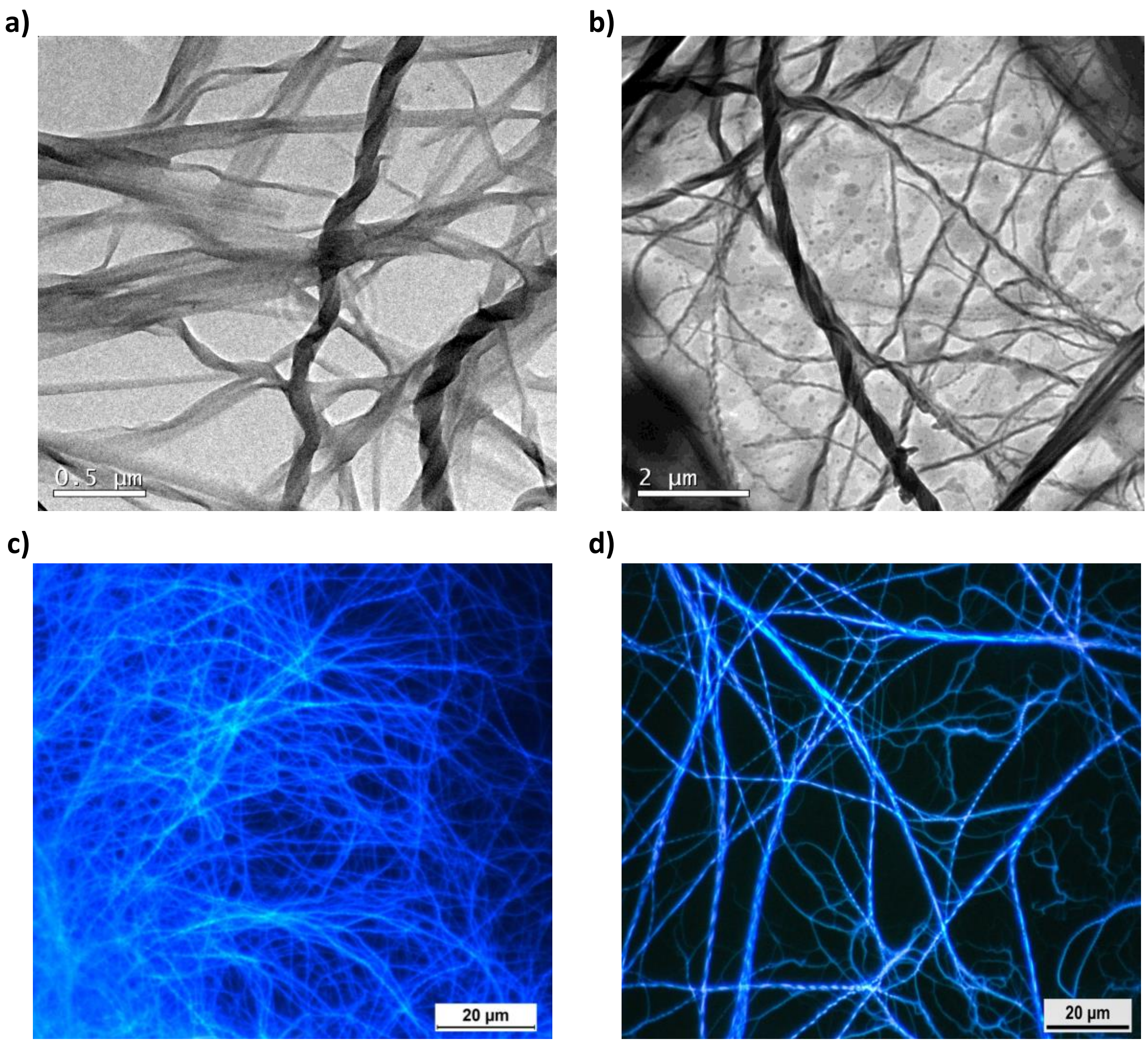

Figure 4.11. TEM images: a) **PE-CN-Chiral** and b) **PE-Chiral**. Fluorescence microscopy images: c) **PE-CN-Chiral** and d) **PE-Chiral.** Samples were prepared from solutions in *n*-decane (c = 5 × 10^{-4} M).

4.2.7. Small Angle X-ray Scattering (SAXS) Studies

In order to understand packing of the molecules in the helical structures formed by **PE-CN-Chiral** and **PE-Chiral**, SAXS studies have been performed in the xerogel state. Figure 4.12a shows the SAXS pattern of the **PE-CN-Chiral** exhibiting two peaks with a reciprocal *d*-spacing ratio of 1:2.[21] The presence of diffraction bands with *d*-spacing of 36.7 Å (001) and 18.3 Å (002) indicate a long range crystalline lamellar type ordering of the molecules. The intense sharp peak at 36.7 Å corresponds to the width of a single 1-D layer of the molecules where dipole-dipole interaction is nullified upon interdigitation of the two oppositely oriented cyano groups present in the extreme ends of **PE-CN-Chrial** molecules. Similarly, **PE-Chiral** also shows an intense small-angle reflection at 34.9 Å and weak reflection at 17.5 Å confirming the lamellar packing (Figure 4.12b).

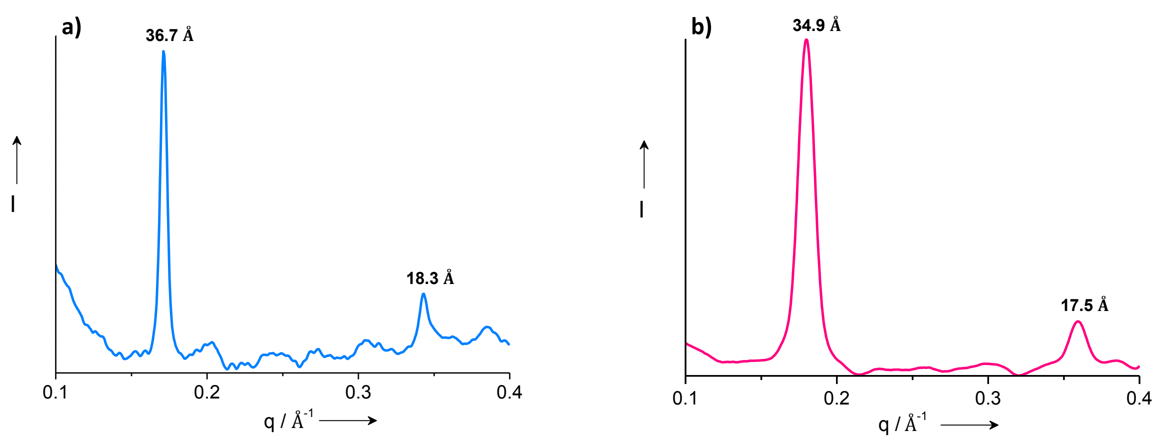

Figure 4.12. SAXS pattern of a) **PE-CN-Chiral** and b) **PE-Chiral** xerogel film.

4.2.8. Chiroptical Studies

CD spectroscopy is the most sensitive and appropriate tool to understand the behavior of chiral assemblies. The chiroptical properties of the **PE-CN-Chiral** and **PE-Chiral** helical assemblies in *n*-decane were investigated by CD spectroscopy. A bisignate CD signal in the vicinity of the lowest molecular singlet transition indicates the formation of non-racemic supramolecular helical assembly.[23] The CD experiments of **PE-CN-Chiral** and **PE-Chiral** were carried out in chloroform and *n*-decane at 25 °C (Figure 4.13). As expected both compounds were CD silent in chloroform (1 x 10^{-4} M) indicating that they exist as monomers in chloroform. This result is in agreement with UV/Vis absorption and emission spectral studies.

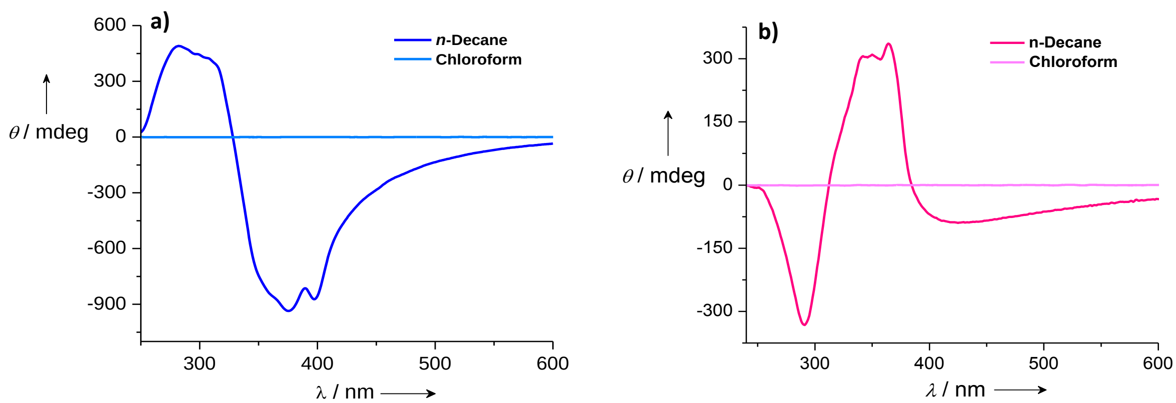

Figure 4.13. CD spectra of a) **PE-CN-Chiral** and b) **PE-Chiral** (c = 5 × 10^{-4} M, l = 1 mm) at 25 °C in chloroform and *n*-decane.

The **PE-CN-Chiral** aggregates in *n*-decane (1 x 10^{-4} M) showed a bisignate Cotton effect with a negative signal at 347 nm followed by a positive signal at 284 nm (Figure 4.13a). The zero crossover point at 322 nm in the CD spectrum close to the absorption maximum indicates an exciton coupled CD signal. However, CD measurements of **PE-Chiral** in *n*-decane (1 x 10^{-4} M) showed an entirely different CD spectrum, when compared to that of **PE-CN-Chiral** (Figure 4.13b). In this case, the CD pattern was found to be reversed where an intense positive signal at 364 nm followed by a negative signal at 291 nm with a zerocrossing at 312 nm was observed.

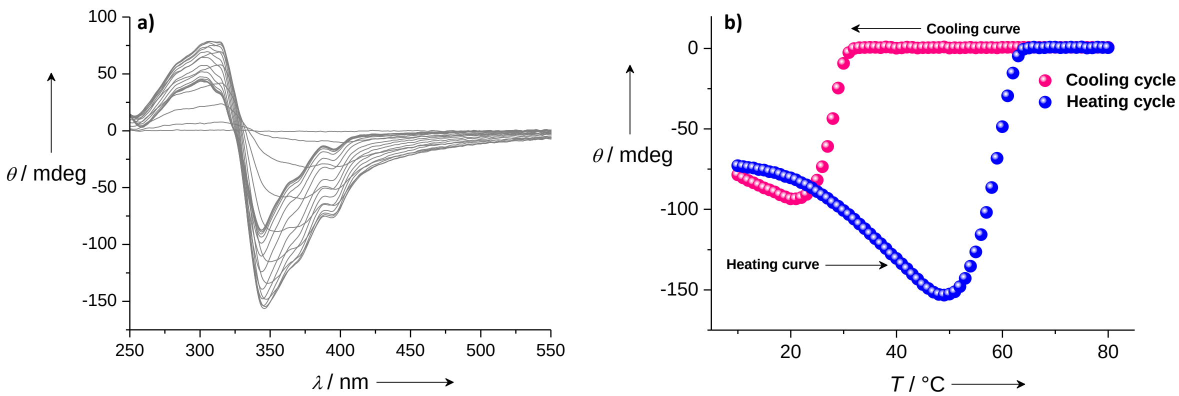

Figure 4.14. a) Temperature dependent CD spectra of **PE-CN-Chiral** (c = 1 × 10^{-4} M, l = 1 mm) in *n*-decane. b) Plot showing the transition of CD intensity at 347 nm with temperature, rate of cooling and heating is 1 K/min.

Variable temperature CD measurement of **PE-CN-Chiral** in *n*-decane (1 × 10^{-4} M) with a rate of 1 K/min revealed an increase in the intensity of the CD signal upon increasing the temperature from 10 to 50 °C (Figure 4.14). However, above 50 °C, a sharp transition of the intense exciton coupled CD signal to a weak signal was taken place, which continued to decrease till the CD signal intensity reaches zero at 62 °C. This is clear from the heating and cooling curves shown in Figure 4.14b. The temperature-dependent CD intensity changes can be explained on the basis of exciton theory. According to the exciton theory, the CD intensity Δ is a measure of the distance between the chromophores and the angle θ between the two transition dipole moments.[24] In general, CD signal has a maximum intensity when θ is 45 or 135°. This angle is generally less than 10° in chiral self-assemblies, especially in gel systems. Therefore, it can be considered that the increase in the CD intensity below 50 °C originates from the increase in θ induced by the partial breaking of hydrogen bonds between adjacent chromophores. The decrease in the CD signal above this temperature is similar to the behavior normally observed in the disassembly and the resulting loss of supramolecular chirality induction.

4.2.9. Effect of Trifluoroacetic Acid on Chiral Assembly

The chiral packing of the **PE-CN-Chiral** molecule is decided by different self-assembling motifs present within the system where the chiral alkyl side chain is responsible for preferential supramolecular handedness of the assembly. The amide group forms intermolecular hydrogen bonding, the rigid *p*-phenyleneethynylene aromatic core gives π-π stacking and the cyano group provides dipolar interaction. As demonstrated in Chapter 2 of the thesis, modulation of any one of these interactions present in the molecular assembly can lead to a change in the molecular packing and thereby give rise to different optical properties. Based on this assumption, we have introduced trifluoroacetic acid (TFA) as a H-bond modulator in the chiral assembly of **PE-CN-Chiral**. The use of TFA in controlling the conformation of peptide assemblies were well established, which prompted us to use TFA for modulating the chiral molecular assembly.[25] At a concentration of 1×10^{-3} M in *n*-decane, **PE-CN-Chiral** aggregates displayed a bisignate CD signal with a negative Cotton effect at 400 nm and a positive Cotton effect at 315 nm with a zero crossover point 342 nm (Figure 4.15a). The solution upon exciting at 340 nm showed an intense blue emission with maximum centered at 432 nm (Figure 4.15b).

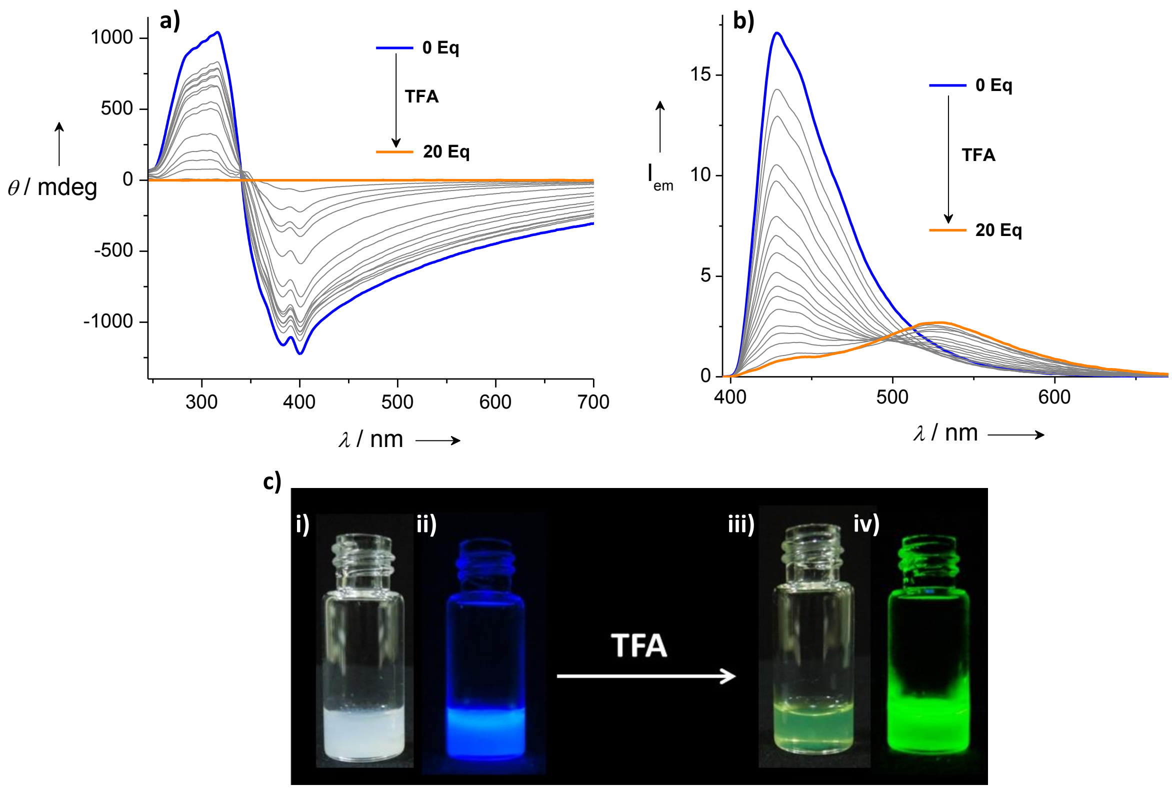

Figure 4.15. a) CD spectra and b) emission spectra of **PE-CN-Chiral** ($c = 1 \times 10^{-3}$ M, $l = 1$ mm) in *n*-decane at 25 °C with addition of varying amounts of TFA, λ_{ex} = 340 nm. c) Photographs of **PE-CN-Chiral** under normal light (i and iii) and UV light (ii and iv) before and after the addition of TFA.

In order to understand the role of TFA in modulating the self-assembly properties of **PE-CN-Chiral**, different amount of TFA was added to an aggregated solution of **PE-CN-Chiral** (c = 1 × 10^{-3} M) in *n*-decane and the corresponding changes were simultaneously monitored by CD and fluorescence spectroscopy (Figure 4.15a and b). A decrease in CD as well as emission intensity of **PE-CN-Chiral** aggregates was noticed upon gradual addition of TFA. After adding 20 equivalence TFA, the CD signal intensity was found to reach zero. However, in the case of emission, addition of TFA results in the formation of a new red-shifted band at 528 nm along with the decrease of emission in the blue region. Figure 4.15c shows that **PE-CN-Chiral** aggregated solution in *n*-decane is opaque and colorless under normal light and blue-emissive upon illumination with UV light at 365 nm. A complete change in appearance as well as emission was observed upon addition of TFA into this solution. In the presence of TFA, the turbid blue solution of **PE-CN-Chiral** aggregates becomes transparent with a green emission.

As mentioned above, in the presence of 20 equivalence of TFA, **PE-CN-Chiral** solution in *n*-decane is CD silent. However, a time dependent evolution of CD signal with opposite Cotton signal to that of initial **PE-CN-Chiral** assembly has been observed (Figure 4.16a and c). After seven days, this system showed an intense positive CD signal at 374 nm followed by a negative CD signal at 280 nm with zero crossover point at 337 nm. This CD change is accompanied with change in emission intensity also (Figure 4.16b and d). The green emission of **PE-CN-Chiral** was observed in the presence of TFA (20 equivalence) showed a time-dependent enhancement in intensity and became saturated after 4 h. This result clearly indicates that addition of TFA induced changes in chiral packing of the **PE-CN-Chiral** assembly resulting in new emissive properties.

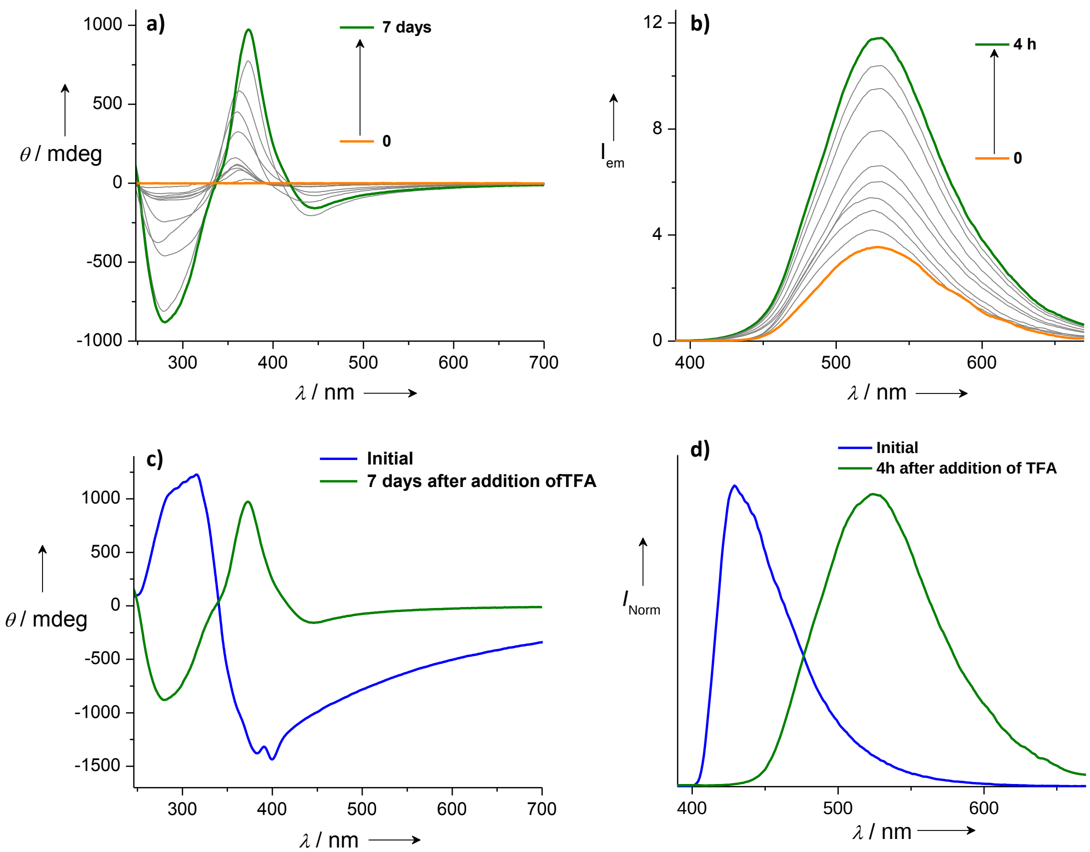

Figure 4.16. Time dependent changes of a) CD spectra and b) emission spectra (λ_{ex} = 340 nm) of **PE-CN-Chiral** after the addition of 20 equiv. of TFA. c) CD d) normalized emission spectra of **PE-CN-Chiral** (c = 1 × 10^{-3} M) in *n*-decane in the absence (blue) and presence of (green) of TFA (20 equivalence).

Fluorescence microscopy images of **PE-CN-Chiral** have revealed the formation of blue emitting rod like structures having length of several micrometers (Figure 4.17a). However, addition of 20 equivalence of TFA resulted in the formation of green emitting entangled thin fiber networks (Figure 4.17b).

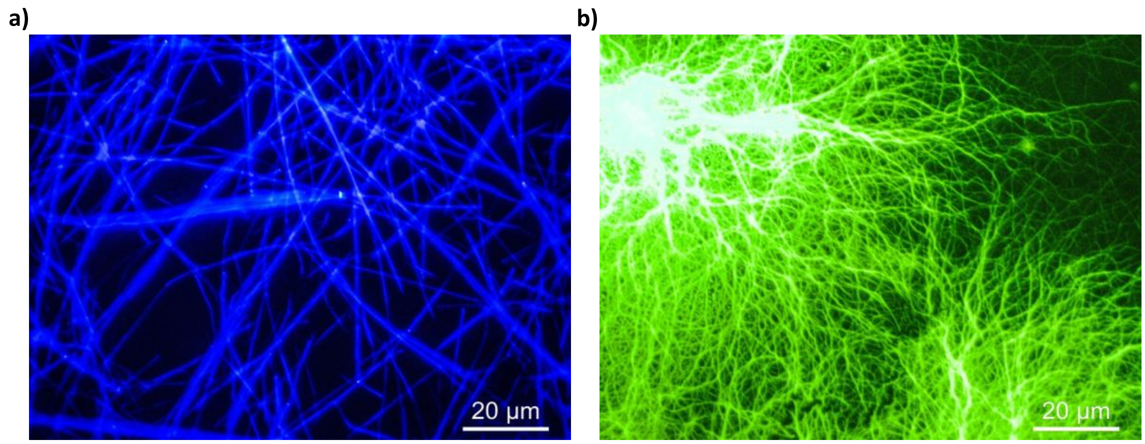

Figure 4.17. Fluorescence microscopy images of **PE-CN-Chiral** ($c = 1 \times 10^{-3}$ M) in *n*-decane a) before and b) after addition of 20 equivalence of TFA.

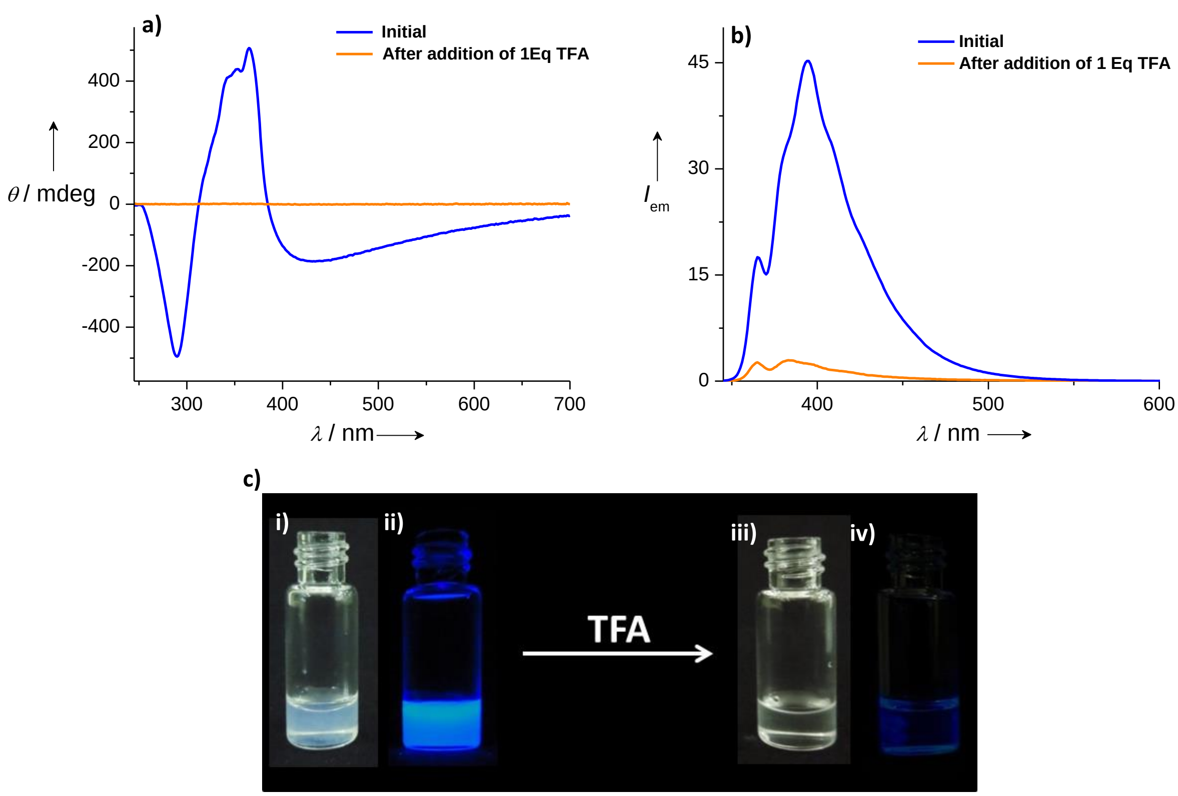

Figure 4.18. a) CD and b) emission spectra (λ_{ex} = 340 nm) of **PE-Chiral** ($c = 1 \times 10^{-3}$ M, l = 1 mm) in *n*-decane at 25 °C before (blue) and after (orange) addition of TFA. c) Photographs of **PE-Chiral** under normal light (i and iii) and UV light (ii and iv) before and after addition of TFA.

In contrast to **PE-CN-Chiral** aggregates, addition of 1 equivalence of TFA to aggregates of **PE-Chiral** ($c = 1 \times 10^{-3}$ M) in *n*-decane causes complete loss of CD signal (Figure 4.18a). This observation shows the disruption of chiral molecular assembly upon addition of TFA. Similarly, the emission spectra also showed a change from intense blue emission of aggregates to very weak monomeric emission (Figure 4.18b). The corresponding photographs display the disappearance of aggregates with the formation of a clear monomeric solution after the addition of 1 equiv. TFA (Figure 4.18c). In this case we have not observed any time dependent changes in CD and emission.

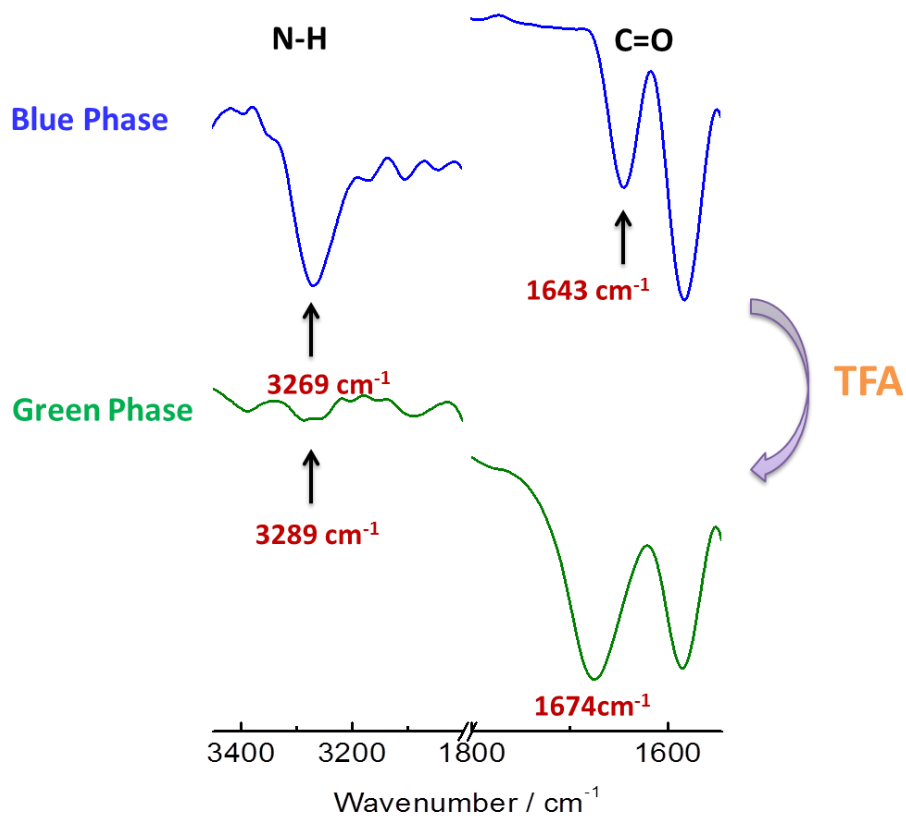

Figure 4.19. FT-IR spectra of **PE-CN-Chiral** film before (blue) and after (green) exposure to TFA vapors.

Addition of TFA to the **PE-CN-Chiral** assembly in *n*-decane can result initially the breaking of chiral assembly by disrupting the amide H-bonding. However, with time the monomeric units can undergo self-organization with the help of π-π stacking, dipole and van der Waals interactions. This has been confirmed with help of FT-IR studies of self-assembled film of **PE-CN-Chiral** exposed to TFA vapors (Figure 4.19). The H-bonded **PE-CN-Chiral** assembly showed N-H and carbonyl stretching frequency at 3269 and 1643 cm^{-1}, respectively.[26] However, upon exposure to TFA vapors both the N-H and carbonyl stretching showed a shift to higher frequency region due to breaking of intermolecular H-bonding.

4.3. Conclusions

In conclusion, we have described the synthesis and supramolecular helicity modulation of two *p*-phenyleneethynylene derivatives **PE-CN-Chiral** and **PE-Chiral** organogelators. With the help of detailed CD and photophysical studies, we have shown that the supramolecular chirality of the **PE-CN-Chiral** assembly could be manipulated with the addition of TFA without changing the inherent molecular chirality of the individual building blocks. After adding TFA, the blue emission of the molecular assembly is changed to green with reversal of CD signal over a period of time. However, such changes have not been encountered with **PE-Chiral** assembly upon the addition of TFA, instead complete disruption of molecular assembly has been observed. This work highlights the importance of stimuli responsive multiple noncovalent interactions in creating the supramolecular helical assembly with tunable helicity and emission.

4.4. Experimental Section

General procedure for the purification, drying of solvents and other common experimental techniques used are described in the experimental section (section 2.4.1) of Chapter 2.

4.4.1. Synthesis and Characterization

Synthesis and characterization of PE-CN-Chiral and PE-Chiral: In a general synthetic procedure, the aryl halide (0.70 mmol), bis(triphenylphosphine)palladium (II) dichloride (10 mol%), and copper (I) iodide (10 mol%) were added to an oven-dried two neck round bottom flask equipped with a magnetic stirring bar. The round bottom flask was then sealed with a rubber septum, evacuated and backfilled with argon three times. Degassed triethylamine (10 mL) was added followed by degassed THF (10 mL) to serve as the co-solvent. After stirring for 5 minutes at room temperature, the alkyne (0.80 mmol) dissolved in 10 mL (1:1) mixture of degassed triethylamine and THF was added and the reaction mixture was stirred at room temperature until the completion of the reaction was noted by TLC. The reaction mixture was extracted using chloroform and washed with dilute hydrochloric acid. The organic layer was washed with brine and dried over anhydrous sodium sulphate and then evaporated under reduced pressure. The crude product was then purified by column chromatography using silica gel as adsorbent.

PE-CN-Chiral: R_f = 0.54 ($CHCl_3$:MeOH, 97:3 v/v); Yield: 57%; m.p.: 156-158 °C; FT-IR (KBr): ν_{max} = 3264, 2953, 2924, 2216, 1915, 1641, 1585, 1512 cm^{-1}; ^1H NMR (500 MHz, $CDCl_3$): δ = 7.83 (s, 1H), 7.68-7.61 (m, 6H), 7.57-7.54 (m, 6H), 7.07 (s, 2H), 4.10-4.02 (m, 6H), 1.91-1.85 (m, 3H), 1.72-1.51 (m, 9H), 1.35-1.32 (m, 9H), 1.20-1.16 (m, 9H), 0.96-0.93 (m, 9H), 0.86-0.87 (m, 18H) ppm; ^{13}C NMR (125 MHz, $CDCl_3$): δ = 165.6, 153.3, 141.7, 138.4, 132.6, 132.1, 131.7, 131.6, 129.6, 128.1, 124.1, 121.8, 119.8, 111.6, 105.8, 93.5, 91.6, 89.4, 88.7, 71.8, 67.8, 39.3, 37.5, 37.3, 36.4, 29.8, 29.7, 27.8, 24.7, 22.7, 22.6, 19.6 ppm; ESI-MS (m/z): $[M+1]^+$ calcd. for $C_{60}H_{78}N_2O_4$, 892.27; found, 892.97.

PE-Chiral: R_f = 0.45 (*n*-hexane:$CHCl_3$, 1:1 v/v); Yield: 60%; m.p.: 143-145 °C; IR (KBr): ν_{max} = 3285, 2957, 2926, 2216, 1651, 1582, 1518 cm^{-1}; ^1H NMR (500 MHz, $CDCl_3$): δ = 7.78 (s, 1H), 7.66 (d, J = 10.0 Hz, 2H), 7.55-7.50 (m, 8H), 7.36-7.35 (m, 3H), 7.05 (s, 2H), 4.09-4.02 (m, 6H), 1.91-1.85 (m, 3H), 1.72-1.51 (m, 9H), 1.35-1.32 (m, 9H), 1.20-1.16 (m, 9H), 0.96-0.93 (m, 9H), 0.86-0.87 (m, 18H), ppm; ^{13}C NMR (125 MHz, $CDCl_3$): δ = 165.7, 153.5, 141.5, 138.2, 132.7, 131.4, 128.5, 123.0, 119.7, 106.0, 103.8, 100.0, 89.3, 72.0, 67.8, 39.3, 37.5, 36.3, 30.0, 29.8, 28.1, 24.8, 22.8,19.6 ppm; ESI-MS (m/z): $[M]^+$ calcd. For $C_{59}H_{79}NO_4$, 866.26; found, 866.61.

4.4.3. Description on Experimental Techniques

Circular Dichroism Spectroscopy (CD): The experiments were performed on a JASCO 810 spectrometer equipped with peltier thermostatic cell holders. Sensitivity, response time and scanning speed were chosen appropriately. CD spectra were recorded as θ in millidegrees for aggregated solutions of **PE-CN-Chiral** and **PE-Chiral** using a quartz cuvette of 1 mm path length at 25 °C.

The experimental techniques for SAXS, SEM, TEM, Fluorescence microscopy and Optical measurements are described in section 2.4.5 of Chapter 2. General procedure for gelation studies and experimental technique for rheological studies are are described in section 3.4.4 of Chapter 3.

4.5. References

[1] F. J. M. Hoeben, P. L. Jonkheijm, E. W. Meijer, A. P. H. J. Schenning, *Chem. Rev*. **2005**, *105*, 1491–1546.

[2] (*a*) W. Li, T. Aida, *Chem. Rev*. **2009**, *109*, 6047–6076; (*b*) L. Brunsveld, H. Zhang, M. Glasbeek, J. A. J. M. Vekemans, E. W. Meijer, *J. Am. Chem. Soc.* **2000**, *122*, 6175–6182.

[3] (*a*) T. Yamamoto, T. Fukushima, A. Kosaka, W. Jin, Y. Yamamoto, N. Ishii T. Aida, *Angew. Chem., Int. Ed.* **2008**, *47*, 1672–1675; (*b*) Y. He, Y. Yamamoto, W. Jin, T. Fukushima, A. Sacki, S. Seki, N. Ishii, T. Aida, *Adv. Mater.* **2010**, *20*, 829–832.

[4] (*a*) V. Dehm, Z. Chen, U. Baumeister, P. Prins, L. D. A. Siebbeles, F. Würthner, *Org. Lett.* **2007**, *9*, 1085; (*b*) Y. Huang, Y. Yan, B. M. Smarsly, Z. Wei, C. F. J. Faul, *J. Mater. Chem.* **2009**, *19*, 2356–2362.

[5] (*a*) E. Yashima, N. Ousaka, D. Taura, K. Shimomura, T. Ikai, K. Maeda, *Chem. Rev.* **2016**, *166*, 13752–13990; (*b*) M. Liu, L. Zhang, T. Wang, *Chem. Rev.* **2015**, *115*, 7304–7397; (*c*) G. Song, J. Ren, *Chem. Commun.* **2010**, *46*, 7283–7294; (*d*) M. A. Mateos-Timoneda, M. Crego-Calama, D. N. Reinhoudt, *Chem. Soc. Rev*. **2004**, *33*, 363–372.

[6] (*a*) K. S. Cheon, J. V. Selinger, M. M. Green, *Angew. Chem., Int. Ed.* **2000**, *39*, 1482–1485; (*b*) K. Tang, M. M. Green, K. S. Cheon, J. V. Selinger, B. A. Garetz, *J. Am. Chem. Soc.* **2003**, *125*, 7313–7323; (*c*) K. Maeda, H. Mochizuki, M. Watanabe, E. Yashima, *J. Am.Chem. Soc.* **2006**, *128*, 7639–7650; (*d*) M. Shigeno, Y. Kushida, M. Yamaguchi, *J. Am. Chem. Soc.* **2014**, *136*, 7972–7980.

[7] (*a*) K. Maeda, N. Kamiya, E. Yashima, *Chem. –Eur. J.* **2004**, *10*, 4000–4010; (*b*) T. Yamamoto, T. Yamada, Y. Nagata, M. Suginome, *J. Am. Chem. Soc.* **2010**, *132*, 7899–7901; (*c*) Y. Nagata, T. Yamada, T. Adachi, Y. Akai, T. Yamamoto, M. Suginome, *J. Am. Chem. Soc*. **2013**, *135*, 10104−10113.

[8] (*a*) N. Koumura, R. W. J. Zijlstra, R. A. van Delden, N. Harada, B. L. Feringa, *Nature* **1999**, *401*, 152−155; (*b*) J. Li, G. B. Schuster, K.-S. Cheon, M. M. Green, J. V. Selinger, *J. Am. Chem. Soc.* **2000**, *122*, 2603−2612; (*c*) D. Pijper, B. L. Feringa, *Angew. Chem., Int. Ed.* **2007**, *46*, 3693−3696.

[9] Y. Li, H. Wang, L. Wang, F. Zhou, Y. Chen, B. Li, Y. Yang, *Nanotechnology*, **2011**, *22*, 135605.

[10] S. Maity, P. Das, M. Reches, *Sci. Rep.* **2015**, *5*, 16365.

[11] Y. Nagata, R. Takeda, M. Suginome, *Chem. Commun*. **2015**, *51*, 11182–11185.

[12] (*a*) Y. Inai, Y. Ishida, K. Tagawa, A. Takasu, T. Hirabayashi, *J. Am. Chem. Soc.* **2002**, *124*, 2466–2473; (*b*) P. A. Korevaar, S. J. George, A. J. Markvoort, M. M. J. Smulders, P. A. J. Hilbers, A. P. H. J. Schenning, T. F. A. De Greef, E. W. Meijer, *Nature* **2012**, *481*, 492–496.

[13] (*a*) R. M. Meudtner, S. Hecht, *Angew. Chem., Int. Ed.* **2008**, *47*, 4926–4930; (*b*) H. Miyake, H. Kamon, I. Miyahara, H. Sugimoto, H. Tsukube, *J. Am. Chem. Soc.* **2008**, *130*, 792–793; (*c*) S. Akine, S. Hotate, T. Nabeshima, *J. Am. Chem. Soc.* **2011**, *133*, 13868–13871; (*d*) F. Freire, J. M. Seco, E. Quinoa, R. Riguera, *Angew. Chem., Int. Ed.* **2011**, *50*, 11692–11693.

[14] Z. Huang, S.-K. Kang, M. Banno, T. Yamaguchi, D. Lee, C. Seok, E. Yashima, M. Lee, *Science* **2012**, *337*, 1521–1526.

[15] M. C. Sicilia, A. Niño, C. Muñoz-Caro, *J. Phys. Chem. A* **2005**, *109*, 8341–8347.

[16] Y. Huang, J. Hu, W. Kuang, Z. Wei, C. F. Faul, *Chem. Commun*. **2011**, *47*, 5554–5556.

[17] F. Freire, J. M. Seco, E. Quiñoá, R. Riguera, *Angew. Chem., Int. Ed.* **2011**, *50*, 11692–11696.

[18] (*a*) J. Mei, Y. Hong, J. W. Lam, A. Qin, Y. Tang, B. Z. Tang, *Adv. Mater*. **2014**, *26*, 5429–5479; (*b*) Y. Hong, J. W. Lam, B. Z. Tang, *Chem. Soc. Rev.* **2011**, *40*, 5361–5388.

[19] (*a*) S. Yao, U. Beginn, T. Gress, M. Lysetska, F. Würthner, *J. Am. Chem. Soc.* **2004**, *126*, 8336–8348; (*b*) F. M. Menger, A. V. Peresypkin, *J. Am. Chem. Soc.* **2003**, *125*, 5340–5345.

[20] B.-K. An, S.-K. Kwon, S.-D. Jung, S. Y. Park, *J. Am. Chem. Soc*. **2002**, *124*, 14410–14415.

[21] (*a*) J.-H. Ryu, E. Lee, Y.-b. Lim, M. Lee, *J. Am. Chem. Soc*. **2007**, *129*, 4808–4814; (*b*) S. Yagai, T. Kinoshita, M. Higashi, K. Kishikawa, T. Nakanishi, T. Karatsu, A. Kitamura, *J. Am. Chem. Soc*. **2007**, *129*, 13277–13287.

[22] (*a*) C. C. Lee, C. Grenier, E. W. Meijer, A. P. H. J. Schenning, *Chem. Soc. Rev.* **2009**, *38*, 671–683; (*b*) G. Gottarelli, S. Lena, S. Masiero, S. Pieraccini, G. P. Spada, *Chirality* **2008**, *20*, 471–485.

[23] A. Lohr, M. Lysetska, F. Würthner, *Angew. Chem., Int. Ed.* **2005**, *44*, 5071 – 5074.

[24] (*a*) N. Berova, L. D. Bari, G. Pescitelli, *Chem. Soc. Rev*. **2007**, *36*, 914–931; (*b*) F. D. Lewis, L. Zhang, X. Liu, X. Zuo, D. M. Tiede, H. Long, G. C. Schatz, *J. Am. Chem. Soc.* **2005**, *127*, 14445–14453.

[25] I. M. Klotz, S. F. Russo, S. Hanlon, M. A. Stake, *J. Am. Chem. Soc.* **1964**, *86*, 4774–4776.

[26] R. Thirumalai, R. D. Mukhopadhyay, V. K. Praveen, A. Ajayaghosh, *Sci. Rep.* **2015**, 5, 9842

Posters Presented in Conferences

1. **R. Thirumalai** and A. Ajayaghosh, A Novel Fluorescent Molecular Self-assembly for Self-erasable Writing with Water and Its Application as Currency and Document Security Label. *14th CRSI National Symposium in Chemistry,* February 3-5, **2012**, Trivandrum, India.

2. **R. Thirumalai** and A. Ajayaghosh, Rewritable Photoluminescent Paper with Water as Ink. *9th JNC Research Conference on Chemistry of Materials*, October 14-16, **2013**, Trivandrum, India.

List of Publications

1. Role of Complementary H-bonding Interaction of a Cyanurate in the Self-Assembly and Gelation of Melamine Linked tri(*p*-phenyleneethynylene)s. S. Mahesh, **R. Thirumalai**, S. Yagai, A. Kitamura and A. Ajayaghosh. *Chem. Commun*. **2009**, 5984–5986.

2. Light Induced Ostwald Ripening of Organic Nanodots to Rods. S. Mahesh, A. Gopal, **R. Thirumalai** and A. Ajayaghosh. *J. Am. Chem. Soc*. **2012**, *134*, 7227–7230.

3. A slippery molecular assembly allows water as a self-erasable security marker. **R. Thirumalai**, R. D. Mukhopadhyay, V. K. Praveen and A. Ajayaghosh. *Sci. Rep*. **2015,** *5*, 9842.

4. Emission Color Tuning of a π-Gelator through Thermodynamic and Kinetic Assembly Pathways**. R. Thirumalai**, Gourab Das, P. Anisha, V. K. Praveen and A. Ajayaghosh. (*To be Communicated*).

5. Acid Induced Modulation of Luminescence and Helicity of a Chiral Assembly. **R. Thirumalai**, Gourab Das, B. Betzy, P. Anisha, V. K. Praveen and A. Ajayaghosh. (*To be Communicated*).

6. **Patent Granted:**
   Fluorescent Material for Self-Erasable Writing, Authentic Security Labeling, Currency Counterfeit Prevention and Processes for the Preparation Thereof. A. Ajayaghosh and **R. Thirumalai**. ***US 9,012,688 B2* (2015)**.